DISSERTATION

PROFILE MAINTENANCE IN BEDROCK STREAMS INCISING SOLUBLE STRATA

Submitted by

Gregory S. Springer

Department of Earth Resources

In partial fulfillment of the requirements

for the Degree of Doctor of Philosophy

Colorado State University

Fort Collins, Colorado

Summer, 2002

ProQuest Information and Learning Company
300 North Zeeb Road
P.O. Box 1346
Ann Arbor, MI 48106-1346

COLORADO STATE UNIVERSITY

May 24, 2002

WE HEREBY RECOMMEND THAT THE DISSERTATION PREPARED UNDER OUR SUPERVISION BY GREGORY S. SPRINGER ENTITLED PROFILE MAINTENANCE IN BEDROCK STREAMS INCISING SOLUBLE STRATA BE ACCEPTED AS FULFILLING IN PART REQUIREMENTS FOR THE DEGREE OF DOCTOR OF PHILOSOPHY.

Committee on Graduate Work

Advisor

Department Head , Acting

ABSTRACT OF DISSERTATION

PROFILE MAINTENANCE IN BEDROCK STREAMS

INCISING SOLUBLE STRATA

This study employs quantitative hypothesis tests to explore variations in channel substrate, geomorphic setting, and incision processes against changes in velocity ($\bar{u}$), shear stress (τ). and unit stream power (ω) in streams incising soluble and insoluble bedrock: Buckeye Creek (14 km^2 drainage area) and Greenbrier River (3800 km^2), West Virginia. Both streams are incising at ≤ 40 m Ma^{-1} and transport coarse, insoluble sediment. The streams are incising by quarrying, abrasion, and corrosion. Comparisons in thirteen stream reaches reveal that τ and ω are 3 to 30 times lower atop soluble versus insoluble bedrock. For constant relative solubility, τ and ω are higher in reaches that interact strongly with hillslopes.

Values of $\bar{u}$ are highest where evidence of abrasion is prominent on insoluble channel elements. Evidence of quarrying is associated with higher values of τ and ω than evidence of corrosion. By inference, the efficiency of corrosion-driven incision on soluble bedrock translates to minimization of mechanical energy expenditure, which is used to calculate τ and ω. Presumably, incision of insoluble strata requires more mechanical energy expenditure for a similar incision rate.

Rapid longitudinal changes in τ and ω are associated with similarly rapid longitudinal sorting and coarse-sediment storage in an alluvial reach in Buckeye Creek. Depth has adjusted in Greenbrier River such that changes in τ are of lesser magnitude. As a result, coarse sediment transport may be continuous across soluble and insoluble

bedrock. Overall, variations of $\bar{u}$, τ, and ω appear to reflect relative substrate solubility, geomorphic setting, and incision processes.

Sculpted forms enhance abrasion and corrosion in both streams by localizing energy expenditure on channel margins. Analyses of the equations for a forced vortex show that the morphology of large sculptures is controlled by channel hydraulics, whereas a mathematical model of erosion by small sculptures reveals that their morphology is dependent on overall channel erosion rates and not simply channel hydraulics. Therefore, corrosion and abrasion in sculpted forms are not controlled absolutely by channel hydraulics, which places a limit on the use of hydraulic variables for modeling channel incision by these phenomena.

Gregory S. Springer
Department of Earth Resources
Colorado State University
Fort Collins, CO 80523
Summer 2002

ACKNOWLEDGEMENTS

Technically, a doctoral degree is an individual achievement. One person receives the degree in return for a period of scientific exploration and mental anguish. In reality, a doctoral degree represents the sum of an individual's effort and the countless acts of compassion bestowed upon him/her. There can be no doubt that I would never have accomplished the task now behind me without the aid and patience of so many others. These people include my stoic mate, loving children, remarkably talented advisor, and tortured office mates. I wish to thank them all.

First, and foremost, I thank Tisha for enduring the hardship of being married to a would-be professor. I can imagine nothing so challenging as being married to doctoral candidate determined to succeed at all costs. Tisha suffered too much; whether one considers the many spouseless hours spent wondering when her husband would end his affair with his work or the long summers spent alone. I thank her for holding our family together through so much hardship.

Who could be more blessed than the father of Cass and Sara? I thank my beautiful children for their unrelenting love. Whatever stresses I may have suffered in any given day I could always look forward to loving hugs and gleeful faces when I arrived home. I certainly have never done anything deserving of such wonderful children, but I am thankful to have been given such bright and caring "buddies".

As hard as I have worked to earn my doctoral degree, I am nonetheless happy to thank my parents and mentors for their direct and indirect support for my aspirations and research. My parents, John and Nancy, gave me the opportunity to earn a BS in Geology, and were it not for their intermittent support since then I would have long since found myself settling for something less than my dream. Following my BS, Steve Kite gave me a model for teaching success, compassion and demanding standards, and I thank him for helping to channel my raw enthusiasm into an MS degree that has led to so much more.

Speaking of compassion and demanding standards... I thank my advisor, Ellen Wohl, for leading by example. I feel fortunate to have had two graduate advisors who ceaselessly work hard and encourage their students to chase their ideas and dreams. Ellen has consistently supported me and suffered through four years of constant hounding.

Some people wear their hearts on their sleeves. I wear my ideas on my sleeves and I thank Ellen for not only tolerating my incessant outbursts of irrational enthusiasm for new ideas, but for encouraging me to pursue them.

Chasing dreams and ideas is never cheap. My family and I have benefited from the generosity of Colorado State University, which gave me a Fellowship, and the Department of Earth Resources, which gave me seed money to start my fieldwork and write grant proposals. I thank Judy Hannah for acceding to Ellen's request for that seed money. I especially thank the Larry Burns Memorial Scholarship program for support that was invaluable at the time when it was received.

The Cave Conservancy Foundation (CCF) deserves my thanks for their generous financial support of my dissertation via a Fellowship. The CCF Fellowship gave me the opportunity to fully implement my research program and buy needed field and office equipment that I will be using for years to come. I thank the National Science Foundation (NSF) for funding my dissertation proposal and thereby allowing me to pursue my research in greater detail than would have been possible otherwise (NSF Grant EAR-0000725). I thank the West Virginia Association for Cave Studies (WVACS) for allowing me to stay at their fieldhouse for three summers and tolerating such a burdensome tenant.

Money aside, my research would have been impossible without my field assistants: Ben Mirable, Greg Gotham, Mark Hekkers, and Julie Foster. I thank them all for their hard work and especially Ben for working at cost during my first field season. I also wish to thank Vince Guaraldi for continued inspiration.

I thank Gene Turner for access to Buckeye Creek Cave and vicinity, but more importantly for being a friend. I have never been entirely sure whether Gene thinks I am crazy or just nearly so. In spite of that, he has consistently been supportive of my work and tolerate of my traipsing about. Thanks Gene!

TABLE OF CONTENTS

Abstract iii

Acknowledgements v

Table of Contents vii

List of Tables xiii

List of Figures xiii

List of Plates xiv

List of Variables xv

Chapter 1: Introduction 1

1.1 Project Introduction 1

1.2 Hypotheses and Principle Assumptions 2

1.3 Research Impetus and Rational 5

1.4 Project Objectives 12

Chapter 2: A Contextual Review of Profile Maintenance In Bedrock Streams 14

2.1 Methods of Profile Maintenance and Bedrock Incision 14

2.1.1 Bedrock Incision and Channel Processes 14

2.1.2 Hydraulic-Based Mechanisms of Bedrock Incision 15

2.1.3 Corrosion and Bedrock Incision 17

2.2 Substrate Resistance 20

2.3 Erosional Profile Forms 24

2.3.1 Profile Form 24

2.3.2 Knickpoints 26

2.3.3 Erosion in Knickpoints 27

2.4 Incision Processes and Resulting Forms Atop Soluble Strata 28

2.4.1 Confounding Variables 28

2.4.2 Channel Adjustments to Rock Solubility 30

2.4.3 Recognizing Channel Adjustments to Soluble Strata 31

2.4.4 Profile Development Atop Soluble Strata 32

Chapter 3: Study Area 40

3.1 Introduction 40

3.2 Buckeye Creek and Catchment 43
3.2.1 Surface Component 43
3.2.1.1 Geology 43
3.2.1.2 Fluvial Architecture 47
3.2.1.3 Model Reaches 50
3.2.1.4 Headwater Geomorphology 52
3.2.2 Subsurface Component 56
3.2.2.1 Subterranean Stream Network 56
3.2.2.2 Buckeye Creek Cave 56
3.2.2.3 Stream Morphology 57
3.2.2.4 Closed-Conduit Flow 58
3.2.3 Development of Buckeye Creek Cave 59
3.2.3.1 Overview of Sequential Passage Development 59
3.2.3.2 Age and Incision Rate 60
3.2.3.3 Passage Morphology 61
3.2.3.4 Development of Active Tier 61
3.2.4 Reach Descriptions 65
3.2.4.1 Reach A 65
3.2.4.1 Reach B 66
3.2.4.1 Reach C 67
3.2.4.1 Reach D 67
3.2.4.1 Reach E 68
3.2.4.1 Reach F 69
3.2.4.1 Reach G 69
3.2.4.1 Reach H 70
3.3 Greenbrier River 71
3.3.1 General Characteristics 71
3.3.2 Renick Reaches 71
3.3.2.1 Mile-27 Reach 73
3.3.2.2 Bone Quarry Reach 73

3.3.2.3 Cathole Reach 74
3.3.3 Canyon Reaches 74
3.3.3.1 Anvil Rock 75
3.3.3.2 Acme Quarry Reach 75
Chapter 4: Modeling Methods 77
4.1 Introduction 77
4.2 Channel Geometry Data 77
4.3 Estimation of Particle Sizes on Streambeds 79
4.3.1 Wolman Counts 79
4.3.2 Sieving 80
4.4 Substrate Resistance Characterization 81
4.3.1 Relative Solubility 81
4.3.2 Bulk Mechanical Resistance 81
4.5 Declaration of Incision Processes 82
4.6 Declaration of Geomorphic Setting 83
4.6.1 Buckeye Creek Catchment 83
4.6.2 Greenbrier River 84
4.7 Modeling in HEC-RAS 84
4.7.1 Open Channel Roughness Estimates 84
4.7.1.1 Buckeye Creek 84
4.7.1.2 Greenbrier River 85
4.7.2 Flood Discharges for Hydraulic Models 86
4.7.2.1 Greenbrier River 86
4.7.2.2 Buckeye Creek Cave 87
4.7.2.3 Buckeye Creek Surface Channel 89
4.7.3 Modeling Technique 90
4.7.3.1 Flow Conditions 90
4.7.3.2 Model Construct 91
4.8 Statistical Analyses 92
4.8.1 Buckeye Creek Reaches 92

4.8.2 Greenbrier River Reaches 94
Chapter 5: Erosion by Sculpted Forms 95
5.1 Chapter Abstract 95
5.2 Introduction 96
5.3 Study Reach Characteristics 101
5.4 Methodology 101
5.5 Results of Field Study 104
5.5.1 Origin of Scallops and Pockets 104
5.5.2 Pocket Morphology and Internal Flow Fields 105
5.5.3 Lateral Potholes 109
5.6 Geometrical Model of Reverse-Flow Pocket Growth 111
5.6.1 Model Concepts 111
5.6.2 Model Construct 113
5.7 Model Results 115
5.8 Discussion 117
5.9 Conclusions 121
Chapter 6: Profile Maintenance in a Fluviokarst Basin 123
6.1 Chapter Abstract 123
6.2 Introduction 124
6.3 Controls on Profile Development in Buckeye Creek 127
6.3.1 General Profile 127
6.3.2 Profile in Buckeye Creek Cave 128
6.4 Methods of Incision and Passage Enlargement 131
6.4.1 Incision Processes 131
6.4.1.1 Overview 131
6.4.1.2 Incision in Study Reaches 132
6.4.2 Lateral and Upward Passage Enlargement 138
6.5 Values of Hydraulic Variables Along the Longitudinal Profile 140
6.5.1 Model Output 140
6.5.2 Sensitivity Analyses 142

6.5.2.1 Evaluation Techniques 142
6.5.2.2 Subcritical vs. Critical Flow 142
6.5.2.3 Roughness Estimates 143
6.5.3 Reach Comparisons 143
6.5.4 Model Results Applied to Quarrying 145
6.6 Discussion 145
6.6.1 Measures of Incision Capability Atop Soluble Strata 145
6.6.2 Profile Maintenance and Stability 147
6.6.2.1 Profile Form 147
6.6.2.2 Inferences about Profile Integration 147
6.6.2.3 Incision by Debris Flows 149
6.6.2.4 Profile Stability 150
6.7 Conclusion 152
Chapter 7: Profile Maintenance in a Large Mountain River 153
7.1 Chapter Abstract 153
7.2 Introduction 154
7.3 Methods of Incision 155
7.4 Results 160
7.4.1 Modeling Output 160
7.4.2 Preplanned Comparisons of Reach Results 160
7.4.2.1 Bone Quarry versus Mile-27 160
7.4.2.2 Values Atop Limestone and Sandstone at Cathole 162
7.4.2.3 Cathole (Ls) versus Mile-27 162
7.4.2.4 Bone Quarry versus Cathole (Ss) 163
7.4.2.5 Cathole (Ss) versus Cathole (Ls) 163
7.4.2.6 Anvil Rock versus Acme Quarry 163
7.5 Evaluation of Reach Comparisons and Hypothesis Tests 164
7.5.1 Concepts 164
7.5.2 Effects of Relative Substrate Solubility and Geomorphic Setting 164
7.5.2.1 Relative Substrate Solubility 164

7.5.2.2 Geomorphic Setting 165
7.5.3 Association of Incision Mechanisms with Hydraulic Variables 166
7.6 Discussion 168
7.7 Conclusions 170
Chapter 8: Profile Maintenance in Bedrock Streams Incising Soluble Strata 172
8.1 Overview of Findings 172
8.2 Discussion: Findings in Context 173
8.2.1 Covariance of Incision Processes and Hydraulics 163
8.2.2 Basin-Scale Models of Bedrock Channels 174
8.2.3 Relationship of Incision Processes to Channel Hydraulics 175
8.2.3.1 Corrosion 175
8.2.3.2 Quarrying and Abrasion 176
8.2.3.3 Sculpted Forms and Incision 176
8.3 Conclusion 177
References Cited 179
Appendix A: Schematics of Study Reaches A-1
Appendix B: Visual Basic Macro for Reduction of Cross Section Data B-1

LIST OF TABLES

Table 3.1: Buckeye Creek study reaches 51
Table 3.2: Greenbrier River study reaches 72
Table 4.1: Planned t-tests for Greenbrier River reaches 94
Table 5.1: Sculpted forms 98
Table 5.2: Pocket summary statistics 103
Table 5.3: Comparisons of pocket morphology statistics 108
Table 5.4: Linear regression of pocket dimensions upon one another 108
Table 6.1: Incision processes and model results for Buckeye Creek 127
Table 7.1: Incision processes and model results for Greenbrier River 157
Table 7.2: Results of hypothesis tests for unit stream power 161

LIST OF FIGURES

Figure 2.1: Plot of pH versus discharge: Greenbrier River 20
Figure 2.2: Example of a concave river profile 25
Figure 2.3: Schematic plan and profile of a fluviokarst basin 36
Figure 3.1: Location and topography of Buckeye Creek basin 41
Figure 3.2: Plan view of Buckeye Creek Cave System 42
Figure 3.3: Locations of Greenbrier River catchment and study reaches 44
Figure 3.4: Simplified geology map of the Buckeye Creek basin 45
Figure 3.5: Stratigraphic column of the Greenbrier Group along Spring Creek 46
Figure 3.6: Pictures of Buckeye Creek in headwaters and upstream end of depression 48
Figure 3.7: Profile of Buckeye Creek and longitudinal distribution of particle sizes 49
Figure 3.8: Buckeye Creek and Spencer entrances to Buckeye Creek Cave System 54
Figure 3.9: Cross sections and picture of boulder deposits in Ninson Hollow 55
Figure 3.10: Cross section through Buckeye Creek Cave 57
Figure 3.11: Passages and channels in Buckeye Creek Cave 62
Figure 3.12: Stream passage within resistant limestone 63
Figure 3.13: Basic geology and fracture patterns in Buckeye Creek Cave 65
Figure 4.1: Longitudinal cross section through a scallop 89

Figure 4.2: Floodwaters entering Buckeye Creek Cave 93
Figure 4.3: Profile and longitudinal distribution of model variables in Watergate 80
Figure 5.1: Sculpted forms in narrow canyon passage 97
Figure 5.2: Schematic diagram of pockets and L vs. W for observed pockets 103
Figure 5.3: Logarithmic plots of axes measurements for lateral potholes 107
Figure 5.4: Cross section through a lateral pothole at two growth stages 116
Figure 5.5: Model results for ds=0.001 m 119
Figure 6.1: Longitudinal profile of Buckeye Creek with reaches labeled 126
Figure 6.2: Normalized profiles of Buckeye and Spring creeks 129
Figure 6.3: Distance stream flow across limestone before sinking 130
Figure 6.4: Longitudinal profile of streambed and siltstone in Buckeye Creek Cave 133
Figure 6.5: Intact bedrock undercut by corrosion in Buckeye Creek Cave 133
Figure 6.6: Floor pothole with grinders in Buckeye Creek Cave 136
Figure 6.7: Pothole-like sculpted forms eroded into boulder in reach B 136
Figure 6.8: Ceiling bells in reach G 137
Figure 6.9: Scallops and a pocket 138
Figure 6.10: Longitudinal distributions of reach variables in Buckeye Creek 141
Figure 6.11: SNK groupings of shear stress as a function of Manning's n values 144
Figure 6.12: SNK groupings of shear stress, unit stream power, and mean velocity 144
Figure 7.1: Irregular, corroded limestone clasts atop a riffle in the Cathole reach 156
Figure 7.2: Quarried block of limestone detached by corrosion in Greenbrier River 156
Figure 7.3: Colluvial apron on banks of Greenbrier River and potholed boulder 158
Figure 7.4: Potholed and abraded sandstone boulders in Anvil Rock reach 159
Figure 7.5: Potholed and scalloped bedrock outcrops in Greenbrier River 167

LIST OF PLATES

Plate 2.1: Selby rock hardness worksheet 23

LIST OF VARIABLES

Variable	Units	Name
ω	$W\ m^{-2}$	mean unit stream power
τ	$N\ m^{-2}$	mean bed shear stress
u and $\bar{u}$	$m\ s^{-1}$	mean velocity
Ω	$W\ m^{-1}$	mean total stream power
ρ	$kg\ m^{-3}$	fluid density
g	$m\ s^{-2}$	gravitational acceleration
Q	$m^3\ s^{-1}$	fluid discharge
S_e	unitless ($m\ m^{-1}$)	energy gradient or slope
V_x	m^3	volume; different subscripts are used for each volume defined
L_r	m	reach length
S_o	unitless ($m\ m^{-1}$)	bed gradient or slope
H_L	m	head loss
w	m	channel or cross section width
h	m	maximum flow depth
U_c	$m\ s^{-1}$	critical entrainment velocity
ρ_s	$kg\ m^{-3}$	density of a solid
D_x	m	diameter or width; different subscripts are used for each diameter defined
C_d	unitless	drag coefficient
C_l	unitless	lift coefficient
μ_f	unitless	friction factor between sliding objects

IAP	unitless	ion activity product
K	unitless	reaction constant
SI	unitless	saturation index
A	km^2	drainage basin area
dz	m	distance of incision
dt	a^{-1}	time period in years
k	unitless	substrate or rock resistance
d_x	phi	x^{th} percentile of particle sizes in a sample
n	unitless	channel roughness or Manning's n
D	m	passage diameter or width
L	mm, cm, m	sculpted form length (along wall)
W	mm	sculpted form width (into wall)
H	mm	sculpted form height (along wall)
υ	$m^2\ s^{-1}$	kinematic viscosity
L_{32}	m	Sauter mean length (L^3/ L^2)
Re^*	unitless	Reynolds number
B_L	unitless	roughness geometry constant
R	m	hydraulic radius
p_x	$N\ m^{-2}$	pressure; different subscripts are used for each diameter defined
C	s^{-1}	vorticity
r	m	radius

ΔV	m^3	volume change in a sculpted form between two points in time
L_t	m	diameter of a circle eroded by a circular sculpted form
y_x	m	distance of wall from some arbitrary point at time x
ds	m	increment of wall retreat or erosion
λ	unitless	ratio of erosion volumes accomplished by a sculpted form (numerator) and through wall translation

Chapter 1

Introduction

1.1 Project Introduction

Bedrock rivers primarily maintain their profiles and incise by quarrying, abrasion, and corrosion. Quarrying and abrasion are mechanical phenomena dependent upon the conversion of potential energy to kinetic and pressure energies, which are associated with the hydraulic forces and local fluid accelerations that detach blocks and accelerate abrasive tools that erode channel perimeters (Baker and Pickup, 1987; Wohl, 1993; Hancock et al., 1998; Whipple et al., 2000a). Models of landscape evolution generally assume that incision capability is positively correlated with unit stream power (ω) and shear stress (τ) and field-based studies have found higher values of ω and τ where strata are more resistant to incision (Baker, 1988; Wohl, 1993; Howard, 1994). This relationship may arise because macroturbulence and large mean channel velocities simultaneously enhance quarrying and increase the local rate of energy expenditure (Baker, 1988), which is one of the variables used to estimate ω and τ. Abrasion may be positively correlated with mean channel velocity ($\bar{u}$) because higher kinetic energies of suspended particles translate to larger impact forces (Hancock et al., 1998). As incision phenomena arising from hydraulic forces in floodwaters, quarrying and abrasion are

ultimately driven by expenditure of potential energy. In contrast, corrosion is less dependent upon expenditure of potential energy because available chemical energy drives the erosion process.

Fundamental differences exist between incision processes driven by chemical and potential energy. These differences can be exploited to establish linkages between channel geometry, hydraulics, and incision processes in bedrock rivers. Presumably, if quarrying, abrasion, and corrosion are all active in adjacent reaches that are not separated by a knickpoint then there must be adjustments to channel processes and morphology. Hypothetically, mechanical energy expenditure should decrease where chemical energy is the primary impetus for incision or the combined effects of mechanical and chemical erosion will destabilize the river profile through excess erosion. Moreover, a profile lacking knickpoints implies that mechanical and chemical processes are coupled between adjacent reaches such that incision rates are spatially congruous, if not uniform. How such disparate reaches are coupled is of particular interest because modeling of river profiles is hampered by limited knowledge of profile integration across multiple substrates.

1.2 Hypotheses and Principle Assumptions

This study uses intra-stream comparisons of modeled hydraulic variables to discern the influence of relative bed solubility on channel processes and morphology in bedrock streams incising soluble and insoluble strata. *The hypothesis is tested that unit stream power and shear stress are least atop soluble bedrock and highest atop insoluble bedrock for reaches of similar geomorphic setting versus the null hypothesis that values*

are similar regardless of bed solubility (Hypothesis I). Hypothesis I is tested by comparing ω and τ between reaches developed atop soluble and insoluble bedrock. The variable $\bar{u}$ is omitted from the statistical test because both ω and τ scale with $\bar{u}$ (Bagnold, 1966). The research hypothesis presumes that quarrying and abrasion of insoluble strata are associated with higher values of ω and τ than corrosion. Therefore, the numerical output used to evaluate Hypothesis I can be used to test a corollary research hypothesis, that ω and τ are least in Buckeye Creek and Greenbrier River where evidence of corrosion is most numerous and highest where evidence of mechanical incision is most numerous. The null hypothesis of no effect is explicitly evaluated in Chapter 6 (Corollary Hypothesis I), but is not stated as an entirely separate hypothesis from Hypothesis I because the rationales are inseparable.

The hypothesis that erosion processes are related to hydraulics can also be evaluated for a particular class of erosion features known as sculpted forms, which are relatively smooth concavities excavated on channel margins. Sculpted forms are complexly related to channel hydraulics because they are excavated by coherent vortices in flow separations, which derive their motion from momentum exchange with the freestream flow (Blumberg and Curl, 1974). The semi-quantitative research hypothesis that incision by sculpted forms is purely a function of hydraulics is evaluated using output from a geometrical model developed for this study. *The associated null hypothesis is that the geometry of sculpted forms is not related to erosion atop adjacent surfaces (Hypothesis II).*

Hypothesis I is only valid for constant geomorphic setting. The role of geomorphic setting on hydraulic variables is evaluated using the hypothesis that stream

reaches abutting valley walls or receiving coarse, insoluble sediment from hillsides will display higher values of unit stream power and shear stress than reaches lacking such confounding influences. *The associated null hypothesis is no effect among different geomorphic settings (Hypothesis III).*

Comparisons are made between reaches in three separate stream segments in two streams. The hypotheses assume that incision rates are similar in the study segments and that magnitudes of hydraulic variables are related to substrate resistance and geomorphic setting. The latter assumption is invalid if the effects of base level fall or knickpoint migration dominate channel processes in either stream. Three previously reported incision rates are used for both streams to establish that incision rates are similar among the three stream segments. It is assumed that the available incision rates are applicable for all reaches in each stream segment because of close reach proximities and a lack of recognizable knickpoints between reaches. Close proximity of adjacent reaches in individual stream segments is further used to minimize the potentially confounding effects of asynchronous response to base level fall or knickpoint propagation upon statistical comparisons. The stream segments are located in different longitudinal positions in the same large basin; therefore no statistical comparisons are made between reaches in separate stream segments because of the possibility of asynchronous response to base level fall or knickpoint propagation.

The hypotheses and assumptions are employed in two slowly incising streams with different basin sizes, network structures, and geomorphic settings. Both streams, Buckeye Creek and Greenbrier River, flow atop soluble and insoluble strata. Buckeye Creek drains a low-order, fluviokarst basin beneath an escarpment comprised of insoluble

clastics. Sequentially, the stream carries insoluble detritus from atop the escarpment, across a karst depression floor, and through a 1.6 km long subterranean channel. The Greenbrier River is a large, base level stream draining a mountainous Appalachian catchment. One stream segment is examined in Buckeye Creek and two in Greenbrier River.

1.3 Research Impetus and Rationale

Understanding relationships between energy expenditure, hydraulics, incision processes, sediment transport, channel geometry, and longitudinal profile development in alluvial and bedrock streams is one of the ultimate goals of modern fluvial geomorphology. Bedrock streams are the least understood of the two types of streams. Bedrock streams play important roles in many landscapes by setting the boundary conditions for landscape development (Howard, 1998; Sklar and Dietrich, 1998). Channel elevations determine local base level elevations, and incision rates strongly influence hillslope gradients (Burbank et al., 1996). Successful modeling of landscape evolution in catchments dominated by bedrock streams is therefore dependent upon modeling channel processes, particularly in mountainous regions (Smart, 1988; Howard et al., 1994).

Longitudinal profiles are the focus of most bedrock stream models because the profiles incorporate basin-scale variables that can be obtained from existing databases and hold implications for landscape development throughout the length of a catchment (e.g., Howard, 1980; Howard, 1998; Snyder et al., 2000). Individual longitudinal profiles can be replicated using theoretical models and descriptive equations if they are relatively

uniform. Concave profiles can often be described using power equations because channel gradients decrease markedly downstream (Howard, 1980; Knighton, 2000). Concave profiles are of special interest to geomorphologists because they imply order, wherein slope changes systematically in response to lengthwise, cumulative changes in driving variables such as discharge and sediment loading (Merritts and Vincent, 1989; Snyder et al., 2000). Successful modeling of longitudinal profile development has proven difficult because even the most uniform profiles are often disrupted by local irregularities that cannot be treated by power laws. As such, various authors have suggested a need for detailed information concerning how profiles develop and are maintained (Hancock et al., 1998; Whipple et al., 2000a). Such studies must encompass reach-scale processes as they relate to basin-scale variables and discern how profile excavation varies longitudinally and by substrate.

The concave longitudinal profiles of stable bedrock streams are excavated and maintained by varying combinations of quarrying, abrasion, and corrosion. Quarrying is the physical detachment of blocks from bedrock surfaces. Abrasion yields minute, solitary grains. The roles of the three erosion processes vary spatially and temporally as a stream incises through strata of varying resistance. Quarrying and abrasion are mechanical processes in which effectiveness as an agent of mass removal is hypothetically dependent upon hydraulic variables such as water velocity (u), bed shear stress (τ), and stream power (Ω)(outgrowth of research Hypothesis I). The latter variables are co-dependent upon a variety of reach and basin scale variables. As an example, stream power can be calculated as:

$$\Omega = \rho g Q S_e , \qquad (1.1)$$

where ρ is fluid density, g is gravitational acceleration, Q is discharge, and S_e is the local energy slope or rate of energy loss per unit length of channel. First-generation models of profile development assume that mechanical incision capability is proportional to stream power and this assumption is quantitatively evaluated in this study.

Longitudinal stream profiles are useful for geomorphic analyses because they quantitatively describe the input of gravitational energy (E_g) into channel systems. Local rate of energy input is calculated herein as:

$$E_g = \rho g V_f L_r S_o \,, \qquad (1.2)$$

where V_f is the volume of fluid being accelerated through a reach of length L_r and S_o is the local bed slope. Incision is accomplished using energy expended at the bed. Additional losses are created by turbulence and sediment transport processes. Energy loss is typically evaluated as the energy gradient (S_e), which is the ratio of H_L to L_r, where H_L is energy loss in units of length. However, the absolute magnitude of energy loss is not an appropriate measure of erosive ability because S_e can be high as a result of losses that do not produce bedrock erosion (e.g., Wohl, 2000). Therefore, the time rate of energy loss is generally used to evaluate the ability of a stream to erode via hydraulic-based mechanisms. Energy loss per unit of time is power and stream power per unit length of channel can be calculated using equation (1.1) with units in Watts m^{-1} (W m^{-1}). Total stream power can be divided by channel width (w) to yield unit or specific stream power (ω) with units of W m^{-2},

$$\omega = \frac{\Omega}{w} \,. \qquad (1.3)$$

Unit stream power may be a particularly useful tool for evaluating the ability to quarry and abrade because instantaneous forces will be greater where more power is expended per unit of channel width (e.g., Baker and Pickup, 1987).

The ability of a stream to erode a particular stratum will change longitudinally as a result of the dependence upon such basin-scale variables as discharge, although channel geometry may be adjusted at the reach-scale to optimize mechanical erosion capabilities for a given rock type (Wohl et al., 1994; Wohl and Ikeda, 1998). As a hypothetical example, if an identical resistant stratum outcrops at two widely separated locations in a stream, then normalized channel width might be less and depth greater at the upstream location because decreased width and increased depth relative to adjacent reaches has the effect of increasing shear stress and stream power for the smaller discharge. One of the reasons stream power is maximized in narrow, deep channels is because of elevated S_e values created by enhanced turbulence and expansion/contraction losses around constrictions (Baker and Pickup, 1987). Shear stress (τ) is, in part, maximized because of its dependence upon channel depth (h):

$$\tau = \rho g h S_e \quad . \qquad (1.4)$$

Precisely how local stream properties reflect adjustments for particular combinations of substrate resistance and hydrology is unknown, although an analysis of channel morphology found statistically significant correlations between descriptive channel classifications and basin- and reach-scale variables (Wohl and Merritt, 2001). Presumably, feedback loops operate over geologic time to adjust local channel geometries such that local hydraulics create the forces necessary to transport sediment supplied to the channel and incise bedrock (Gilbert, 1877; Mackin, 1948; Miller, 1991a,b;

Snyder et al., 2000). Longitudinal changes in substrate resistance will therefore produce systematic changes in the longitudinal distribution of energy losses and hydraulic forces in graded rivers that are recognized, in part, on the basis of unbroken, concave longitudinal profiles. These changes are believed to occur in concert with variations in erosion processes (Hancock et al., 1998).

Coupled changes in reach-scale energy losses, hydraulic forces, and incision processes must occur because energy losses scale positively with force magnitudes, and individual incision processes do not occur until hydraulic variables achieve some minimum magnitude (Baker, 1988). For instance, the forces required to quarry blocks from massive strata are presumably too great to be generated by stream discharges below some critical threshold (Baker, 1988). As a result, abrasion is common atop massive, resistant strata (e.g., Hancock, et al., 1998; Whipple et al., 2000a). The ability to abrade scales with the kinetic energy of particle impacts, which are proportional to the squares of particle velocities (Hancock et al., 1998). The energy required to sustain high velocities is presumably derived from increases in local bed slope and is aided by decreases in channel area (e.g., Wohl and Ikeda, 1998; Wohl and Merritt, 2001). Sculpted forms, concavities containing coherent vortices, are often the loci of abrasion and enhance energy loss because they direct particle attacks at specific locations on channel margins and generate turbulent mixing on their streamwise faces (Blumberg and Curl, 1974; Hancock, et al., 1998). Resistant strata in stream channels are often associated with abrasion, sculpted forms, steep bed gradients, elevated water velocities, and enhanced energy loss (Hancock et al., 1998; Wohl, 1993). How differences in substrate resistance

are expressed in reaches dominated by quarrying is less clear and the process is probably quite variable among different substrates.

Elucidation of how reach-scale energy losses, hydraulic forces, and incision processes vary in streams such that uniform, concave longitudinal profiles are maintained is complicated by a lack of studies concerning reach-scale incision processes, interactions with confounding variables, and profile development in streams flowing atop multiple strata. Bedrock erosion typically occurs during high magnitude, low recurrence floods that present considerable practical and safety obstacles to detailed studies of incision processes (Tinkler and Wohl, 1998). The diversity of geologic, hydrologic, climatic, and historical variables found in streams is broad. As a result, comparisons of any two streams or stream segments cannot be interpreted unequivocally, although multivariate comparisons of stream properties can assist identification of controlling variables (Wohl and Merritt, 2001). Carefully designed natural experiments that compare selected variables through multiple reach comparisons could simultaneously shed light on profile maintenance in bedrock streams flowing atop multiple substrates. This approach is used herein. The methodology does not allow causality to be definitively recognized, but the affect of controlling variables can be used to draw tentative inferences about cause and effect.

Perennial, corrosive streams flowing over and through soluble strata offer unique opportunities to identify reach-scale adjustments of channel processes and geometry. Quarrying and abrasion are mechanical phenomena ultimately driven by gravitational energy, but corrosion is driven by available chemical energy. Studies have failed to show that chemical aggressiveness is adjustable by changes in channel hydraulics, although

access to bedrock may be adjusted by deposition (White, 1988). Therefore, a bedrock stream that is incising primarily through corrosion should display hydraulic adjustments that minimize values of hydraulic variables associated with mechanical incision.

Hypothetically, feedback loops would suppress high magnitudes of incision-related hydraulic variables in bedrock rivers corroding through soluble strata. Channel gradients would decline rapidly as mechanical and chemical incision operated in tandem after a soluble unit was breached by incision. Lower channel gradients would deprive physical processes of the energy necessary to drive incision. Eventually channel geometry and processes would balance the separate roles of physical and chemical processes.

The considerable differences that separate mechanical and chemical phenomena may translate to adjustments of channel geometries that are more discernable than in systems adjusting hydraulic variables for mechanical incision alone. There is no reason to suppose that the purported hydraulic adjustments should be any different from those that occur atop strata that are non-resistant to mechanical erosion. If so, discernment of hydraulic adjustments in streams incising soluble strata could be useful for interpreting channel hydraulics and geometry in other bedrock streams.

Hydraulic adjustments may be most evident in slowly incising streams in tectonically quiescent settings because rapid uplift probably increases mass flux in transit through a system and the amount of bedrock that must be eroded to maintain a stable profile (e.g., Wohl, 1993; Whipple et al., 2000a). The increased energy input required to remove and transport the extra mass would presumably exceed available chemical energy at some finite threshold. Adjustments to channel architectures and processes may be

dramatic well below this threshold. If so, the adjustments could be recognized through quantitative comparison of incision processes in reaches atop soluble and insoluble reaches and as a function of geomorphic setting (Hypotheses I and III).

1.4 Project Objectives

This study exploits differences in the nature of physical and chemical incision to quantitatively identify longitudinal adjustments to channel substrates in bedrock streams. Identifying hydraulic adjustments will shed direct light on how reach-scale energy losses, hydraulic forces, and incision processes are coupled in bedrock rivers. However, such adjustments are almost certainly a function of drainage basin scale. Therefore, it is an objective of this study to discern how streams adjust to substrate resistance at radically different scales of drainage basin area and length.

Knowledge concerning longitudinal adjustments of stream processes as functions of substrate resistance and other geomorphic variables will directly aid interpretation and development of profile models. Currently, modelers are hindered by a lack of knowledge concerning linkages between basin-, reach-scale, and confounding variables (Sklar and Dietrich, 1998; Snyder et al., 2000). The latter include the influence of hillslope processes on river incision and wall interactions in caves. Furthermore, knickpoints cannot be modeled because these bed-gradient irregularities are often associated with such poorly understood phenomena as sculpted forms and abrasion. In light of these problems, it is an objective of this study to quantitatively evaluate the influence of selected geomorphic variables on incision, and to numerically describe particular erosion phenomena that are common in knickpoints.

Discerning the nature and roles of channelized processes in eight study reaches in a fluviokarst terrain is a secondary objective of this study. As partially reviewed by Ford and Williams (1989), White (1988), and Gillieson (1996), existing studies of karst hydrology have largely focused on groundwater flow under Darcian conditions, origins of flow routes, and aqueous geochemistry. Macroscopic channels have received considerably less attention despite their acknowledged importance in water and sediment transport (Coward, 1975; Atkinson, 1977; Gale, 1984). Knowledge of channel processes will directly aid landscape evolution studies that utilize clastic cave sediments and should eventually lead to an understanding of how bedrock erosion in fluvial and karst terrains are related to one another.

Chapter 2

A Contextual Review of

Profile Maintenance In Bedrock Streams

2.1 Methods of Profile Maintenance and Bedrock Incision

2.1.1 Bedrock Incision and Channel Processes

Energy expenditure is believed to correlate with erosional resistance of bedrock in bedrock streams because harder, more massive rocks presumably require larger forces to erode (Hancock et al., 1998; Whipple et al., 2000a,b; Wohl and Merritt, 2001). Shear, lift, and drag forces are the principal forces that detach blocks of bedrock (Hancock et al., 1998). Drag forces are created by pressure differences across blocks, and passing vortices. Turbulence is generated by flow acceleration and deceleration associated with obstacles to flow (e.g., blocks). Turbulence is one of the principal mechanisms of energy dissipation in streams and an important erosive agent (Matthes, 1947). Hence, larger drag forces must be associated with larger energy losses. Shear and lift forces are not uniquely associated with turbulence because shear forces arise from velocity gradients near objects whereas lift forces arise from pressure gradients spanning blocks and the adjacent, moving fluid. Forces may be particularly strong where critical flow prevails and waves

dramatically steepen water surfaces (Tinkler, 1997). Nonetheless, shear and lift are enhanced by vortices generated in floodwaters because vortices can produce intense, local changes in both pressure and velocity gradients. Large pressure fluctuations associated with macroturbulence and critical flow enhance forces on channel beds and may be responses to resistant strata (Matthes, 1947; Tinkler, 1997).

2.1.2 Hydraulic-based Mechanisms of Bedrock Incision

Shear, lift, and drag forces can detach or mobilize blocks from channel surfaces. Quarrying is the removal of blocks en mass from bedrock surfaces by shear, lift, and drag forces. Antecedent processes such as weathering, sculpting, and wedging usually aid these erosion phenomena. Wedging is accomplished by roots on channel margins and hydraulic insertion of small clasts into discontinuities during floods (Hancock et al., 1998). Weathering loosens binding forces acting across discontinuities that bind individual blocks by removing cements and chemically converting minerals to secondary weathering products including clays. In general, intact bedrock will not be detached by any but the highest magnitude, lowest return interval floods until weathering has prepared blocks for detachment (Hancock et al., 1998; Wohl, 2000).

Sculpting is the preferential erosion of block surfaces or margins by persistent vortices. The most well known of all such processes is potholing, wherein a vortex forms atop a bedrock depression, entrains small stones, and repeatedly impacts or slides grinder stones within the depression (Alexander, 1932). Abrasion created by impacts and sliding deepens the depression, which has the effect of maintaining the formative vortex. Potholing is believed to be an important means of channel incision in and of itself, but potholing also aids quarrying by detaching blocks and weakening inter-block attachment

forces. Other forms of sculpture include lateral potholes, flutes, scallops, and undulating walls. These latter concavities lack grinders and are carved by abrasion and/or corrosion (Allen 1971; Blumberg and Curl 1974; Zen and Prestegaard, 1994; Hancock et al., 1998; Wohl et al., 1999).

Massive strata outcropping in streams are often associated with evidence of abrasion and potholing because quarrying is suppressed by large block sizes (Hancock et al., 1998; Whipple et al., 2000a,b). Shear stress and unit stream power values in reach-scale segments containing potholes and abundant sculptures are typically higher than in adjacent reaches that lack such phenomena (e.g., Wohl, 1993). This study evaluates the corollary hypothesis developed in conjunction with Hypothesis I, that values of τ and ω reflect the ability of a stream to quarry, abrade, and corrode. The hypothesis is evaluated by interpreting the outcomes of distributions of τ and ω using statistical tests and qualitative interpretations.

Relative abilities to quarry may also be roughly approximated by comparing mean cross-section velocities to critical entrainment velocities for unprotected boulders on the channel bed. Carling et al. (2002) present an equation for the critical velocity (U_c) necessary to entrain an unprotected boulder on a channel bed. The velocity necessary to quarry must necessarily be higher because of attachment and normal forces between the intact block and surrounding bedrock. Values of U_c are estimated herein for intact, protected blocks on the channel bed. If cross-section velocities are insufficient to move unprotected blocks of equal size then it will be assumed that the stream is simultaneously incapable of quarrying. The formula is,

$$U_c = \sqrt{\frac{2(\rho_s - \rho)gD_b}{\rho} \frac{\mu_f}{C_d + [C_l \mu_f (D_b + D_c]}} \quad , \qquad (2.6)$$

where ρ_s is the block density (2500 kg m^{-3} for limestone), g is gravitational acceleration, D_b and D_c are the b and c axis lengths for the boulder, C_d is the boulder drag coefficient (calculated as 1.995 from equations in Carling et al., 2002), C_l is the lift coefficient for the obstacle (C_l=0.09 for near-critical flow), and μ_f is the friction factor between the block and underlying surface. The average value of μ_f reported by Carling et al. (2002) was 0.7, which is used herein.

2.1.3 Corrosion and Bedrock Incision

Experimental results reveal that corrosion rates of exposed calcite in channels or conduits are independent of water velocity and presumably all other hydraulic forces (White, 1988). Sediment accumulation is reported to shield carbonate streambeds from corrosion and to cause cave passages to preferentially widen (White, 1988; Ford and Williams, 1989). Why fluids passing through sediments on the bed (hyporheic flow) are apparently ineffective at eroding buried cave streambeds deserves additional study, although the presence of carbonate grains in bed sediments may cause the slowly recharged pore waters to become saturated. By inference, incision of channel beds in surface streams is probably influenced by sediment shielding because of the velocity dependence of hyporheic corrosion. Periodic mobilization and rearrangement of sediment accumulations may be required for incision. Hypothetically, the physical energy needed to expose the bed and transport sediment would provide a lower limit to values of mean velocity, shear stress, and unit stream power in sediment-charged reaches being incised

by corrosion alone. Sediment flux, caliber, and composition would determine the values of mean velocity, shear stress, and unit stream power needed during floods for periodic access to the bed.

The process of corrosion is well understood despite uncertainties about the circumstances under which it occurs. Corrosion by streams is driven by chemical energy derived from ions in aqueous solution. Carbonic acid supplies the majority of ions in natural waters and is derived from atmospheric and biologically produced carbon dioxide dissolved in water and supplied from the atmospheric reservoir and soils. The associated reaction is generally represented as,

$$H_2O + CO_2(aq) \Leftrightarrow H_2CO_3 \ , \qquad (2.7)$$

where aq indicates that the gas is dissolved in aqueous solution. Carbonic acid disassociation can be represented in the following manner,

$$H_2CO_3 \Leftrightarrow H^+ + HCO_3^- \ , \qquad (2.8)$$

where the production of disassociation products is controlled by aqueous geochemistry and the reaction constant. Calcite corrosion can be represented as,

$$CaCO_3(solid) + H^+ + HCO_3^- \Leftrightarrow Ca^{+2} + 2HCO_3^- \ . \qquad (2.9)$$

Corrosion is driven by the H^+ ion, but the available chemical energy and reaction direction are not strictly a function of pH. Reaction direction and aggressiveness with respect to calcite are determined by relative values of the ion activity product (IAP) and reaction constant (K). Values of IAP are calculated using the mineral specie being dissolved. Corrosion of calcite can be represented as,

$$CaCO_3 \Leftrightarrow Ca^{+2} + CO_3^{-2} \ , \qquad (2.10)$$

and the associated reaction constant at STP is 4.90×10^{-9}. Values of IAP for this reaction can be calculated as,

$$IAP = \frac{[Ca^{+2}][CO_3^{-2}]}{[CaCO_3]}, \qquad (2.11)$$

where effective concentration values are substituted for the species in brackets. If IAP<K, then the reaction described by equation (2.10) proceeds from left to right, the solution is said to be undersaturated, and corrosion predominates. For IAP>K, the reaction proceeds from right to left, the solution is oversaturated, and precipitation is probable. For convenience, the state of solid/liquid interactions is often reported as saturation indices (SI) where,

$$SI = \log\left(\frac{IAP}{K}\right). \qquad (2.12)$$

A mineral exposed to an aqueous solution is in equilibrium with respect to the solution when SI=0. Undersaturation prevails for SI<0 and saturation prevails for SI>0 (White, 1988; Ford and Williams, 1989).

Geochemical data are virtually non-existent for the Buckeye Creek basin, but the United States Geological Survey (USGS) has occasionally measured pH of the Greenbrier River upstream of the study reaches at USGS gage 03182500. As seen in plots of these data, pH tends to decline as discharge increases (Figure 2.1). Floodwaters travel more quickly and have less interaction with channel margins because the cross sectional area of flow increases much more quickly than perimeter length. As a result, floodwaters are more corrosive than baseflows and can accomplish greater erosion; baseflows may

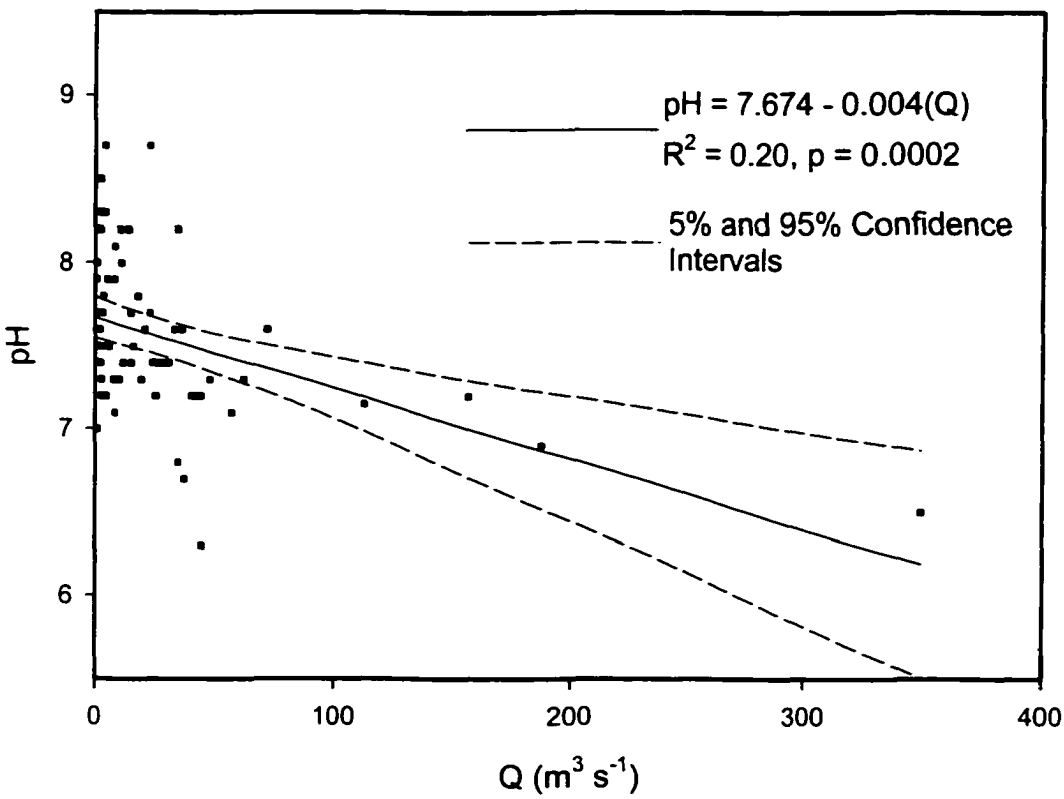

Figure 2.1: Plot of pH as a function of discharge (Q) at USGS gage 03182500. Data obtained from the USGS NWIS Web server (http://water.usgs.gov/nwis/).

not be the most effective agents of channel incision in streams flowing atop carbonates (White, 1988; Ford and Williams, 1989).

2.2 Substrate Resistance

Numerous field studies have found statistical correlations between unit stream power and quantitative measures of substrate resistance in channels (Wohl et al., 1994; Wohl and Ikeda, 1998; Whipple et al., 2000b; Wohl and Merritt, 2001). Factors influencing the resistance of rock beds to quarrying and abrasion include joint and fracture spacing, degree and type of cementation, Mohs hardness values of rock grains,

compressive strength, and tensile strength (Hancock et al., 1998; Wohl et al., 1999; Sklar and Dietrich, 2001). Massive strata are difficult to erode because block sizes may be so large as to be effectively immovable (Hancock et al., 1998). Well-cemented or crystalline rocks comprised of hard resistant minerals offer substantial resistance to abrasion. Therefore, massive strata comprised of hard, insoluble, crystalline mineral grains are the most resistant to stream erosion (Hancock et al., 1998; Whipple et al., 2000a). Chemical reactivity is an important component of overall rock resistance and indirectly affects rock resistance to physical erosion because the most soluble mineral grains, calcite and dolomite, are relatively soft (Mohs hardness of 3 and 3.5, respectively). Soluble grains decrease the overall resistance to erosion in chemically aggressive waters and their dissolution directly influences a variety of processes. For instance, corrosion-widening of joints and fractures may aid block detachment and thereby enhance quarrying.

The most commonly used techniques for quantifying rock resistance in channels rely upon the physical characteristics of channel bedrock and do not explicitly incorporate chemical reactivity in their estimations. The most widely used resistance scale is Selby rock-mass strength (Selby, 1980). The Selby method was originally devised for analyzing hillslopes, but is widely employed in stream channels with few or no modifications (e.g., Wohl and Merritt, 2001). As used in channels, rock strength is estimated on the basis of compressive or intact rock strength, degree of weathering, joint spacing, orientation of joints relative to flow direction, joint widths, joint continuity, and groundwater outflow (Plate 2.1).

Intact rock strength is determined using the mean of ten or more readings from a Schmidt rock hammer. The hammer measures rebound of a spring-loaded steel rod after

the rod impacts a surface. Gage values can be converted to compressive strength values if a calibration curve is known, but geomorphologists traditionally use uncorrected gage values. The average value for a given rock is used to assign one of five point values (see Plate 2.1). Weathering, joint orientation, and joint continuity are qualitatively assigned to point categories. Joint spacing, joint widths, and groundwater outflow categories are assigned on the basis of numerical values that are usually estimated. Statistical comparisons of Selby rock-mass strength, total stream power, and unit stream power generally yield significant correlations between the resistance index and hydraulic variables (Wohl and Merritt, 2001). These results are tacitly interpreted to reflect localization of energy expenditure atop resistant strata such that long-term incision is comparable atop all strata (e.g., Wohl and Merritt, 2001).

Tensile strength has been proposed as another discriminant of rock resistance because tensional forces cause bedrock fragments to be dislodged upon impact of sediment grains (Johnson, 1972; Sklar and Dietrich, 2001). Tensile strengths of a wide variety of rocks including sandstone, mudstone, granites, basalts, and tuffs correlate strongly with abrasive wear in rock abrasion mills (Sklar and Dietrich, 2001). However, abrasion is only one means of river incision. It is unclear whether tensile strength is related to resistance to quarrying because blocks separate along discontinuities with attachment strengths determined by cementation and degree of weathering between blocks and not grains. Carbonates have relatively high tensile strengths in comparison to other sedimentary rocks and therefore plot among rocks with relatively low erosion rates in the mill experiments of Sklar and Dietrich (2001). These results may be representative of natural limestone erosion in streams where incision is driven by rare, large floods and

Field Site: Date:
Lithology:
Sample No.:

Hammer Readings

SELBY ROCK-MASS STRENGTH

Intact Rock Strength	Weathering	Joint Spacing	Joint Orientation	Width of Joints	Continuity of Joints	Outflow of Groundwater	TOTAL RATING
100-60 (20 pts)	Unweathered (10 pts)	>3 m (30 pts)	Steep dips into slope, cross joints interlock (20 pts)	<0.1 mm (7 pts)	None continuous (7 pts)	none (6 pts)	100-91
60-50 (18 pts)	Slightly Weath. (9 pts)	3-1 m (28 pts)	Mod. dips into slope (18 pts)	0.1-1 mm (6 pts)	Few continuous (6 pts)	trace (5 pts)	90-71
50-40 (14 pts)	Mod. Weath. (7 pts)	1-0.3 m (21 pts)	Horiz. or nearly vert. dips (hard rx only) (14 pts)	1-5 mm (5 pts)	Continuous, no infill (5 pts)	slight (4 pts) (25 l/min/10 m²)	70-51
40-35 (10 pts)	Highly Weath. (5 pts)	30-5 cm (15 pts)	Mod. dips out of slope (9 pts)	5-20 mm (4 pts)	Continuous, thin infill (4 pts)	moderate (3 pts) (25-125 l/min/10 m²)	50-26
35-10 (5 pts)	Complet. Weath. (3 pts)	<5 cm (8 pts)	Steep dips out of slope (5 pts)	>20 mm (2 pts)	Continuous, thick infill (1 pts)	great (1 pts) (>125 l/min/10 m²)	<26

Weathering

Unweathered: Parent rock showing no discoloration, loss of strength, etc...
Slightly Weath.: Slightly discolored, especially adjacent to discontinuities; intact rock not noticeably weaker than fresh rock.
Mod. Weath.: Rock is discolored throughout more of its mass, but less than half the rock mass is decomposed and disintegrated; alteration has penetrated discontinuities which may be zones of weakly cemented alteration products or soil.
Highly Weath.: Rock is discolored through; discontinuities may be open and have discolored surfaces; up to one half of rock mass is decomposed and disintegrated so that it can be excavated with rock hammer.
Complet. Weath.: Rock is discolored and changed to soil, but some original rock fabric and texture is preserved.

Plate 2.1: Field worksheet used to calculate Selby rock-mass strength. Intact rock strength is measured using a Schmidt rock hammer (see text for discussion).

not corrosion by baseflow or moderate floods (e.g., streams in arid regions). Conversely, incision of soluble strata in perennial streams may be accomplished independent of abrasion rates and physical resistance. Therefore, tensile strength may have limited applications for studies of quarrying and corrosion.

This study utilizes the Selby method as one means of substrate resistance characterization. The effectiveness of corrosion-based incision is crudely estimated by comparing incision processes atop quartz sandstones, shale, and high calcite limestones. A long-term record of aqueous geochemistry would be more useful for estimating the ability of corrosion to affect incision, but such a record would need to extend for a geologically meaningful time and there is no way of obtaining such a record at present.

2.3 Erosional Profile Forms

2.3.1 Profile Form

Longitudinal stream profiles are two-dimensional representations of channel thalwegs or valley floors. Elevation is plotted as a function of distance from either river source or mouth (Figure 2.2). Profiles of bedrock rivers often display local increases in gradient and abrupt offsets known as knickpoints (Figure 2.2). Profiles displaying systematic declines of channel elevation are generally considered to be in equilibrium and at grade; the distribution of energy expenditure in the stream is adjusted to reflect the energy needed to maintain synchronous incision in all reaches and the river is adjusted to local base level (Merritts and Vincent, 1989). Theoretically, smooth profiles are most easily attained atop a single substrate because bed resistance remains fixed and channel

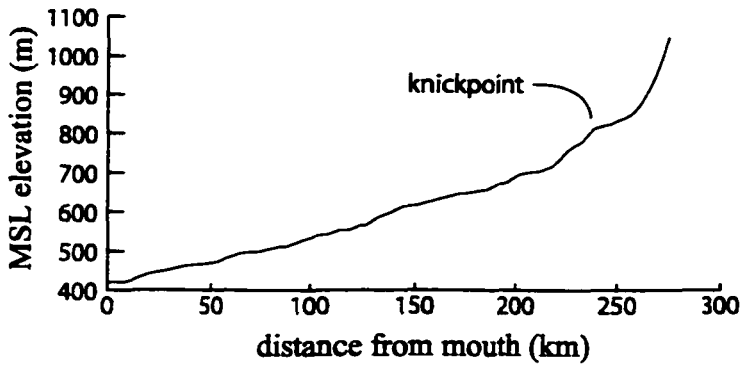

Figure 2.2: Example longitudinal profile of a bedrock stream. The overall profile is relatively smooth, but note the many upward and downward convexities. Such convexities may be associated with variations in bed lithology, hillslope processes, influxes of sediment or water from tributaries, glacial history, and knickpoint propagation.

processes need only be adjusted for downstream increases in discharge (e.g., Merritts and Vincent, 1989; Snyder et al., 2000).

Early models of channel incision and profile development assumed that local incision rates are proportional to stream power or shear stress. These variables are assumed to reflect a balance between local driving and resisting forces; incision occurs when instantaneous forces overwhelm substrate resistance. Erosive forces scale with discharge and the local energy gradient. Discharge generally increases as a positive power function of basin area (A)(Howard, 1994). Local energy expenditure in a graded stream should balance the input of gravitational energy supplied by elevation loss in the associated reach. Therefore, S_e can be approximated as the local bed slope (S_o), which varies as a power or log function in smooth, concave profiles. Assuming S_o varies as a

power function, the exponent can be obtained from regression of longitudinal profile data. Applying this reasoning, incision can be modeled using the equation:

$$-\frac{dz}{dt} = kA^m S^n \quad , \qquad (2.13)$$

where dz/dt is the change in bed elevation per unit of time, k is rock resistance, and m and n are the empirically determined exponents describing longitudinal changes in A and S, respectively (Howard, 1994; Howard, 1998).

Application of equation (2.13) to a variety of streams has produced mixed results. The equation has been used to successfully model profiles, but can not be applied universally because k values must be empirically fitted, leaving the equation with no free variables because we cannot independently know dz/dt and k (Snyder et al., 2000; Whipple et al., 2000b). Use of the equation is further limited by confounding variables. For instance, longitudinal changes in the quantity and caliber of colluvial sediment delivered to the channel affect channel processes. All such variables must be subsumed by k, but values of k are unknown as unique functions of substrate resistance, let alone other influences (Snyder et al., 2000). This study tests the effect of lithology, hillslope interactions, sediment input, and basin size on local driving forces in an attempt to determine some of the variables that must be included in next-generation models of longitudinal profile development.

2.3.2 Knickpoints

The assumption that smooth, uniform profiles reflect equilibrium conditions is inherited from studies of alluvial streams (Mackin, 1948; Merritts and Vincent, 1989). Knickpoints are found in alluvial streams where they can be attributed to disequilibria

associated with propagation of base level fall and stream disturbance (e.g., Ritter et al., 1999). Knickpoints in bedrock streams have been interpreted similarly although some knickpoints have remained at fixed locations over geologically long periods of time. This has led some researchers to suggest that equilibrium and grading in bedrock streams need not be expressed solely as smooth, uniform profiles (Snow and Slingerland, 1987; Pazzaglia et al., 1998). Alluvial streams are free to alter channel resistance and energy expenditure by varying sediment calibers and fluxes. The distribution of substrate resistance is fixed in bedrock streams, therefore it is probable that systematic incision can only be made by varying the distribution of energy expenditure systematically, but non-uniformly. For instance, the distribution of stream power may not vary as a power function of area and slope (Snow and Slingerland, 1987). In fact, energy expenditure should reflect the distribution of substrate resistance and not just basin drainage area. This study indirectly tests this hypothesis by examining the distribution of terms dependent upon energy expenditure, ω and τ, in longitudinal profiles with significant variations in substrate resistance by examining variations in stream power as a function of relative rock solubility.

2.3.3 Erosion in Knickpoints

Erosion mechanisms in knickpoints are often different from those operating in adjacent reaches. For instance, abrasion is common in knickpoints atop resistant strata and sculpted forms are most commonly present in channel constrictions. The mere presence of a dramatic change in longitudinal form is problematic for researchers who model landscapes and channels because first-generation, power law-based approaches cannot describe the irregularities. This problem is further compounded by a lack of

knowledge concerning how sculpted forms and abrasion are related to basin-scale variables and localized erosion in knickpoints (Hancock et al. 1998; Whipple et al., 2000a,b). Partially solving these problems may show how future modelers might accommodate knickpoints in profile models using empirical laws or through physically-based models of individual erosion processes. Knickpoints are found in the Greenbrier River. Sculpted forms are numerous in several of these knickpoints, but are most abundant in an especially narrow channel constriction in Buckeye Creek Cave. The abundance and diversity of sculpted forms in this locale offer a unique opportunity to analyze the controls on sculpted form growth. These analyses shed light on the relationship of sculpted forms to knickpoint erosion because the large populations of sculpted forms are amenable to statistical analyses. This study uses statistical analyses of sculpture geometry and geometrical modeling to quantitatively explain how sculpted forms are related to one another and erosion in the constriction. These analyses are also used to indirectly evaluate the relationship of corrosion and abrasion in sculpted forms to another potential control: channel hydraulics.

2.4 Incision Processes and Resulting Forms Atop Soluble Strata

2.4.1 Confounding Variables

Longitudinal changes in unit stream power and bed gradient may reflect local adjustments to substrate resistance, but gradient is just one of many adjustable variables and unit stream power can only serve a proxy for a multitude of other variables associated with incision. As previously mentioned, cross-sectional area generally decreases as a stream flows onto more resistant strata (Whipple et al., 2000b). This has

the effect of increasing stream power because mechanical energy gradients increase in such settings (Wohl, 1993), and because unit stream power is maximized as a result of a dependence upon width (see equation 1.5). However, sources of energy dissipation often change in tandem with incision processes, and confounding variables may overwhelm the effects of substrate resistance in determining channel processes. For instance, influxes of coarse sediment from hillslopes influence channel processes (Sklar and Dietrich, 1998; Snyder et al., 2000; Sklar and Dietrich, 2001). However, the magnitudes of channel response are unknown and of vital interest to landscape modelers because of their influence on k in equation (2.13), and the need to create second-generation models that explicitly treat a wider variety of variables.

Deciphering the effect of individual variables, such as colluvial sediment supplied to the channel, requires independent knowledge concerning correlations between substrate resistance, hydraulics, and incision processes. Theoretically, if these co-dependent relationships are approximately understood, then space substitution could be used to discern the effect of additional variables. For instance, if process relationships were unraveled in a reach lacking hillslope interactions or other obvious confounding variables, then it might be possible to decipher the influence of other variables by examining nearby reaches atop the same strata but with additional variables. This approach requires detailed investigation of multiple river reaches and has not been tried previously, although Wohl and Ikeda (1998) did compare adjacent streams with different substrates to infer substrate influences on channel processes.

2.4.2 Channel Adjustments to Rock Solubility

Theoretically, the partial independence of corrosion from hydraulic variables should produce measurable differences between hydraulic variables atop soluble strata relative to adjacent insoluble strata in systems wherein corrosion is an effective means of incision. Long-term incision by corrosion should be limited primarily by access to the bed and not by the ability to quarry and abrade (e.g., White, 1988; Ford and Williams, 1989). Hypothetically, reach-average values of hydraulic variables in a mature system should reflect the need to convert potential energy to energies associated with bed incision. Therefore, stream channels incising by corrosion of soluble strata may display values of unit stream power, shear stress, and mean velocity that are lower than values found in adjacent reaches or that are less than expected of streams in similar settings. Channel geometries help dictate hydraulic variables, therefore channel cross sections and slopes should show systematic deviations atop soluble strata. For instance, stream widths may increase atop soluble strata because this would distribute stream power across a wider portion of the bed and increase hydraulic radius. These adjustments would increase the bed area available for corrosion and enhance non-erosive energy dissipation.

Hydraulic adjustments in cave streams should be especially pronounced and necessary for incision. Roughness in surface streams is provided by vegetation, but vegetation is absent in caves except as logjams. As a result, relative roughness will effectively decrease as a stream flows into a cave from a surface channel unless the cave passage presents additional roughness elements. Long-term, subterranean hydraulic adjustments might take the form of increased channel widths, decreased channel gradients, increased hydraulic radii, pools, or boulder obstructions. Adjustments need not

be associated with closed conduit flow, because free-surface flow prevails in many cave streams. For instance, Coward (1975) found that the majority of subsurface flow in West Virginia fluviokarst is free surface. Channel processes are the principal component of erosion and fluid transfer in such terrains because up to 80% of subsurface water is transmitted by stream channels in caves (Atkinson, 1977; Gale, 1984).

2.4.3 Recognizing Channel Adjustments to Soluble Strata

Cause and effect are often difficult to discern in fluvial systems. Confounding variables obscure the role of substrate resistance in determining channel processes, and causality may not be directly discernable in even the simplest systems. For instance, valley widths are commonly greater in shales than atop more resistant strata and stream gradients are typically less steep atop shales (Hack, 1957). The observed properties of valley widths and channel gradients atop shale could be hydraulic adjustments. Energy expenditure atop the less resistant strata, shales, is employed on lateral incision and other processes that do not directly aid vertical incision. Overall energy expenditure atop the shales may be equal to that atop adjacent resistant strata, or it may be less. In either case, more energy may be expended upon vertical incision in reaches developed atop resistant strata. Alternatively, wider valley widths could be the natural result of more efficient hillslope transport of fine material produced by shales and more rapid weathering.

Streams flowing atop soluble strata offer a unique opportunity to help recognize cause and effect because of the significant differences between erosion processes. For instance, if there are statistically significant differences between hydraulic variables in adjacent reaches atop soluble and insoluble strata, and values are less in the carbonate reach, then it would seem reasonable to attribute the difference to decreased physical

energy expenditure upon the soluble bed (Hypothesis I). If, as shown herein, the mechanisms of adjustment are readily discernable, then it may be possible to explicitly tie reach-scale energy losses, hydraulic forces, and incision processes together. More importantly, hydraulic adjustments atop soluble strata may be similar to adjustments atop especially weak strata such as shales. Subsequent studies could explore this possibility by looking for similarities between channels developed atop physically and chemically non-resistant strata.

2.4.4 Profile Development Atop Soluble Strata

Caves and karst streams possess many similarities with other bedrock streams that potentially allow them to be used to advance our knowledge of fluvial systems. White and White (1968) report that vadose, free-surface, cave streams have morphologies equivalent to bedrock surface channels. Deike and White (1969) report that stream meanders within Missouri caves are described by the same morphological relationships as those found within surface streams. The similarity between non-karst terrains and karst terrains is most dramatic in fluviokarst terrains. As the name implies, fluviokarst terrains are those in which surface streams and valley networks are an integral part of the landscape. Such terrains contrast dramatically with holokarst wherein the surface drainage network has been almost completely disrupted and obscured by subsurface piracy and subsequent denudation.

Surface streams are commonly diverted underground where incision of a clastic caprock exposes an underlying carbonate unit within fluviokarst terrains. Small surface streams may be diverted underground at the clastic/carbonate contact (White, 1988), but larger streams often flow across carbonates for considerable distances (Miller, 1996).

Subsurface piracy routes may mimic the drainage pattern initially developed upon a clastic caprock or divert flow beneath surface drainage divides into adjacent catchments. Regardless of subsurface flow routes, such fluviokarst basins commonly preserve a valley network inherited from antecedent surface streams; the valley network develops upon a clastic caprock and is largely preserved upon incision of the underlying carbonates, and channelized flow predominates (White, 1988; Ford and Williams, 1989).

Within some mature fluviokarst basins, surface streams flow across the clastic-carbonate contact and onto low gradient floodplains within a topographically enclosed karst depression. Streams flow directly into a cave upon reaching the opposite wall of the depression. The distance that a stream flows before entering the subsurface has been shown to be a function of contributing basin area (Smart, 1988; Miller, 1996). The cave transmits stream flow beneath depression slopes and eventually discharges the water at a spring. Position of the spring may be controlled by lithology, structure, or base level (Ford and Williams, 1989; White, 1988).

Cave streams and their initial profiles evolve from groundwater pathways that are preferentially enlarged because of relatively high permeabilities (Palmer, 1991). Passage growth eventually slows and a channel may be abandoned for a lower passage without incision of intervening bedrock. Gradients and channel characteristics inherited from a nascent stage will complicate profile analyses unless there is clear evidence that the pathways that guided early passage development do not control the modern stream profile. Bedding planes served as the initial pathways in Buckeye Creek Cave, but now lie as much as 15 m above the active channel. The cave stream has incised multiple lithologic units, flows across folds, and has entrenched 25 m-deep meanders against

bedrock dip. These observations suggest that channel geometry is no longer guided by gradients and boundary roughness characteristics inherited from groundwater flowpaths, and other factors now guide channel evolution. White (1988) concludes that just such an evolution is to be expected as fluviokarst streams mature, and Palmer (1977) uses such criteria to infer as much for the Mammoth Cave System of Kentucky. Theoretical models indirectly predict this result; Palmer (1991) showed that after cave passages reach a critical size, corrosion enlargement proceeds extremely slowly and passage growth becomes largely independent of corrosion phenomena.

Apparently, the deductions of White and Palmer are in direct agreement; as cave passages mature, changes in base level elevation, sediment flux, and other factors become the most important controls on profile evolution. Even if corrosion is still the predominant means of channel erosion, extrinsic variables dictate long-term changes in gradient and sediment supply, thereby affecting overall erosion rates (e.g., Granger et al., 2001). However, if these assumptions are invalid, this research will be able to show why they are invalid. For instance, geometric data and hydraulic modeling may reveal that channel evolution does not significantly modify initial channel parameters such as bed gradient. Or, the longitudinal profile may adjust to base level changes by periodic abandonment of older passage tiers because shear stress is too low to permit physical processes from incising the channel, while corrosion is simultaneously hindered by sediment shielding of the bed (e.g., White, 1988).

White and White (1983) examined the longitudinal profiles of streams passing through fluviokarst basins in Tennessee. Longitudinal stream profiles were found to display a break in slope at the base of enclosed karst basins when fitted with a

logarithmic function. When extrapolated beyond the downstream end of the basin, longitudinal profiles intersected base level. This and other evidence led White and White to conclude that, in general, such karst streams exhibit the profiles, gradients, and mouth elevations that one would predict for surface streams draining the same basin.

That a karst stream would possess the profile of a surface stream draining an equivalent catchment is intriguing. Consider a hypothetical surface stream with headwaters upon an erosional escarpment (Figure 2.3A). In a mature landscape, the longitudinal profile would follow a transition from high gradient, bedrock and colluvium-lined tributaries atop the escarpment to a lower gradient, alluvium-lined channel near the mouth of the catchment. The longitudinal profile would be adjusted to local base level and channel hydraulics. Cross section and plan form would be adjusted to prevailing basin characteristics such as runoff, sediment supply, and relief (Leopold et al., 1964; Knighton, 1998). Lower reaches of the stream would likely possess a floodplain several times the width of the stream. Flooding would be accommodated by overflow of the stream onto the floodplain and changes in runoff and sediment supply could be accommodated by adjustment of channel cross-section or slope.

In a karst stream, the longitudinal profile would follow a transition from high gradient, bedrock and colluvium-lined tributaries atop the escarpment to a low gradient reach within the floor of a topographically enclosed karst basin. Within the depression, the stream would enter an underground segment in a cave and thence arise at a spring near base level (Figure 2.3B). The cave stream may become pipe-full during floods, but otherwise meets many of the criteria of a bedrock stream; resistant channel

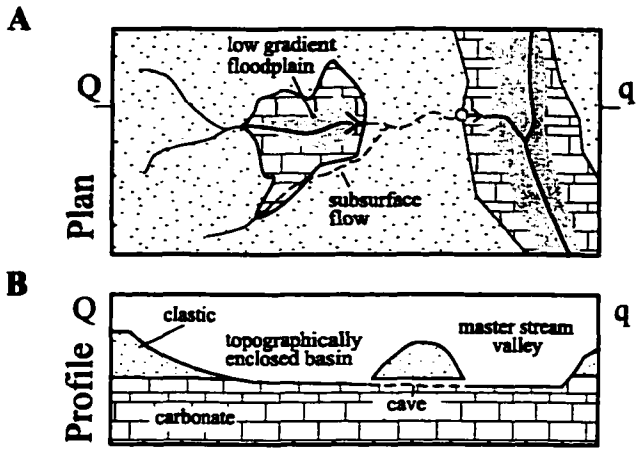

Figure 2.3: Schematic plan and profile of a fluviokarst basin. A: Surface streams enter karst depression, flow across depression floor, and enter cave. Water rises at a spring alongside a master stream. B: Profile of fluviokarst stream.

boundaries, limited sediment supply, large stage changes as discharge increases, and zones of flow separation where slackwater sediments may accumulate. Thus, downstream changes in stream morphology of the non-karst stream are typified by decreasing confinement and increasing sediment loading and alluvium. In contrast, the karst stream is typified by abrupt changes in channel and valley form, culminating in marked stream confinement within a subsurface conduit at the downstream end of the longitudinal profile and isolation from the direct effects of hillslope processes. Yet, according to White and White (1983), both streams grade to base level and possess similar longitudinal plans, gradient, and mouth elevations. Although this conclusion is at odds with the breaks in slope atop the floors of the karst basins they examined, the general similarities between longitudinal profiles are intriguing. Hypothetically, the two systems should receive equal amounts of energy input, in the form of discharge. However, each

dissipates the energy through very different channel and flow processes, although with similar results as quantified by longitudinal profiles.

Regardless of whether we accept White and White's (1983) conclusions about the similarity of surface and subsurface streams, numerous authors have reported grading of subsurface streams to surface streams (e.g., Palmer and Palmer, 1975; Johnson and Gomez, 1994; Pease et al., 1994; Farrant et al., 1995). Incipient subsurface pathways are commonly guided by lithologic and structural variables (e.g., joints and faults) that provide preferential flow routes or act to perch cave streams (White, 1988; Palmer, 1987; Ford and Williams, 1989; Palmer, 1991). Within such streams, profiles do not grade to base level, but display numerous lithologic and structurally controlled knickpoints. By inference, as a cave system adjusts its longitudinal profile to local base level, such variables as discharge, sediment load, base level elevation, and channel hydrology will progressively become the most important controls on stream profile, channel geometry, and erosion. White (1988) reaches this conclusion as well.

That cave streams do grade to local base level implies that they, like surface streams, are capable of modifying their longitudinal profile and channel form to most efficiently balance energy input and dissipation (e.g., Leopold et al., 1964). Although this result is not surprising, it is important when considering the relationship between cave and surface streams. However, as previously discussed, cave streams are at least superficially similar to bedrock streams. Thus, a karst stream must dissipate energy in ways different from a surface stream draining a similar catchment with downstream alluvial reaches.

Confinement of floodwaters by bedrock streams produces elevated water velocities, boundary shear stress, and energy dissipation at flow transitions and constrictions (e.g., Baker and Pickup, 1987; Wohl, 1992; Wohl et al., 1994). By analogy, cave streams may dissipate energy in a manner similar to bedrock streams. Yet, as shown by White and White (1983), the longitudinal profile of surface streams within karst depressions are adjusted to local base level; the position of local base level must be transmitted to the surface stream via the cave connecting the two (Figure 2.3). Hence, the cave stream and alluvial reach are coupled. The transition from alluvial to cave or bedrock stream is accomplished without interruption of the longitudinal profile despite the different natures of the two channel segments for the hypothetical basins. As previously discussed, the mechanism by which coupling is maintained without a break in profile is unknown. This study uses the results of reach-scale studies in Buckeye Creek basin to suggest a hypothesis for the relationship between the alluvial and bedrock reaches in the fluviokarst basin.

On the surface, storage of floodwaters atop broad, low gradient depression floors may attenuate flow and decrease velocity head, thereby regulating energy expenditure such that grade may be maintained. If this is the case, the depression floor represents not just an adjustment to base level, but also an adjustment to the transition from surface to subsurface stream. Hence, the landform should experience lowering at a pace comparable to incision of the cave and base level streams; the flat depression bottom does not represent in-filling by slackwater sediments from backflooding of the cave. Rather, the flat depression floor should be shallowly underlain by bedrock and is therefore a fluvial adjustment to a subsurface piracy. Bedrock is observed on the floors of many fluviokarst

depressions. White and White (1983) describe relict bedrock karst depression floors preserved above active, low gradient floodplains within the depressions. These surfaces grade to ancient base level positions, as defined by base level straths, and may themselves be straths.

The possibility that some karst streams effectively regulate energy dissipation, such that alluvial and cave or bedrock reaches are coupled, offers potential insight into the processes governing energy expenditure in karst and other fluvial settings. For instance, is storage of karst floodwaters within a surface depression and in ponded cave passages analogous to surface storage of floodwaters in tributary mouths and behind constrictions? How is it that localized zones of accelerated energy expenditure do not disrupt the longitudinal profile of cave streams? These are among the problems addressed in this research as a cave stream is used to infer correlations between reach-scale energy losses, hydraulic forces, and incision processes. However, a general theory of these linkages awaits still more case studies.

Chapter 3

Study Area

3.1 Introduction

This study examines two bedrock streams in southeastern West Virginia. The smaller stream, Buckeye Creek, drains a 14 km^2, topographically enclosed fluviokarst basin near Renick, West Virginia (Figure 3.1). The basin lies on the eastern margin of the Appalachian Plateau physiographic province atop gently folded Mississippian sandstones, siltstones, shales, and limestones. The climate is humid temperate with an average rainfall of ~125 cm a^{-1}. Buckeye Creek exits the surface catchment through Buckeye Creek Cave System and resurges through springs on the banks of Spring Creek. Spring Creek, drainage area 245 km^2, acts as local base level and drains highlands to the west of Buckeye Creek (Jones, 1997).

The Buckeye Creek Cave System encompasses three caves known to be physically and hydrologically connected (Buckeye Creek, Spencer, and Rapps caves) (Figure 3.2). Buckeye Creek Cave is a large cave whose entrance is also the Buckeye Creek stream sink. Aggregate passage length is 6 km; the modern stream passage accounts for 1.6 km of this distance. Rapps Cave is a 1.6 km-long complex of abandoned

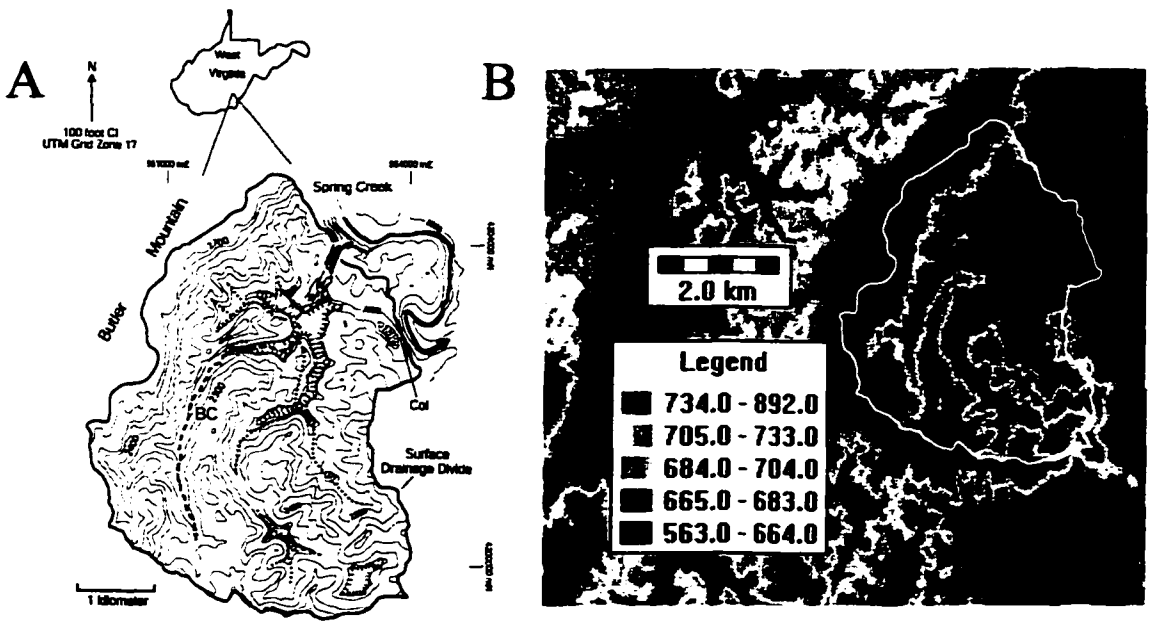

Figure 3.1: Location and topography of Buckeye Creek drainage basin. A: Topographic map with plan view of Buckeye Creek Cave overlaid. B: Surface plot of drainage created from 30 m DEM created by U.S. Geological Survey (http://www.datadepot.com). Concordant ridges are upheld by Mauch Chunk sandstones (west and south) and Greenville Shale (northeast). Cave plan from Dasher and Balfour (1994).

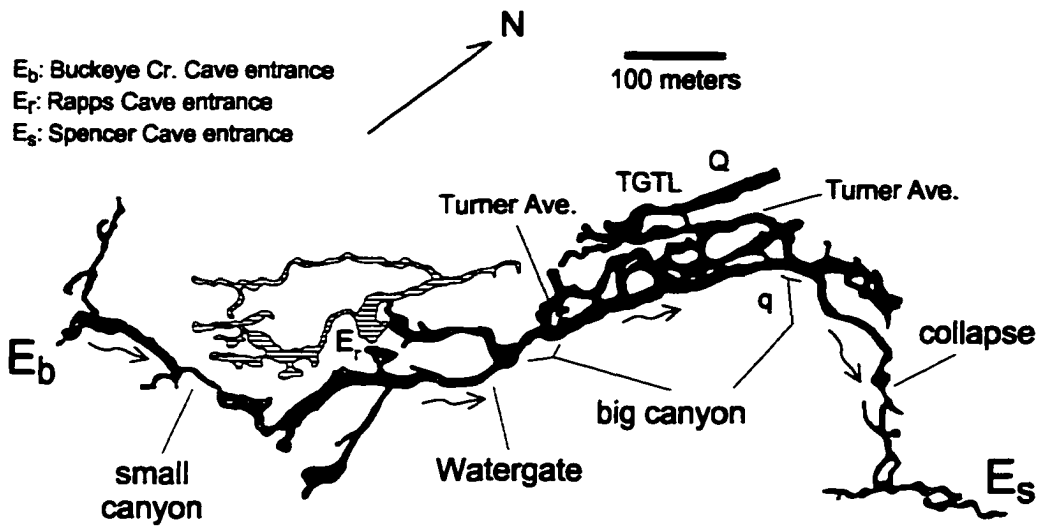

Figure 3.2: Plan view of Buckeye Creek Cave System. Rapps Cave (hatched) is not directly accessible from the rest of the system. Arrows denote flow direction. Cross section line Q-q is shown in Figure 3.10 and discussed in the text.

stream passages that were once part of Buckeye Creek Cave. Collapse has segmented Rapps from Buckeye Creek Cave proper, although the two exchange air and water (Dasher and Balfour, 1994). Spencer Cave is the name given to the Buckeye Creek spring and associated passages. The cave is directly connected to Buckeye Creek Cave, but was named before this was known (Dasher and Balfour, 1994). Henceforth, the stream sink and primary passages will be referred to as Buckeye Creek Cave. The name Spencer Cave will be used to denote the downstream entrance, spring, and nearby passages. Karst features of the Buckeye Creek drainage basin are the subject of a monograph that also presents overviews of basin geology, geomorphology, and hydrology (Dasher and Balfour, 1994).

The larger stream, Greenbrier River, is a south-flowing tributary of the New River with a drainage area of 3800 km^2 (Figure 3.3). The catchment straddles the boundary

between the Appalachian Plateau and Valley and Ridge physiographic provinces. The river principally flows along strike atop Paleozoic sandstones, siltstones, shales, and carbonates. The carbonates first outcrop 175 km downstream of the headwaters and underlie two segments of the river wherein portions of this study were conducted (Figure 3.3). The climate is humid temperate and mean annual precipitation declines toward the river mouth from a high of 152 cm a^{-1} to 100 cm a^{-1} (Jones, 1997). The New River acts as base level for the Greenbrier River.

3.2 Buckeye Creek and Catchment

3.2.1 Surface Component

3.2.1.1 Geology. The surface catchment of Buckeye Creek preserves a dendritic network of valleys with floors underlain by limestones of the Greenbrier Group (Figures 3.1 and 3.4-5). Headwaters are developed atop Mauch Chunk sandstones, siltstones, and shales. Two resistant sandstones underlie concordant ridge tops on the western margins of the basin (Figure 3.1). Denudation has removed these sandstones from the eastern side of the catchment where lower concordant ridge tops are primarily upheld by thin sandstones and siltstones. The Lillydale and Greenville shales cap ridges surrounding limestone-floored valleys. All sub-basins receive clastic sediment from ridges in their headwaters, and Buckeye Creek itself rises atop Mauch Chunk sandstones on Butler Mountain (Figure 3.1).

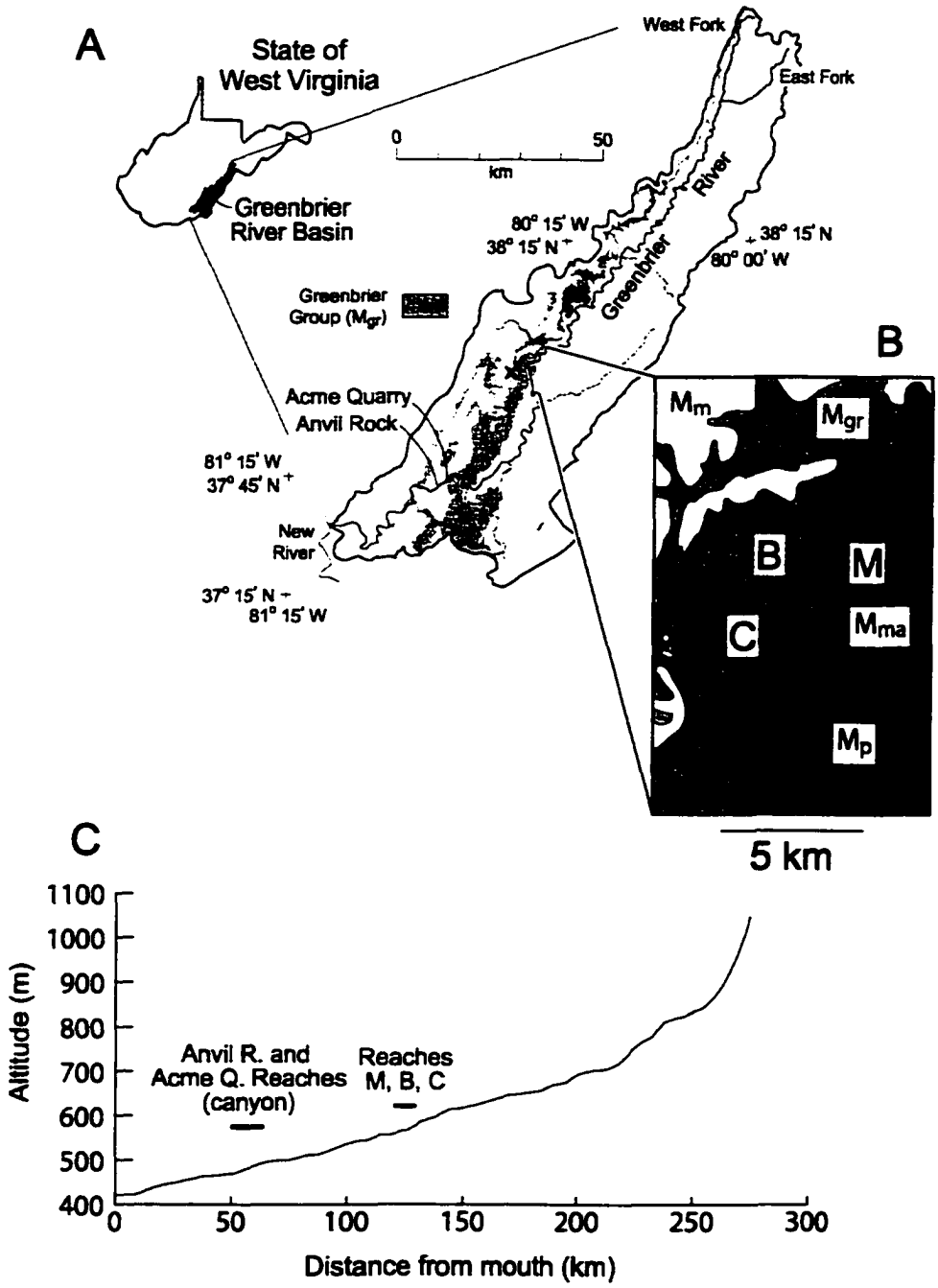

Figure 3.3: A: Locations of Greenbrier River catchment and study reaches. Large X identifies Buckeye Creek basin. B: Detailed geologic map and location of Mile-27 (M), Bone Quarry (B), and Cathole (C) reaches. Maccrady Formation is denoted as Mma. Mm denotes Mauch Chunk sandstones and shales overlying carbonates of the Greenbrier Group (Mgr). Black rectangle identifies Renick. Geology from Cardwell et al. (1968). C: Longitudinal profile of Greenbrier River with study reach locations.

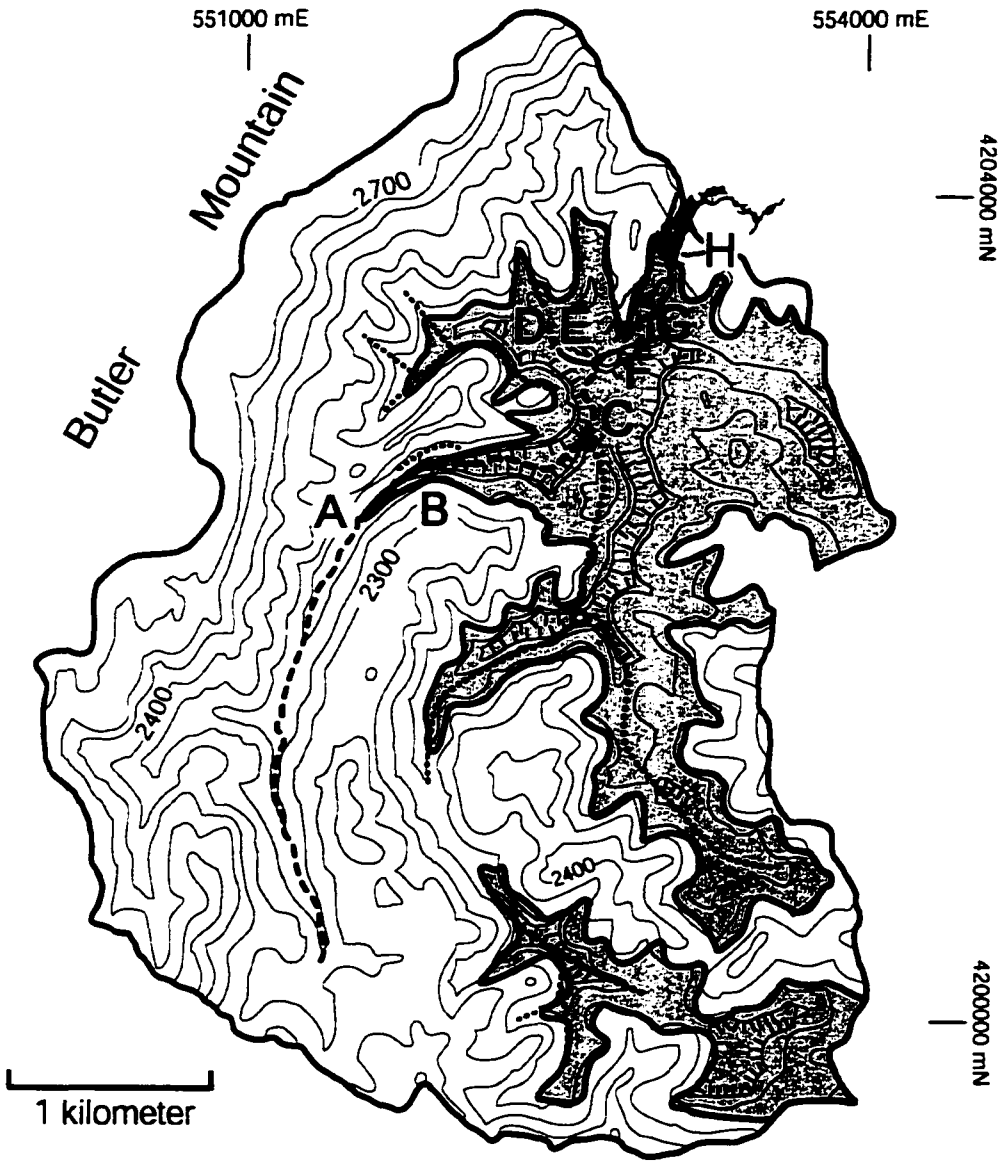

Figure 3.4: Simplified geology map of the Buckeye Creek basin. Shading denotes Greenbrier Group. White denotes Mauch Chunk. Long dashes denote surface stream (Buckeye Creek) and short dashes denote subsurface flow routes. Solid circle is Upper Buckeye Creek Spring. Hollow circle is a karst window where collapse of the valley floor into a flooded cave passage has created a small pond. Geology and flow routes from Dasher and Balfour (1994).

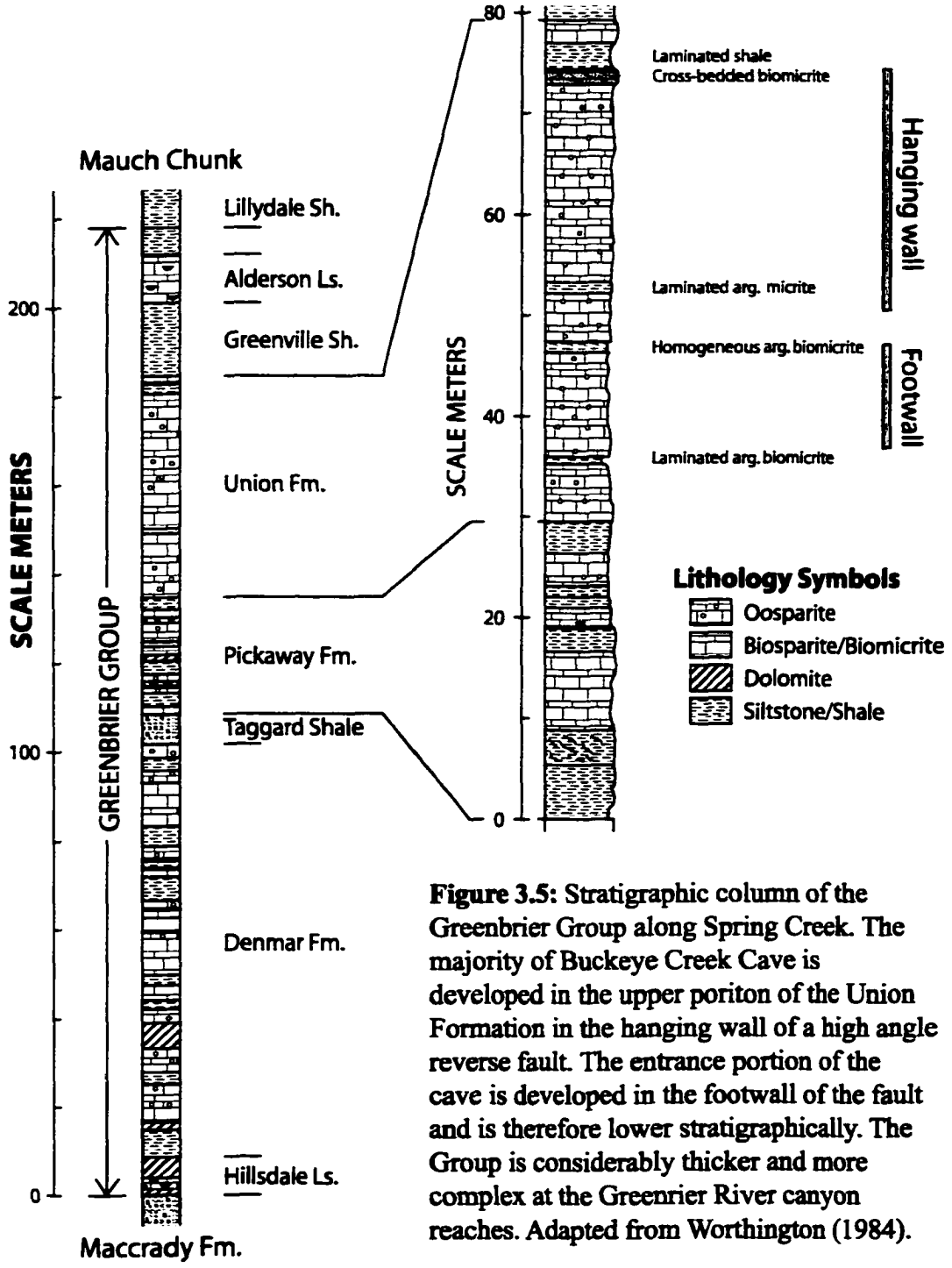

Figure 3.5: Stratigraphic column of the Greenbrier Group along Spring Creek. The majority of Buckeye Creek Cave is developed in the upper poriton of the Union Formation in the hanging wall of a high angle reverse fault. The entrance portion of the cave is developed in the footwall of the fault and is therefore lower stratigraphically. The Group is considerably thicker and more complex at the Greenrier River canyon reaches. Adapted from Worthington (1984).

3.2.1.2 Fluvial Architecture. The surface course of Buckeye Creek begins on the eastern slopes of Butler Mountain, a 200 m high escarpment (Figure 3.1). A coarse veneer of sediment mantles bedrock in reaches incising clastics. Stream widths average 4 m atop the clastics, and the overall gradient from source to cave is 0.03 m m^{-1}. Stream morphology is predominantly cobble runs atop clastic strata, but changes abruptly where the stream reaches limestones of the Greenbrier Group. A small waterfall marks the contact. Bed gradient downstream of the waterfall is steep, and cascade morphology is maintained until the stream enters the depression floor and a high floodplain appears on river left (Figure 3.6).

The stream narrows to 2-to-3 m wide on the depression floor and the gradient is 0.01 m m^{-1}. Mean sediment size, as determined from Wolman counts and sieving, gradually diminishes from small boulders to coarse gravel as the stream flows across the depression floor (Figure 3.7). The surface course of Buckeye Creek ends abruptly where it enters Buckeye Creek Cave (Figures 3.5 and 3.7). The stream once followed an easterly course to Spring Creek, but denudation has virtually erased this route except for a prominent col on the edge of the Spring Creek valley (Figure 3.1). Buckeye Creek has incised at least 31 m since the col was abandoned. As determined by this author and reported in Dasher and Balfour (1994), magnetostratigraphy of clastic sediments in Buckeye Creek Cave reveals that the upper-most cave passages are in excess of 0.788 Ma old. Hence, the col was abandoned no more recently than mid-Pleistocene.

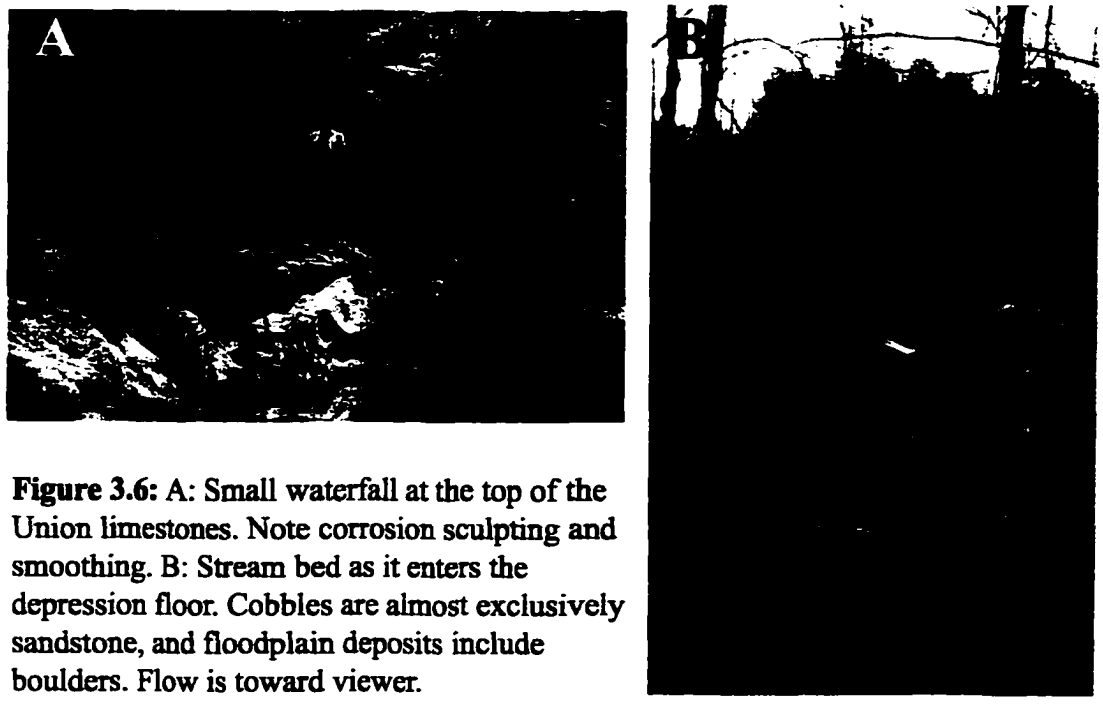

Figure 3.6: A: Small waterfall at the top of the Union limestones. Note corrosion sculpting and smoothing. B: Stream bed as it enters the depression floor. Cobbles are almost exclusively sandstone, and floodplain deposits include boulders. Flow is toward viewer.

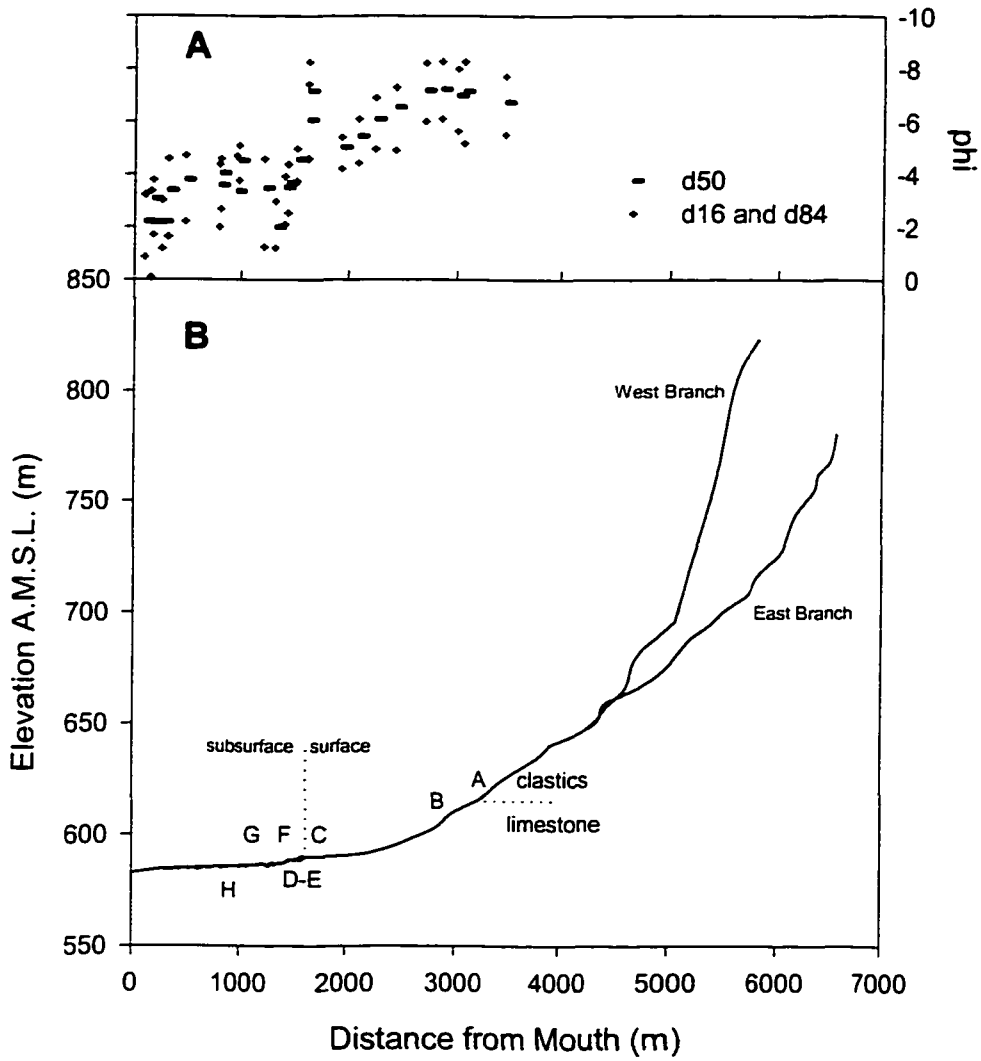

Figure 3.7. A: Distribution of particle sizes along Buckeye Creek as determined from Wolman counts and sieving. Median size peaks where stream enters limestone and karst depression. B: Longitudinal profile of Buckeye Creek. Letters identify study reaches described in Table 3.1.

The majority of tributary valleys are dry valleys with their streams flowing through cave systems beneath adjacent valley walls. Buckeye Creek is perennial except for a 1-km stretch between the carbonate-clastic contact and a major spring, Upper Buckeye Creek Spring. Unknown conduits divert water from the ephemeral reach during base flow and deliver the water to Upper Buckeye Creek Spring. Tributaries rising upon Butler Mountain are generally perennial, although base flow discharges are mere trickles. All such tributaries sink into the underlying carbonates upon reaching the carbonate-clastic contact (Dasher and Balfour, 1994).

Extensive, though thin, deposits of cobbles, sand, and silt mantle most valley bottoms. Sediments with elevations within 5-10 m of the entrance to Buckeye Creek Cave have been attributed to greater flood stages during the Pleistocene (Dasher and Balfour, 1994). These sediments include 5 m of laminated fine sediments beneath an extensive dry valley, The Racetrack (Figure 3.1). These same sediments are exposed in a terrace 40 m west of the cave entrance. The monotonous deposit of laminated silts and clays records a period of extensive fluvial deposition. These sediments once mantled virtually the entire depression floor, but have since been eroded from the vicinity of the cave entrance and surface stream by meandering of Buckeye Creek. In-filling by the fine-grained sediments created a low-relief surface throughout the 1-km long Racetrack. The surface is undisturbed except for two sinkholes.

3.2.1.3 Model Reaches. Eight reaches of Buckeye Creek were chosen for modeling (Figure 3.7)(Table 3.1). The surface reaches include portions of a headwater reach and three segments atop the depression floor. These reaches collectively sample the stream as it flows from atop clastic rocks and across the depression floor. The

Table 3.1: Buckeye Creek Study Reaches

Reach	Descriptors	Length (m)	Gradient ($m\ m^{-1}$)	Cross sections	bedrock or alluvial	Morphology	Bed Lithology	Drainage Area (km^2)	Selby rock resistance	Compressive strength[a]	d_{50} (phi)[a]
A	Headwater	42.3	0.044	10	bedrock	cascade, run	Shale	3.5	-	too soft[b]	-7.2
B	Upstream depression floor	53.0	0.029	12	alluvial	run	Limestone[c]	3.9	-	-	-7.2
C	Depression floor	75.3	0.005	9	alluvial	pool-riffle	Limestone[c]	10.4	-	-	-5.0
D	Depression floor; cave entrance	142.4	0.016	26	mixed	pool-riffle	Limestone	10.4	78	64 ± 2	-7.2
E	Cave	118.9	0.009	17	bedrock	cascade, pool-riffle	Limestone	13.4	76	64 ± 2	-4.6
F	Narrow canyon	65.1	0.003	20	bedrock	forced pool	Limestone	13.4	88	65 ± 2	-3.7
G	Large, tubular	77.0	0.004	12	bedrock	pool-riffle	Limestone	13.4	66	67 ± 2	-3.5
H	Large canyon	99.8	0.000	15	alluvial	pool-riffle	Limestone[c]	13.4	66	69 ± 2	-3.6

[a] Mean ± one standard deviation. Minimum n for compressive strength is 10. Minimum n for Wolman count d_{50} is 100. Sieving used for reaches F-H.

[b] Surface of massive shale is too soft for safe use of measurement device.

[c] Limestone underlies alluvium at an underdetermined depth.

subterranean reaches include the cave entrance and reaches that are drawn from each of the three large stream passage segments in the cave (Figure 3.8). Segments include large passages that occasionally flood to their ceilings, a narrow canyon, and a perennially vadose canyon.

3.2.1.4 Headwater Geomorphology. Evidence of mass wasting phenomena is ubiquitous on the slopes of Butler Mountain. Boulder streams typically occupy the axes of steep, low-order basins. The boulder streams originate beneath the sandstone caprock on Butler Mountain as broad sheets that narrow as they are funneled into incised hollows. The boulder streams are convex upward and heavily vegetated. Widths are generally less than 10 m atop carbonates at the base of Butler Mountain (Figure 3.6A). The boulder streams deliver coarse sediment to the karst network. Much of this sediment is stored in alluvial fans at hollow junctions on the karst depression floor. Stream channels are absent from atop most fans because small swallets divert water at the top of Union limestones. Deep soil weathering profiles observed in barrow pits, heavily weathered boulder surfaces, and boulder lags atop the fans suggest that the deposits are either relicts from the Pleistocene, or that sediment is supplied infrequently. Evidence of debris flows is most pronounced at the downstream terminus of the boulder streams. Deposits display pronounced upward convexities and boulder levees (Figure 3.9). Headward-migrating channels flank the boulder streams. These channels are preferentially eroding shales and siltstones of the Mauch Chunk and Greenville Shale because of the substantial resistance offered by the boulder streams (Figure 3.9A).

Channels whose headwaters do not include either of the resistant Mauch Chunk sandstones lack boulder streams, but hollow axes may be filled with more than 1 m of

gravel-sized Greenville Shale clasts or massive sands. The sands are 4 m thick in stream cuts in the principle valley that supplies discharge to Buckeye Creek Spring.

Extensive gravel and cobble deposits on the depression floor, Buckeye Creek floodplain, and inside Buckeye Creek Cave represent the insoluble sediment supplied to the karst drainage network by headwater streams; sediments generated atop headwater slopes must eventually be borne out of the basin. However, gravels predominate in cave streams of the basin and coarser sediments are stored in the alluvial fans and hollow axes. By inference, either transport of coarse sediment is episodic, or weathering decreases sediment caliber until transport is possible. Both phenomena are probably important for long-term denudation; extensive *in situ* weathering is observed atop all fan surfaces, and large cobbles are present in a 5-to-6 m thick fill in an abandoned passage of Buckeye Creek Cave. The insoluble detritus carried as bedload atop soluble strata in the Buckeye Creek catchment affects long-term incision by limiting access to the bed and by influencing channel hydraulics (e.g., White, 1988; Ford and Williams, 1989). The channel gradient must be sufficiently steep and the hydraulic forces sufficiently vigorous that the mass flux of solids balances that delivered to the stream network. Significant quantities of sediment may be carried as suspended sediment, but a gravel bed morphology and gravel deposits preserved in abandoned passages testify to the importance of bedload in long-term erosion of the catchment.

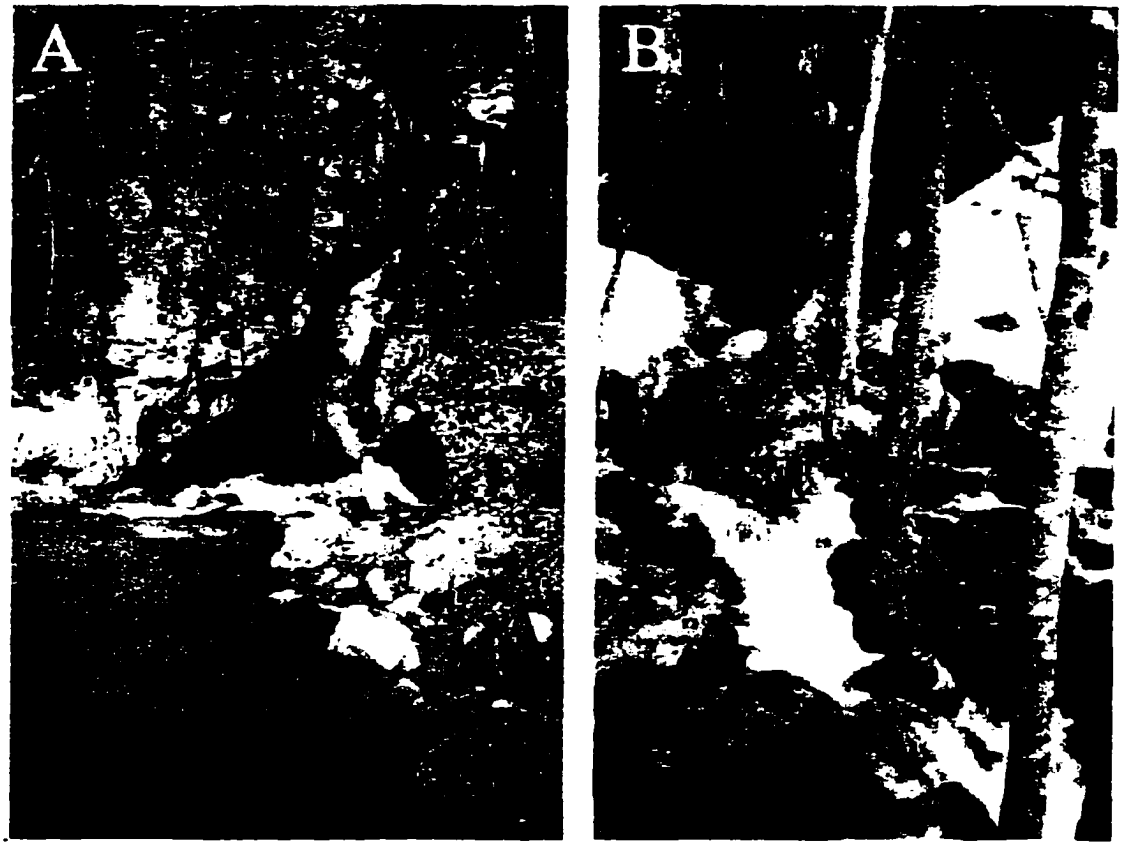

Figure 3.8: Entrances to the Buckeye Creek Cave System. A: Buckeye Creek flowing into the entrance of Buckeye Creek Cave during high water. The cascade in the cave mouth is caused by limestone boulders shed from the overlying cliff. B: Buckeye Creek overflowing through the Spencer Cave entrance during a flood. Larger floods fill the entire entrance and the melt line records higher stages for this flood. Both pictures taken in January 1996.

A

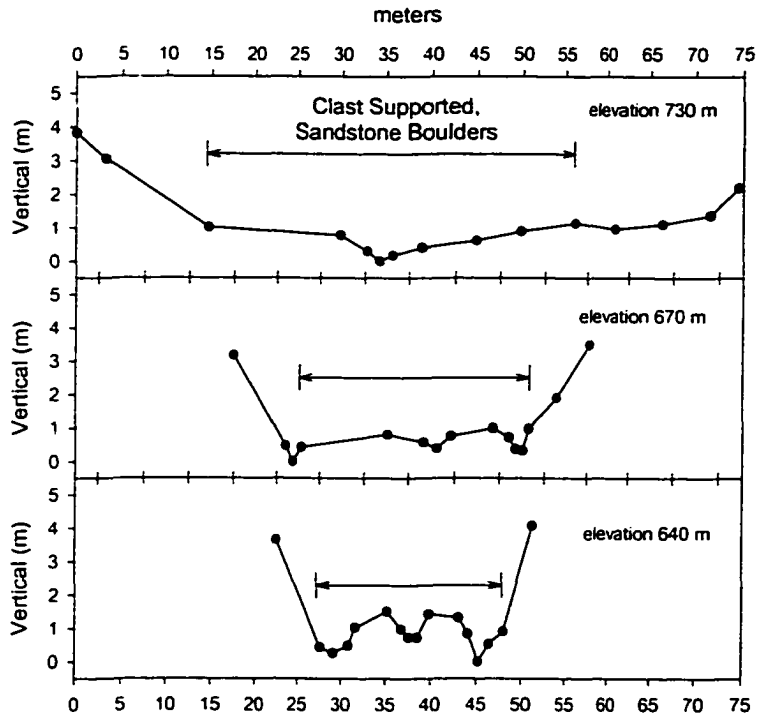

B

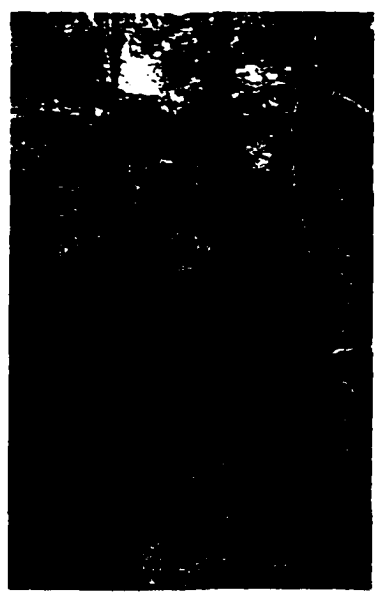

Figure 3.9: A: Cross sections of boulder streams and deposits in Ninson Hollow on Butler Mountain. Lowest cross section coincidental with top of Union Formation. B: Boulder levee identified in lowest cross section. Channels on either side are incised into shales and siltstones and are partially filled with boulders undercut from adjacent deposit.

3.2.2 Subsurface Component

3.2.2.1 Subterranean Stream Network. Cave exploration, dye traces, and geomorphic associations reveal that subsurface drainage in the Buckeye Creek basin is primarily vadose and epiphreatic (Dasher and Balfour, 1994). No systematic stream gage or aqueous geochemistry data are available for Buckeye Creek. Flow routes are shown in Figure 3.4. The most extensive epiphreatic segments, stream passages at or near the water table and which are perennially or ephemerally pipe-full, are those associated with Upper Buckeye Creek Spring. Submerged passages extend from a karst window to within a thousand feet of the spring (Figure 3.4). The accessible stream passage is dominated by a gravel streambed, deep pools, and short runs. Gravel and cobble beds in 0.5-to-2 m high passages characterize other tributary cave streams in the Buckeye Creek basin. Closed conduit conditions may prevail during floods, but perennially flooded segments are few and the cave streams are generally not representative of the water table position (Dasher and Balfour, 1994; Jones, 1997).

3.2.2.2 Buckeye Creek Cave. Buckeye Creek Cave contains the largest and most extensive subterranean stream channel in the basin. Buckeye Creek flows directly into the cave through the Buckeye Creek entrance and exits the cave 1.6 km later beneath or through the Spencer Cave entrance (Figures 3.8). The Spencer Cave entrance is connected to the remainder of the cave system by a 120-m long passage where air space above the stream is generally 1-to-10 cm. The Spencer entrance acts as an overflow for the passage, which reaches Spring Creek directly via the cave during base flow and small floods (Figure 3.8). The overall gradient of the cave stream is 0.01 m m^{-1}.

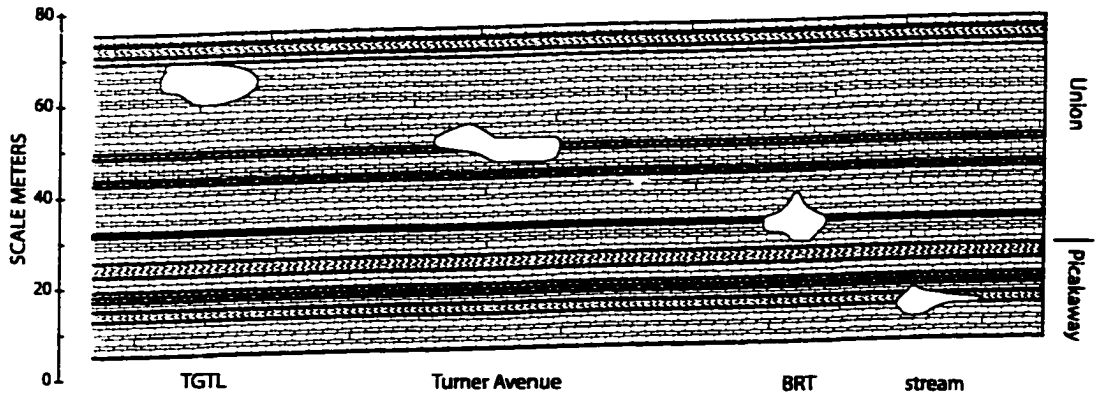

Figure 3.10: Cross section through cave along line Q-q in Figure 3.2. The highest passage, Too Good To Last (TGTL), was the first to form. The cave subsequently abandoned TGTL and two succeeding levels. The average incision rate is calculated as $29 < dz/dt < 64$ m Ma^{-1}, but vertical separation between the levels indicates that incision is episodic. Cross section data from Dasher and Balfour (1994). Stratigraphy from Worthington (1984).

The stream passage is the lowest and youngest of four tiers or cave levels (Figure 3.10) (Dasher and Balfour, 1994). The upper three tiers are similar in form to the modern stream passage; large elliptical tubes dominate passage shapes. Plan forms of the active and abandoned passages are gently meandering. Cave survey data and analyses of cross sections through the tiers show no discernable differences in passage gradients, although gradients of the abandoned tiers are difficult to reconstruct because of substantial fill and collapse (Dasher and Balfour, 1994).

3.2.2.3 Stream Morphology. Morphology of the cave stream connecting the stream entrance to the spring is pool-riffle. Clast sizes are predominantly gravel and the channel has the appearance of a typical gravel bed stream; fine-grained and gravel point bars extend from bend apices, silt banks line passages, and pebble and gravel clusters are the most common bedform. Exceptions to this rule include a 50-m-long cascade and limestone boulder bed at the upstream cave entrance and two large pools downstream of

the cascade. The first pool is bedrock-lined and maintained by a bedrock lip at the downstream end where water enters a substantially larger pool. Fine sediments mantle the pool bottom and river left bank. Bedrock forms the river right bank. The pool-riffle morphology is also absent in a short canyon located 120-m from the Buckeye Creek entrance (Figure 3.2).

3.2.2.4 Closed-Conduit Flow. Closed conduit flow has occurred almost system-wide at least twice since 1940. Passage heights in the active stream tier average 6 m and reach a maximum in excess of 20 m. The relatively large passage sizes prevent frequent closed conduit flow except behind three constrictions: the Watergate (described below), an unnamed collapse, and a small passage upstream of Spencer Cave (Figure 3.2). The collapse and small passage at Spencer Cave are found near the downstream terminus of the cave. The collapse occurs where the cave passage is enlarging in the downstream direction by stoping, which is vertical enlargement by collapse of passage ceilings. A boulder measuring 5 m wide, 5 m high, and 7 m long almost completely blocks the lower portion of the cave stream at the collapse, and the small passage begins a further 100 m downstream. As a result, backflooding produces pipe-full flow even during small floods. Pipe-full flow extended up to 300 m upstream of the collapse at least four times between June 1999 and January 2002 in a passage that averages 8 m wide and 6 m high. The backflooding significantly affected flow depths as much as 500 m upstream of the collapse.

The Watergate is a 30 m long constriction near the middle of the cave where ceiling height drops to only 1 m while width remains relatively constant. A pool fills the constriction and air occupies only 10-to-20 cm of the passage cross-section during base

flow. Flooding has caused the Watergate to become pipe-full twice during the course of this study, but closed-surface flow only spanned the 30-m length of the constriction; backflooding did not fill upstream passages, although backflooding did produce flow depths immediately upstream of the Watergate that were twice those found more than 150 m upstream of the constriction.

3.2.3 Development of Buckeye Creek Cave

3.2.3.1 Overview of Sequential Passage Development. Dasher and Balfour (1994) investigated the development and geomorphic history of Buckeye Creek Cave. Cave development began with diversion of Buckeye Creek from its easterly surface course into a north-flowing, strike-oriented passage that is near the contact of the Greenville Shale and Union Formation. This passage, known as Too Good To Last, is a 10-to-15 m wide, 2-to-10 m high elliptical tube developed along low-angle reverse faults and bedding planes. A few minor gravel deposits are found in the passage, but extensive silt and collapse deposits obscure the original stream channel. The silts are presumably slackwater deposits created by flooding from lower passages after abandonment of Too Good To Last.

Too Good To Last was abandoned when the stream was diverted to a lower tier, Turner Avenue (Figures 3.2 and 3.10). This process has been repeated two more times to form the BRT passage and the active stream tier. The four discrete levels are generally separated by bedrock and linked by small connecting passages or collapses. Each level exploits sub-horizontal planar discontinuities except where short canyons follow vertical joints. Tiers are separated by siltstones and nodular chert layers that perched overlying passages and capped phreatic passages below. By inference, groundwater enlarged

pathways below each stream tier until the lower passage captured the stream from the older, overlying passage. The lower passages may have had competitive advantages because insoluble gravels and cobbles armored floors of the higher stream passages (e.g., White, 1988). Just such a process is occurring near the Spencer Cave entrance where the active cave stream drops into a lower passage and has partially abandoned a larger passage that now acts as an overflow route. The vertical avulsion of the stream without incision of intervening bedrock violates the assumption that the vertical depth of incision, as parameterized as $\delta z / \delta t$, equals the vertical thickness of bedrock eroded (e.g., Howard, 1994).

3.2.3.2 Age and Incision Rate. The magnetostratigraphy of fine-grained cave sediments in Buckeye Creek Cave reveals that the cave is no younger than mid-Pleistocene (Dasher and Balfour, 1994). Silts immediately overlying gravels in Too Good To Last display reversed magnetic polarity and are therefore no younger than the Brunhes/Matayama magnetic chron boundary of 0.788 Ma (Spell and McDougall, 1992; Dasher and Balfour, 1994). Too Good To Last lies 50 m above the active stream tier; therefore the maximum incision rate is 62 m Ma^{-1}. Paleomagnetically reversed sediments are found in lower passages separated by normal polarity sediments at intermediate elevations. If the intervening normal sediments are from the normal polarity Jaramillo sub-chron in the Matayama chron, then sediments in Too Good To Last must be older than 1.01 Ma and younger than 1.77 Ma (Berggren et al., 1995). The minimum incision rate calculated using the older chron boundary is 29 m Ma^{-1}. Therefore, the incision rate ($\delta z/\delta t$) for Buckeye Creek in the cave is estimated as $29 \leq \delta z/\delta t \leq 64$ m Ma^{-1}.

The incision rate of Spring Creek is unknown, but the nearby Greenbrier River is incising at 40 m Ma^{-1} (Figure 3.3)(Springer et al., 1997). The range calculated for Buckeye Creek brackets the incision rate for the master stream, which implies that Buckeye Creek is incising at a rate comparable to streams elsewhere in the fluvial network.

3.2.3.3 Passage Morphology. The stream passage is a gently meandering series of long elliptical tubes and short canyon passages (Figure 3.11). Cross sections of the tubes are wider than tall. The canyons are composed of two types. Narrow canyons are found at the cave entrance and 120 m further downstream where cave development followed intersecting, rectilinear joints. These canyons are 1.5-to-3 m wide and 6 m high. Much larger canyons are found downstream of the Watergate where upper-level, abandoned stream tiers are intersected by the modern stream passage. These canyons achieve heights in excess of 20 m and widths average 15 m. The larger canyons have never experienced pipe-full flow since their discovery in the late 1940's. Their height and a complete absence of sediment reworking, slackwater deposits, or flotsam on surfaces more than 20 m above the stream suggest the passages have not been pipe-full for a considerable length of time, if ever.

3.2.3.4 Development of Active Tier. The active stream tier developed as two discrete segments. The channel extending 300 m from the entrance began as small elliptical tubes atop an irregular bedding plane between a sparsely jointed, fossiliferous biomicrite and an underlying biomicrite containing stringers of hardened claystone that accumulated along irregular planes of pressure solution (Figure 3.12). The complex three-dimensional network of interlocking, insoluble stringers causes the lower unit to be

Figure 3.11: Passages in Buckeye Creek Cave. A: Entrance passage. B: Large canyon where stream intersects upper levels. C: Youthful slot-like canyon 300-m from entrance. D: Watergate. Note scallops on ceiling. Photos A, B, and D courtesy of Ed McCarthy.

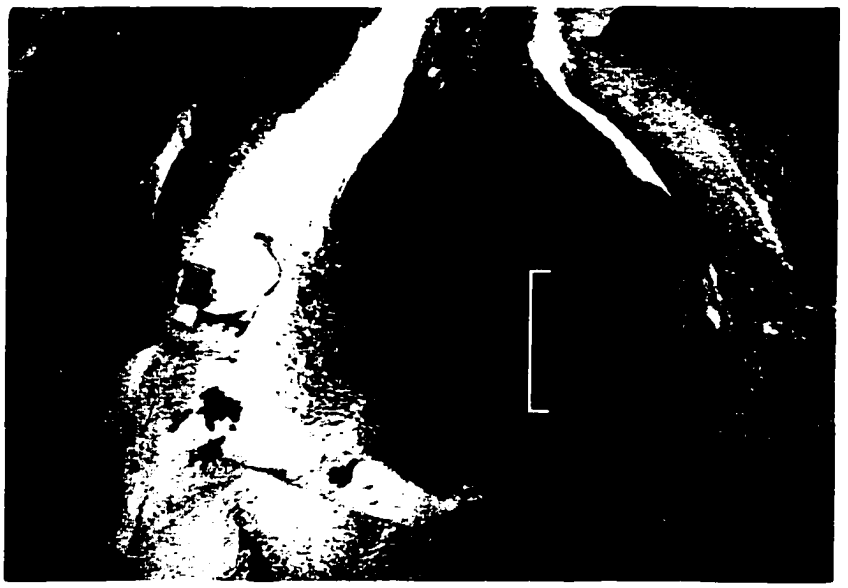

Figure 3.12: Stream passage developed in resistant limestone containing insoluble claystone stringers created during pressure solution. Bracket identifies claystone zone. Passage is located at the downstream terminus of the small canyon. Note that the passage follows a prominent joint and the bedding plane.

resistant, and centimeter-scale fins and nodules of claystone project from associated cave walls. The passage ends abruptly where the stream makes a 90° turn to river left and enters a narrow canyon. The entrance passage once continued toward the east, but is now plugged by breakdown collapse and silt. This passage was probably once continuous with the large stream passage at the downstream end of the 120 m long canyon, but encroachment of the valley wall caused collapse of the meander. This collapse is expressed as two breakdown complexes immediately downstream of the canyon.

The 120 m long, joint-controlled canyon diverts the stream around the collapse and abruptly ends where the passage intersects a reverse fault. The canyon and entrance passages are developed in the footwall, and the hanging wall is composed of micrites overlying a 30 cm thick siltstone and underlying, well-jointed micrite (Figure 3.5). The

siltstone guided cave development along the remaining 1.2 km of the active stream passage leading to Spencer Cave except for a short stretch at the Watergate where a phreatic loop extended through and below the siltstone. In general, passage development began with growth of broad, low elliptical tubes atop the siltstone. Incision eventually breached the siltstone, which crumbles when dry and therefore weathers quickly to form recessed notches in passage walls. Lateral removal of the siltstone and underlying micrite is causing passage widening.

Vertical stoping and corrosion are important throughout the active stream tier. Vertical stoping is occurring as passage walls are undercut by lateral widening in the entrance passage, collapsing as ceiling joints are widened, and lateral erosion of the siltstone. Collapse occurs along bedding planes at the Watergate where the mechanically weak siltstone lies slightly above the passage ceiling. Progressive downstream collapse of the Watergate ceiling is opening the constriction in a manner analogous to waterfall migration on a channel bed. Eventually, the collapse will reach the large canyon at the Watergate terminus and thereby open this constriction.

The importance of stoping for passage growth is especially evident in the entrance passage. Smooth-walled elliptical tubes with widths of ~2.5 m are preserved on passage ceilings at two locations in the passage. The tubes are on the underside of large, fractured blocks of bedrock that protrude from the ceiling. Azimuth and spacing measurements of joints in adjacent walls show high fracture densities with an azimuthal distribution that is considerably less peaked than those on other walls (Figure 3.13). The fracturing reflects active collapse of the walls in association with undercutting and stoping; several

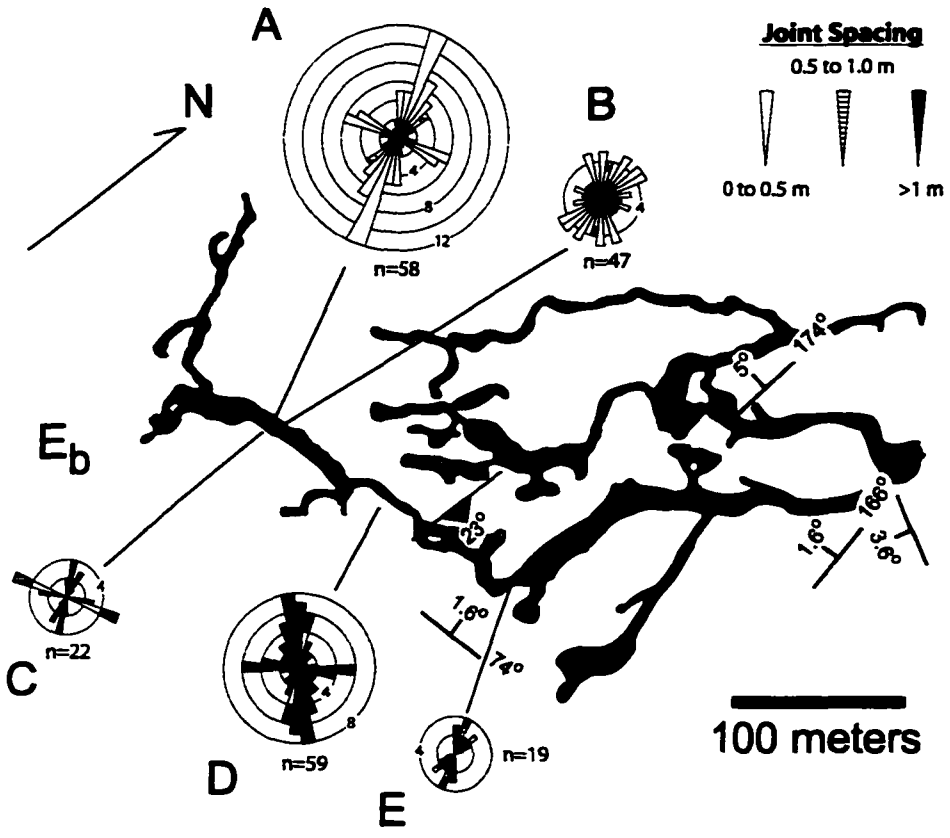

Figure 3.13: Basic geology and fracture orientations in the southern portion of Buckeye Creek Cave. E_b denotes Buckeye Creek Cave entrance. Bimodal joint patterns reflect tectonic jointing for sites A and C-E. However, active wall collapse and stoping at B cause fracture orientations to be more evenly distributed.

decimeter-scale blocks fell from the walls and ceiling during the two-year duration of this study. Presumably, the observed tubes were once part of the formative tube, which has since been almost completely obliterated by collapse and incision. Similar tube remnants are found downstream of the canyon atop the siltstone.

3.2.4 Reach Descriptions

3.2.4.1 Reach A. This reach was chosen from many possible locations in the headwater portion of Buckeye Creek. This particular locale was chosen because it lies away from a county road (Buckeye Creek Road), which parallels the creek for

approximately 1.5 km upstream of the karst depression. As a headwater reach, the channel segment receives coarse, insoluble sediment directly from adjacent hillslopes and upstream sources. Sediments in the reach are entirely sandstone and shale except for some limestone gravel supplied from the county road upstream of the reach. Median clast size is -7.2 phi (Figure 3.7).

The reach is relatively steep and underlain by sparsely jointed shale (Table 3.1). A run morphology prevails throughout the reach, therefore cross sections were surveyed at similar distances from one another (Appendix A). The downstream end of the reach lies at the shale/limestone contact (Figure 3.6B). The shale is quarried by the stream as multi-decimeter blocks, which quickly decompose on the stream bed to form small unconsolidated piles of gravel-sized material. The gravelly material was not observed to persist downstream of the limestone waterfall.

3.2.4.2 Reach B. This reach lies at the upstream terminus of the floodplain developed on the floor of the karst depression (Figure 3.6B). This particular reach was chosen because it is largely separated from Buckeye Creek Road by the floodplain and has not been narrowed by road construction. Insoluble sediments are supplied from upstream and include numerous coarse, sandstone boulders that are isolated from one another by cobbles and coarse gravel. The surfaces of some of these boulders display complex sculpted forms. No bedrock exposures were observed in the reach, including in scour pools around boulders and beneath a culvert 150 m downstream of the reach terminus. Minor excavations in the reach yielded no bedrock. Sculptures orientations are appropriate for the reach flow direction, hence it was inferred that the reach is alluvial and the coarse bed is rarely mobilized because abrasion of insoluble surfaces is a

relatively slow process (Hancock et al., 1998). However, the length of time required to generate the observed sculptures is unknown. Median clast size is -7.2 phi.

The reach maintains a run morphology throughout (Table 3.1)(Figure 3.6B). Cross sections were surveyed at similar distances from one another because of the run morphology (Appendix A). Although there is no direct evidence to substantiate the supposition, it is possible that debris flows are important for delivering the coarse sediment to this reach because the sandstone boulders are found on floodplain surfaces and floating in cobble matrices in channel banks. Alluvial fans with large accumulations are found elsewhere in the basin where tributaries debouch from confined channels. However, those tributaries have drainage areas that are an order of magnitude less than the 3.9 km^2 catchment at reach B and the tributary channels are boulder streams, lacking a discrete central channel such as Buckeye Creek (Figure 3.9).

3.2.4.3 Reach C. This reach lies 40 m downstream of Upper Buckeye Creek Spring on the floor of the karst depression. This particular reach was chosen because it is entirely separated from Buckeye Creek Road, receives the combined discharges of the spring and the headwaters linked to reaches A and B, and lies atop the depression floor (Table 3.1). The overlying hillslopes are entirely composed of limestone and all sandstone clasts are supplied from upstream. Median clast size is -5.0 phi. Pool-riffle morphology is maintained throughout this and adjacent reaches. Cutbanks, 1-to-1.5 m deep, in silt loams form both banks. No bedrock was observed in the channel bed or banks. Shallow excavations failed to find bedrock beneath the channel bed.

3.2.4.4 Reach D. This reaches extends from 30 m upstream of the Buckeye Creek Cave entrance to 110 m downstream of the entrance. The surface reach is incised 1.5 m

into silt loams atop the depression floor. Pool-riffle morphology is maintained throughout the reach except for the entrance region, which includes the first 40 m of the cave (Table 3.1). This region is laden with coarse limestone talus from a 7 m high cliff and bedrock hillslope that overlies the cave entrance. The talus temporally forces a cascade morphology on the stream. The cascade is washed out during large floods (discussed in Chapter 6).

The entrance is relatively narrow and forms a constriction (Figure 3.8A)(Appendix A). The passage enlarges abruptly 30 m downstream of the entrance where overall passage widths increase to as much as 20 m. The stream channel is consistently 4-to-6 m wide throughout the subterranean reach, except in the vicinity of the entrance constriction. Banks of silt loam form one or both banks of the channel downstream of the passage expansion. These banks have been smoothed by floodwaters, but undercutting is causing some bank erosion.

3.2.4.5 Reach E. This reach begins a few meters downstream of reach D. Passage width is consistently ~9 m (Appendix A). Passage and channel cross sections are relatively uniform and pool-riffle morphology is maintained throughout the reach (Table 3.1). The reach was chosen to sample a lengthy stretch of a large passage that extends from the entrance reach to the narrow canyon, which terminates the relatively large passages downstream of the cave entrance. Only ~20 m of the large passage is omitted from the reach, hence the modeled reach should be fairly representative of the stream segment as a whole.

The stream channel is consistently 4-to-5 m wide throughout the reach. Banks of silt loam form one or both banks of the channel. These banks have been smoothed by

floodwaters, but undercutting is causing some bank erosion. Banks are steep, verging on vertical. Sawed wood, tin and leather artifacts, and steel machinery components are found in scattered bank exposures. These objects and banks may have been deposited following a catastrophic flood in the mid-1940's, which largely flooded the depression floor (Dasher and Balfour, 1994). The stream has either eroded through the 2-m-thick deposit or a continuous channel was maintained throughout the deposition event. In either case, the channel gradient appears to be fixed at the reach scale by intermittent bedrock outcrops on the streambed.

3.2.4.6 Reach F. This reach begins 15 m downstream of reach E. The reach spans all but the last 30 m of a narrow canyon that separates large passages on either side. The canyon follows rectilinear joints, but passage corners have been smoothed by erosion to a sinuous planform. The reach was chosen because it is the narrowest stream passage in Buckeye Creek (1.5-to-2 m)(Appendix A). The reach gradient, 0.003 m m^{-1}, is less steep than either adjoining reach (Table 3.1).

Passage walls and floors in the canyon are entirely limestone except for short patches of gravel, which were rearranged after at least three floods during the two years of fieldwork. Sculpted forms are found up to 5 m above the streambed. As discussed in Chapter 4, some of these sculpted forms are useful for paleodischarge calculations and they record the approximate depth in the canyon for the estimated discharge (e.g., Pisarowicz and Maslyn, 1981).

3.2.4.7 Reach G. This reach is located in a 10-to-20 m wide passage, which lies between reach F and the Watergate constriction. This reach was chosen because cross sections and channel beds are wider than preceding reaches (Appendix A). Ceiling

heights vary between 6 and 10 m. Bedrock exposure in the channel bed is largely along the margin of the bed where it abuts a passage wall. The opposite bank is always a finely laminated silt loam with no artifacts or macroscopic wood. A fossil recovered from similar banks nearby was determined to be Pleistocene in age (Dasher and Balfour, 1994); the banks are presumably not historic deposits. The bed is largely composed of sandstone-derived gravel and pool-riffle morphology is maintained throughout (Table 3.1).

3.2.4.8 Reach H. This reach was chosen from the largest stream passage in the cave. The reach begins shortly downstream of a major passage expansion caused by intersection of the modern stream passage with an overlying passage, which elsewhere lies to the north of the active stream passage. Ceiling heights are not directly determinable, but are known to exceed 20 m based upon interpolation (Dasher and Balfour, 1994).

The gradient in reach H is the lowest of all the surveyed reaches. The surveyed value of 0.0004 is rounded to 0.000 in Table 3.1 because of significant figures (Table 3.1). The bed is consistently 6 m wide and composed of sandstone-derived gravel (Appendix A). Pool-riffle morphology is maintained throughout the reach, although a large boulder produced by wall collapse does created a large forced pool on river left near the center of the reach. Such boulders enhance bed scour and pool formation by generating flow separation along their margins (Thompson et al., 1999). However, the pool is not continuous in the vicinity of the boulder because of shoaling and bar formation along the river right channel margin.

3.3 Greenbrier River

3.3.1 General Characteristics

Five reaches of the Greenbrier River, West Virginia were chosen for hydraulic modeling on the basis of hillslope composition (limestone versus limestone plus resistant clastics) and substrate resistance (readily corroded versus resistant to corrosion). Reaches with and without resistant clastic sediments capping valley walls were selected to compare the effects of coarse, insoluble sediment on stream processes. Similarly, reaches were selected that contained clastic and carbonate strata to compare river processes atop different strata. The Greenbrier River is a perennial, unregulated bedrock stream draining a mountainous, ~4000 km^2 catchment with an overall stream gradient of 0.001 m m^{-1} (Figure 3.3). Riffles atop boulders and cobbles alternate with mixed bedrock- and cobble-floored pools. The river profile is concave, but displays numerous local concavities and convexities (Figure 3.3). The five reaches chosen for this study include three near Renick, West Virginia and two in an unnamed canyon (Figure 3.3 and Table 3.2).

3.3.2 Renick Reaches

The Greenbrier River flows atop Paleozoic sandstones and shales for 175 km below the river source, but gently meanders across strike for 9 km near Renick, West Virginia where it incises limestones of the Greenbrier Group. The valley and riverbed are entirely composed of limestone for 5 km at Renick (Figure 3.3). Flood discharge is effectively constant along the reach because no major tributaries enter the river. No significant subsurface diversions of the Greenbrier River are known, although small caves are found in some riverbanks. Locally, catchment area is 1790 km^2 and the river is incising at a rate of 40 m Ma^{-1} (Springer et al., 1997).

Table 3.2: Greenbrier River Reaches

Reach	Length (m)	Gradient ($m\ m^{-1}$)	Cross sections[a]	Bed lithology(s)	Valley Wall Lithology(s)	Selby rock resistance	Compressive strength[b]	d_{50} (phi)[b,c]	Ls Fract. (%)[d]
Anvil Rock	860	0.002	7 (3)	Limestone	Limestone	95	59.7 ± 3.2	-7.94 ± 1.03	8.00
Acme Quarry	780	0.002	7 (3)	Limestone	Clastics+Ls	92	65.7 ± 1.6	-7.86 ± 0.88	10.67
Mile-27	640	0.001	6 (3)	Sandstone	Ls+Clastics	80	49.8 ± 1.1	-7.50 ± 1.14	0.01
Bone Quarry	720	0.002	8 (4)	Limestone	Limestone	77	59.3 ± 2.9	-7.30 ± 0.81	0.67
Cathole	1450	0.000[e]	4 (2)	Limestone	Limestone	86	59.3 ± 2.9	-7.95 ± 0.86	4.33
			2 (0)	Shale		34	too soft[f]		
			6 (2)	Sandstone		77	55.1 ± 2.8		

[a] Total number of cross sections with number of riffles in parentheses.

[b] Mean ± one standard deviation. Minimum n for compressive strength is 10.

[c] Wolman counts of clast sizes were made atop riffles except at Anvil Rock where counts are from a bar. Minimum n is 100.

[d] Percent of bed clasts composed of limestone (minimum n is 100).

[e] Calculated gradient is 0.0003, but rounding yields a value of 0.000 because of averaging across a 1-km-long pool.

[f] Friable shale is too soft and fractured for safe use of measurement device.

The Greenbrier River is a major tributary of the New River. Knickpoints are presumed to have migrated through this drainage network in response to creation of the modern Ohio River drainage network beginning approximately 2.65 Ma (Granger et al., 2001), but there is no evidence that such knickpoints are still extant in the examined reaches of Greenbrier River (Sasowsky et al., 2002). Therefore, local gradients are assumed to reflect long-term incision processes for the purposes of this study.

3.3.2.1 Mile-27 Reach. This reach is located at the Mile-27 trail marker of the Greenbrier River trail north of Renick (M in Figure 3.3B). The Mile-27 reach is incised into thin-bedded, quartz sandstones of the Price Formation. The river flows onto overlying limestones 2-km downstream of the Mile-27 reach because the river is flowing obliquely across the dip. As a result, the river-right valley wall is composed of limestones and the river-left valley wall is composed of sandstones and siltstones of the Price Formation. Pool-riffle morphology is maintained throughout the reach and bedrock is exposed briefly on the river-right bank and in discontinuous patches throughout the pools. Bed clasts are coarse cobbles and fine boulders derived from upstream sources. The river is not receiving coarse sediment from either valley wall.

3.3.2.2 Bone Quarry Reach. This reach is at the northern end of Renick and begins beneath a local landmark, Bone Quarry (B in Figure 3.3B). The quarry is located high on the valley wall and does not affect the river. The reach is incised into medium to thick-bedded micrites. A thin calcareous siltstone is exposed at the downstream terminus of the reach in a riffle. Valley walls are entirely composed of limestone, and numerous caves are known to exist in the valley wall. The river is diverted by subsurface paths near the upstream end of the reach during extended droughts, but the associated spring is small

and the quantity of water diverted is visually estimated as 1-5 $m^3 s^{-1}$ (Jones, 1997). Pool-riffle morphology is maintained throughout the reach. Pool floors are typically limestone. Riffles are developed atop coarse sandstone cobbles and fine boulders derived from upstream sources. The river does not abut either valley wall, nor does it receive coarse sediment from the valley walls.

3.3.2.3 Cathole Reach. This reach is located ~1.5 km downstream of Renick and includes a pool known locally as The Cathole (C in Figure 3.3B). The reach spans the contact between the Greenbrier Group carbonates and clastic rocks of the underlying Maccrady Formation. The upstream terminus lies atop medium to thick-bedded micrites and beneath a bedrock cutbank on river right. The downstream terminus is incising thin to thickly bedded sandstones of the Maccrady Formation beneath a cutbank on river left. Siltstones and shales of the Maccrady Formation are exposed on the riverbed as the river crosses the narrow valley floor between the limestone and sandstone outcrops.

The Cathole reach is the longest of the five study reaches. Overall morphology is pool-riffle, but the reach is dominated by a 1-km-long pool (The Cathole) that extends from atop the limestones to the sandstone outcrop. Normal pool depths are 1-to-3 m. Thin, plate-like sandstone boulders quarried from the channel bed and river left bank are found throughout the downstream end of the pool. The overlying valley walls are composed of limestone and do not supply coarse sediment to the channel except beneath bedrock cutbanks at the upstream and downstream termini of the reach.

3.3.3 Canyon Reaches

The canyon reaches are located ~60 km downstream of Renick where the Greenbrier River has turned across strike. The river flows in a canyon at the southern end

of Muddy Creek Mountain along the cross-strike course (Figure 3.3A). Locally, massive sandstones cap canyon walls and sandstone mega-boulders mantle hillslopes and channel margins. The river profile displays an upward convexity within the canyon even though the bed is composed of limestone (Figure 3.3C). Locally, drainage area is 3380 km^2 and the river is incising at a rate of ≤ 40 m Ma^{-1} (Shank and Sasowsky, 2001).

3.3.3.1 Anvil Rock. This reach is located at the southern terminus of Muddy Creek Mountain in the narrowest segment of the canyon. The river is incised into massive, sparsely jointed oolitic and micritic limestones of the Greenbrier Group. Prominent bedrock banks line the river-right bank. Large sandstone boulders reach the channel as boulder streams and colluvial aprons. The largest boulder is Anvil Rock, with axis lengths of 15, 8, 6 m. Boulder deposits form channel constrictions and extremely coarse bars. The reach is best described as having a rapid-pool morphology. Low water pool depths are 4 m.

3.3.3.2 Acme Quarry. This reach is located adjacent to Acme Quarry at Fort Spring, West Virginia (Figure 3.3A). The reach is near the upstream terminus of the canyon. Acme Quarry is located upstream of Anvil Rock where a low limestone ridge prevents sandstone boulders from reaching the riverbed. The river is incised 17 m below a strath on river right and massive boulders from cliff collapse mantle a third of the right bank. The largest boulders are 5-m cubes. Several floodwater injection caves found in this reach contain paleoflood deposits and peak stage indicators (PSIs) for the historical flood of record (Springer, 2002). The river is incised into massive, sparsely jointed oolitic and micritic limestones of the Greenbrier Group. Pool-riffle morphology predominates

and patchy bedrock exposures are maintained throughout pools. Maximum low water pool depths average 1.5 m.

Chapter 4

Data Collection and Flow Modeling

4.1 Introduction

Specific categories of data were collected for all reaches examined in this study. The categories include channel geometry, sediment size, substrate resistance and composition, types of erosion features on the channel bed, and geomorphic setting. Additional data were collected in selected reaches. These data include sizes of sculpted forms and paleostage indicators (PSIs) for historic floods. Estimates of hydraulic variables were generated from HEC-RAS, a one-dimensional step-backwater program, using the geometry data and estimates of channel roughness. This chapter describes the manner in which the various types of data were collected, generated from models, or analyzed.

4.2 Channel Geometry Data

The thirteen stream reaches examined in this study were modeled using HEC-RAS, a one-dimensional open channel step-backwater model (Hydrologic Engineering Center, 1998a,b). HEC-RAS requires multiple cross sections for each modeled reach. The

distance between each cross section must be known and exit slopes are required for each reach.

Cross section data, distances between cross sections, and exit slopes can be obtained from XYZ data collected using theodolites. A TopCon total station, a laser theodolite with the ability to calculate XYZ positions relative to the survey instrument, was used to survey twelve of the modeled reaches. The remaining reach was surveyed using a transit, stadia rod, and fiberglass tape (reach C in Buckeye Creek). Distances from the instrument were directly determined for reach C using the fiberglass tape. Elevations were relative to an arbitrary benchmark set near the margins of the reach. Standard trigonometric relationships were used to convert the raw data to XYZ coordinates in Microsoft Excel, a spreadsheet program (Microsoft Corporation, 2001). Exit slopes were estimated by surveying the thalweg of riffles upstream and downstream of reach termini. Slopes were calculated as the difference of thalweg elevations divided by the distance between thalweg points.

XYZ cross-section data must be converted to two-dimensional data with distance expressed as distance from the river left end point. These calculations were made using a Visual Basic macro written in Excel. The macro converts the cross-section data to distance from river left end station (Microsoft Corporation, 2001). The macro uses trigonometry to place all cross-section stations on a single line running between cross section end stations (Appendix B). Distances between cross sections are given as distance from three points in each cross section: thalweg and points that delineate the beginning of overbank flow on river left and right. Thalweg distances were determined by calculating the distance between the lowest survey points in adjoining cross sections. Overbank

distances were similarly obtained, although the overbank stations were declared on the basis of field observations of changes in bank slope or local roughness. For instance, large hardwood trees flank surface channels and flow is presumably rougher within the trees. Therefore, overbank stations were set where large trees appeared on channel banks.

Individual channel cross-sections were surveyed atop riffles or rapids and in intervening pools. Cross sections were generally surveyed near the middle of each riffle or rapid depending upon the relative water velocities at those positions. The middle of the riffle was chosen except where high velocities prevent standing in that location. Pool cross-sections were surveyed in the deepest portion of the pool, which allows HEC-RAS to better characterize changes in channel shape (Hydrologic Engineering Center, 1998a,b). Additional cross sections were sometimes surveyed in pools if the pool thalweg did not change semi-linearly between riffles. Pool-riffle morphology is not present in reaches A and B of Buckeye Creek. As a result, cross sections were surveyed at roughly equal intervals along the channel.

4.3 Estimation of Particle Sizes on Streambeds

4.3.1 Wolman Counts

A wide range of particle sizes was encountered in the thirteen reaches (Tables 3.1 and 3.2)(Figure 3.7). The largest particles were boulders and coarse cobbles in headwater channels and in the Greenbrier River. Particle sizes of all particles coarser than -4 phi were estimated using Wolman counts (Wolman, 1954). A total of 100 clasts were measured at each Wolman count location. For consistency, riffles and runs were preferentially chosen for measurement localities. Multiple Wolman counts were

performed in all Greenbrier River reaches and lithology was noted for all clasts measured.

Data from individual Wolman counts were entered into Microsoft Excel, where the data were sorted in descending order. The 50th particle measurement in the sorted data was taken to be d_{50}, which is the median size of clasts on the streambed. The 16th and 84th particle measurements were similarly assumed to be representative of the 16th and 84th percentiles or d_{16} and d_{84} (Wolman, 1954).

4.3.2 Sieving

Sieving was used to determine values of d_{16}, d_{50}, and d_{84} where the bulk of bed grains were finer than -4 phi, which was the coarsest sieve screen available for use. Sediment samples were collected in plastic bags and sieved in a Rotap shaker. Sieve screens were stacked from -4 phi to 4 phi. Screen spacing was 0.5 phi and multiple sieve runs were required for the coarsest samples because the necessary stack heights exceeded that capacity of the machine. Therefore, the samples were first sieved from -4 phi to 0 phi. Material passing 0 phi was then sieved again with finer screens. The mass of grains on each sieve was determined on an electronic balance sensitive to 0.01 gram.

Data from sieve results were entered in Microsoft Excel. The results were graphically plotted as a spline curve with percent finer on the y-axis and particle size on the x-axis. Values of d_{16}, d_{50}, and d_{84} were then determined by using a right triangle to measure upward from the x-axis to the point on the spline curve corresponding to d_{16}, d_{50}, and d_{84} on the y-axis.

4.4 Substrate Resistance Characterization

4.4.1 Relative Solubility

Reaches were preferentially selected where Buckeye Creek and Greenbrier River flow atop limestone and sandstone. The limestones are from the Greenbrier Group. Limestones in the selected reaches are greater than 95% pure (McCue et al., 1939). The sandstones were chosen from the Price and Maccrady formations. The sandstones are composed of quartz grains and cemented by quartz and iron. No arkosic grains were observed in hand specimens. Although quartz sandstones are slightly soluble in natural waters, they are virtually insoluble in comparison to limestones (White, 1988). Therefore, the relative solubility of each rock type is reported as soluble and insoluble (limestone and sandstone, respectively). Presumably, the soluble limestones are less resistant to chemical erosion in the study reaches.

4.4.2 Bulk Mechanical Resistance

Hydraulic variables are positively, though complexly, correlated with rock-mass strength (Wohl and Merritt, 2001). Intact rock strength was determined using the mean of ten or more readings from a Schmidt rock hammer on planar bedrock surfaces and a standardized worksheet (Plate 2.1)(Selby, 1980). This methodology does not account for differences in chemical resistance, which is notable because the limestones consistently yielded higher rock-mass strengths than sandstones in Greenbrier River (Table 3.2).

Hammer readings were obtained away from joints or other discontinuities. For consistency of readings, hammer orientation was either vertical or horizontal for all readings from a given locality because the spring-loaded hammer appeared to give slightly different readings when the plunger was aligned horizontal versus vertical.

Observation of bedrock outcrops was used to assign one of five point values for degree of weathering, joint orientation relative to channel surfaces, joint continuity, joint width, and groundwater outflow (Plate 2.1). Degree of weathering is the least quantitative variable on the worksheet and extra emphasis was placed on consistent declaration of degree of weathering.

4.5 Declaration of Incision Processes

Evidence of incision mechanisms was sought during data collection in all bedrock reaches examined in Buckeye Creek and Greenbrier River. Mechanically driven incision processes, such as quarrying and abrasion, occur during floods, which prevent direct observation of bed erosion. As a result, incision by quarrying and abrasion is declared on the basis of erosion features observed in channels rather than by direct observation of incision phenomena (e.g., Wohl, 1993; Hancock et al., 1998; Whipple et al., 2000a,b).

Quarrying was identified on the basis of step-like ledges with missing and detached blocks. Abrasion was identified by the presence of potholes with grinders, sculpted forms, and smooth surfaces that appear relatively unweathered (Hancock et al., 1998). The unweathered, smooth surfaces were most clearly associated with abrasion on the upstream sides of boulders in the Anvil Rock reach, which occasionally displayed lineations that diverge in directions that seem appropriate for streamlines of flow passing over and around the boulders.

Corrosion was identified by the presence of scallops and corrosion tubes in soluble strata (Blumberg and Curl, 1974; White, 1988; Springer et al., 1997). Many sculpted forms can be created by abrasion and corrosion, so anastomose tubes and

corrosion pitting were especially valuable evidence of corrosion (Springer, 2002a). Using these criteria, the principle incision mechanisms in each reach were identified.

Corrosion was evident in all limestone reaches. Evidence of abrasion was only observed in reach B in Buckeye Creek and Anvil Rock in Greenbrier River. Abrasion is especially evident where large boulders constrict the channel at Anvil Rock. Sandstone boulders display potholes up to a meter in diameter, flutes on upstream faces, and complex sculpted forms on downstream faces.

4.6 Declaration of Geomorphic Setting

4.6.1 Buckeye Creek Catchment

Geomorphic processes vary as a function of basin area, hillslope interactions, and a variety of other variables (Hack, 1957). For instance, reaches A and B in Buckeye Creek lie closer to debris flow-generating tributaries and receive coarser sediment from hillslopes than downstream reaches. Geomorphic elements on the surface in the Buckeye basin include stream segments inside and outside of the karst depression. The depression was defined as all surfaces downstream of the 1950-foot contour elevation, which is the highest closed contour line on the associated 1:24000 Williamsburg topographic map. The remaining stream segments are those that lie in Buckeye Creek Cave and which occur in a completely different geomorphic setting than surface reaches upstream of the cave entrance. The broad divisions among geomorphic locations in Buckeye Creek Cave are used in discussions concerning changes in stream processes from reach to reach.

4.6.2 Greenbrier River

The role of geomorphic setting is explicitly investigated in Greenbrier River using Hypothesis III. Reaches were classified and chosen on the basis of their interaction with adjacent hillslopes. Reaches are classified as either having minimal interaction, bedrock cutbanks, or receiving coarse sediment directly from hillsides. Minimal interaction refers to reaches that are isolated from valley walls by floodplains or terraces (Bone Quarry and Mile-27 reaches). In contrast, other reaches have vertical cliffs lining one bank. These bedrock cutbanks are associated with coarse sediment generated by rockfalls and local cliff collapses (Acme Quarry, Anvil Rock, and Cathole reaches). Anvil Rock also receives large, sandstone boulders from adjacent hillslopes because overlying canyon walls are capped by a resistant sandstone. The geomorphic setting of each reach is used in discussions and analyses in Chapter 7.

4.7 Modeling in HEC-RAS

4.7.1 Open Channel Roughness Estimates

4.7.1.1 Buckeye Creek. HEC-RAS requires knowledge of channel roughness (Manning's n). Values of n can be determined iteratively if water-surface elevation(s) and discharge are known for a flood. The observed discharge is entered into HEC-RAS and n varied until the computed water-surface elevations match the observed values. This technique could not be applied in Buckeye Creek because no large floods occurred during the course of this study and there is no historic gage record. Therefore, roughness was visually estimated for surface and subsurface channels. Thick vegetation, coarse bed sediments, and small channel sizes characterize surface segments. Small willows and

grasses grow in the channel atop the depression floor and greenbriers cover adjacent banks and floodplain surfaces. Hardwood trees mantle channel banks in the headwaters and large woody debris is common in the channel. On the basis of the observed roughness elements, Manning's n was estimated as 0.04 throughout the surface reaches.

Channel cross-sections are extremely uniform in the cave reaches except in the vicinity of the cave entrance. Channels are smooth-sided trapezoids or rectangular. Thick vegetation is absent and channel banks are often streamlined from erosion and smoothing by previous floods. Therefore, Manning's n was estimated as between 0.03 and 0.05 in the cave. The lesser values were used where the channel is uniform and straight with a gravel bed (Figure 3.11A). Higher values were used only in constrictions and atop coarse sediments (Figures 3.6, 3.8A, and 3.11C).

4.7.1.2 Greenbrier River. A water-surface elevation and discharge are known for the flood of record in the Acme Quarry reach of the Greenbrier River (Springer, 2002). The discharge is an estimate provided from USGS stream gage #03183500 at Alderson, WV. The stream gage is located 5 km downstream of Acme Quarry, but the only intervening tributaries are derived from the immediate valley walls. The water-surface elevation was obtained in a small cave in the channel banks on river right at Acme Quarry. The PSIs consist of rings of silt and organic material on passage ceilings and walls. Millimeter-scale Styrofoam balls were used to identify the rings as being historic deposits (Springer, 2002). The height of the rings above the thalweg was determined using the TopCon laser theodolite. Survey paths were not straight; therefore multiple survey legs were used in the cave.

The lack of higher deposits, similarity of reconstructed flow depths to resident observations of the historic flood, and the association of the deposits with abundant flotsam derived from damaged residences strongly suggested that the highest deposit is the product of the flood of record, which caused extensive damage to several towns upstream of the reach (Springer, 2002).

A Manning's n value was calculated using the PSI and discharge estimate. Normal depth was assumed at the downstream boundary and Manning's n was varied in the Acme Quarry reach until the computed water surface matched the stage known for the record 2650 $m^3 s^{-1}$ discharge at the midpoint of the reach. A value of n=0.041 reproduced the known stage. The estimated Manning's n value was then used to approximate channel roughness for large floods in the other reaches of Greenbrier River. Values of n=0.045 were used in all reaches except at Anvil Rock where a Manning's n of 0.051 was used because of the coarse boulder bed and prominent constrictions.

4.7.2 Flood Discharges for Hydraulic Models

4.7.2.1 Greenbrier River. Representative discharges are necessary for hydraulic models of flooding in bedrock rivers. The 100-year flood has been used in some studies for which gaging records are available, but paleodischarges are commonly recovered by matching computed water-surface profiles to the highest available paleostage indicators (e.g., Wohl et al., 1999). Both methodologies are adopted in this study.

Discharges for the 100-yr flood are used in all of the Greenbrier River reaches. Flood magnitudes with longer return periods may be more important than the 100-yr flood for channel incision, but existing gaging data do not allow reliable calculation of the magnitude of floods with greater return intervals (e.g., 500-yr flood). Choice of the

100-yr flood does not represent an assumption that it is the most effective flood for geomorphic change. Rather, the choice is one of convenience in the face of limited data concerning the size of channel altering floods.

Modeled discharges were estimated using gage records and the flood recurrence analysis program EMA (England, 1999). A 71-year record of annual peak discharges is available for the Renick reaches using U.S. Geological Survey (USGS) gage #03182500 at Buckeye, WV. A 105-year record of annual peak discharges is available for the canyon reaches using USGS stream gage #03183500 at Alderson, WV. The 100-yr flood at the Buckeye gage is estimated as 1800 $m^3 s^{-1}$. The 100-yr flood at Alderson is estimated as 2300 $m^3 s^{-1}$.

4.7.2.2 Buckeye Creek Cave. Paleodischarges can be estimated in caves using scallops. Scallops are geometrical arrangements of asymmetrical concavities that form by corrosion and abrasion of channel margins. The population statistics of scallops are discretely related to passage size and some formative discharge (Blumberg and Curl, 1974; Lauritzen et al., 1985; Lauritzen and Lundberg, 2000). The walls of several reaches of the Buckeye Creek Cave stream are covered with scallops and therefore amenable to paleodischarge calculations.

The largest collection of scallops is in the canyon (reach F), downstream of the entrance passage. Empirical and theoretical work by Blumberg and Curl (1974) and Curl (1974) established that the relationships between scallop lengths (L), channel width (D), and mean flow velocity ($\bar{u}$) in straight reaches of parallel-walled channels can be described by a set of equations that are combined herein to yield:

$$\bar{u} = \frac{\upsilon}{L_{32}} Re^{*}[2.5(\ln \frac{D}{2L_{32}} - \frac{3}{2}) + B_L] \ . \qquad (4.1)$$

where υ is kinematic viscosity. L_{32} is the Sauter mean scallop length (L^3/L^2), Re^* is the Reynolds number calculated using the shear velocity, and B_L is a roughness geometry coefficient. Blumberg and Curl (1974) determined that Re^* and B_L are constants with approximate values of 2200 and 9.4, respectively. Thus, by measuring D and L and choosing a temperature-dependent value of υ, we can obtain an estimate of the mean flow velocity ($\bar{u}$) and secondarily a discharge estimate.

Scallops are concavities excavated where laminar jets of fluid impinge on adjacent surfaces (Figure 4.1). The distance an individual jet travels is a function of its own momentum and the momentum of fluids it is passing through. Eventually, each jet destabilizes and turbulence results. The now turbulent fluids impact the wall, which is preferentially eroded at the point of reattachment. The distance to the onset of turbulence is inversely proportional to the rate of momentum exchange between intra- and extra-jet fluids. Momentum exchange rates are highest for large Reynolds number flows, e.g. floods, therefore floods cause shorter reattachment lengths. Floods are also the most erosive events in caves, therefore the mean velocity of the most geomorphically effective floods in karst conduits will determine the size of scallops on passage walls (Blumberg and Curl, 1974; Curl, 1974; Lauritzen et al., 1985).

Measurements reveal that L_{32} = 4.6 cm in straight reaches of the canyon. Assuming a water temperature of 10° C, the mean pipe-full velocity in the canyon is

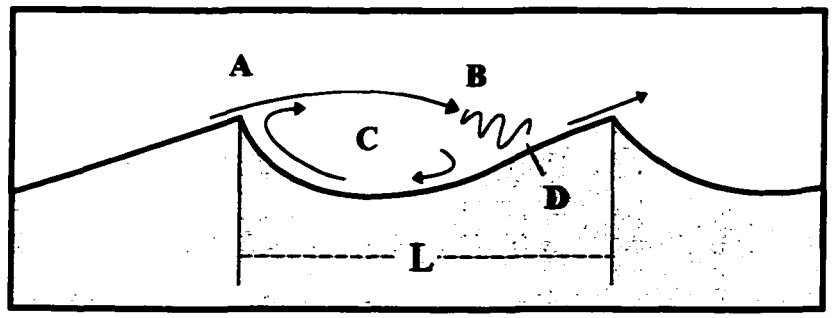

Figure 4.1: Longitudinal cross section through the center of a scallop. A is a laminar jet within the turbulent boundary layer. B is onset of turbulence in the laminar jet caused by interaction with adjacent fluids. C is a recirculating, coherent vortex in the concavity (scallop). D is the location locus of jet reattachment, which is also the site of greates erosion. L is the length of the scallop. Modified from Blumberg and Curl (1974).

estimated as 0.90 m s^{-1} and discharge as 9.5 m^3 s^{-1}. Lauritzen et al. (1985) found empirically that scallops record the upper-most flood regime, suggesting that the velocity and discharge estimates are representative of a relatively infrequent, but formative flow. Validation of this technique has come from comparisons of scallop-based discharge estimates and direct gaging of flood flows (Lauritzen et al., 1985; Lauritzen and Lundberg, 2000).

4.7.2.3 Buckeye Creek Surface Channel. This study examines flow in three discrete reaches of the Buckeye Creek surface channel. However, the only paleostage known for surface flooding in the Buckeye Creek basin is the high water mark associated with the flood of record at the entrance to Buckeye Creek Cave. Gene Turner, owner of the cave, reports that a flood in the mid- or late-1940's reached the first floor windowsills of a residence standing 80 m from the cave entrance. However, this stage was associated with backflooding created by the entrance constriction. Therefore, the stage is only useful for estimating maximum hydrostatic pressure at the pipe-full cave entrance.

Paleodischarge estimates made using scallops in Buckeye Creek Cave each yield instantaneous runoff values of approximately 0.7 $m^3 km^{-1} s^{-1}$. Instantaneous runoff rates generally increase headward, so the calculated value is probably low for headwater channels (Smith et al., 1996). The value represents high magnitude, low recurrence interval floods that are known to be the most effective agents of channel change in bedrock streams (Lauritzen et al., 1985; Baker, 1988). Therefore, the instantaneous runoff value of 0.7 $m^3 km^{-1} s^{-1}$ was multiplied by reach catchment areas to yield discharge values that are presumably large floods (Table 3.1).

The instantaneous runoff value used for Buckeye Creek is lower than those calculated using the 100-yr flood for both the Renick reaches. Instantaneous runoff for each location is estimated as approximately 1 $m^3 km^{-1} s^{-1}$ on the basis of discharge estimates made using EMA and drainage areas obtained from USGS DEMs. The assumption that large, cave-filling floods cannot generate larger values of ω and τ than those obtained from the open channel models should not be made. This study is conducted under the assumption that the modeled open channel flood provides a useful datum with which to begin a quantitative exploration of hydraulic adjustments in streams flowing across multiple substrates. Further work should examine the hydraulics of cave-filling floods.

4.7.3 Modeling Technique

4.7.3.1 Flow Conditions. Thirteen reaches in Buckeye Creek and the Greenbrier River were modeled using HEC-RAS. The model assumes uniform, gradually varied flow (Hydrologic Engineering Center, 1998b). HEC-RAS calculations may be performed under assumptions of subcritical, critical, and mixed flow regimes. Subcritical flow was

assumed for all reaches except the Buckeye Creek headwater reach (labeled D in Figure 3.7). The headwater reach is steep and includes several abrupt bed drops associated with channel-spanning boulders and bedrock steps. Therefore, mixed flow conditions were assumed. Small hydraulic jumps form in the entrance of Buckeye Creek Cave during small floods, but witness observations and photographs of large floods indicate that subcritical flow prevails in the cave mouth during large floods despite a steep bed gradient and coarse bed (Figure 4.2). Presumably, a series of constrictions in the first 25 m of the stream induce large flow depths and maintain subcritical flow.

4.7.3.2 Model Construct. The construct and equations applied in HEC-RAS are discussed in a manual that accompanies the program (Hydrologic Engineering Center, 1998b). In brief, HEC-RAS utilizes an open-channel version of the energy equation to calculate water-surface profiles. Channel geometry is entered, but the user must also specify roughness values (n), discharge, and at least one boundary condition.

A boundary condition, such as the water-surface elevation at the downstream cross section for subcritical flow, is used to begin calculations. Large floods did not occur on either stream during this study and paleostage indicators are absent in Buckeye Creek Cave. Therefore, normal depth was presumed to prevail at downstream boundaries. HEC-RAS estimates normal depth by assuming that local energy expenditure, as measured by the energy slope (S_e), equals input of potential energy into the system as measured by the bed slope (S_o). Discharge (Q) divided by cross-section area (A) is substituted for mean velocity in the Manning equation, which is then solved for the depth that satisfies the relationship:

$$\frac{Q}{A} = \frac{R^{2/3} S_o^{1/2}}{n} \quad , \qquad (4.2)$$

where R is hydraulic radius. HEC-RAS requires input of the channel slope downstream of the terminal cross section. This value is averaged with the bed slope between the terminal cross section and first upstream cross section to yield the bed slope used in the calculation (Hydrologic Engineering Center, 1998b).

4.8 Statistical Analyses

4.8.1 Buckeye Creek Reaches

Model output for Buckeye Creek is used to evaluate the corollary hypothesis developed in conjunction with Hypothesis I, that Buckeye Creek has adjusted flow properties to minimize τ and ω where incision can be accomplished primarily by chemical phenomena. A total of eight reaches were modeled in Buckeye Creek. The sheer number of comparisons in large datasets increases the likelihood of falsely declaring significant differences when each datum is compared to another using t-tests. Therefore, the eight reaches in Buckeye Creek are statistically evaluated using the Student-Newman-Keuls (SNK) multiple comparison test. The SNK procedure is also used in sensitivity analyses in Buckeye Creek.

The SNK procedure yields groups of means lacking significant differences. The SNK procedure, like other multiple comparison techniques, was developed to minimize the number of falsely declared differences during comparisons of many means. The SNK procedure attempts to minimize comparison errors by ranking means and then performing step-wise comparisons that factor in rank and mean differences (Ott, 1992). As a result,

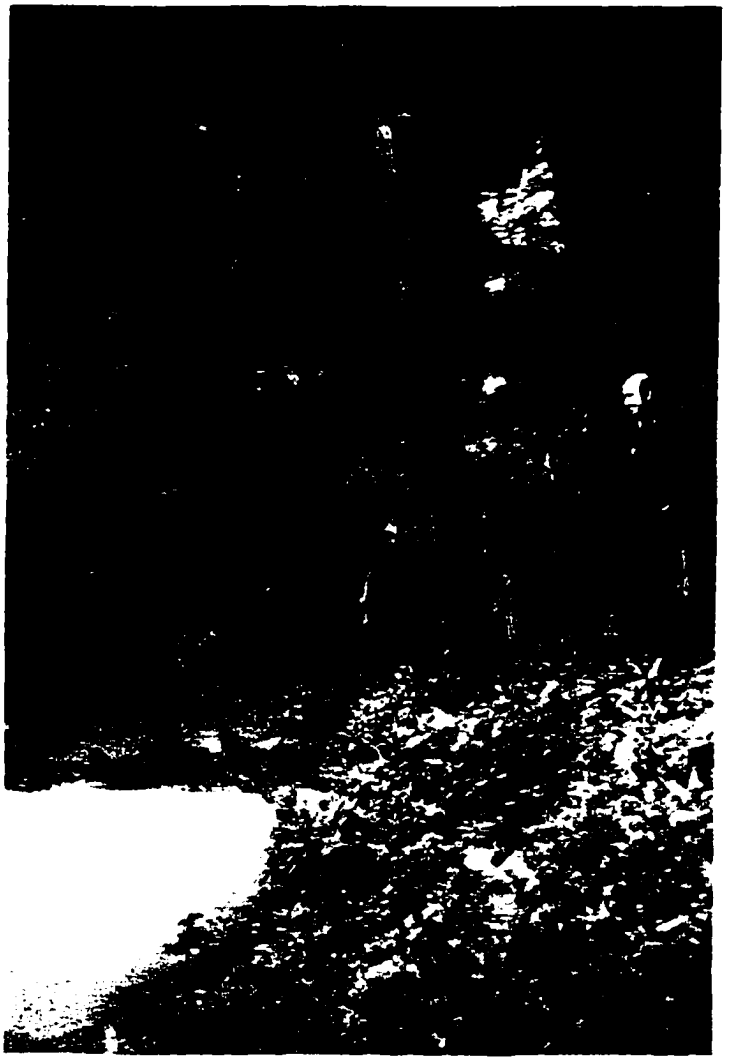

Figure 4.2: Undated photograph of floodwaters entering Buckeye Creek Cave. The flood is believed to have been caused by remnants of Hurricane Agnes in late June, 1972. Flow depth in the cave mouth is approximately 3.5 m. Note lack of a hydraulic drop in cave mouth. Photograph courtesy of Dr. David Culver (American University).

the SNK procedure is more conservative and the results are more readily interpreted than a large table of individual comparisons (Ott, 1992).

4.8.2 Greenbrier River Reaches

Reaches of the Greenbrier River were chosen to allow comparisons of τ and ω as functions of substrate and geomorphic setting. As a result, the preplanned comparisons are statistically analyzed using Student t-tests of mean values of τ and ω between selected reaches. The six planned comparisons and related variables are shown in Table 4.1. Four of the comparisons hold either substrate or geomorphic setting constant. The remaining two comparisons are influenced by interactions; neither set of controlling variables is held constant.

Table 4.1: Planned T-tests for Greenbrier River Reaches

Hypotheses Tested	Reaches Compared	Substrate Comparison[a,b]	Geomorphic setting Comparison[a,b]
I	Bone Quarry vs. Mile-27	Ls vs. Ss	No Cutbank vs. No Cutbank
I	Cathole (Ls) vs. Cathole (Ss)	Ls vs. Ss	Cutbank vs. Cutbank
I, III	Cathole (Ls) vs. Mile-27	Ls vs. Ss	Cutbank vs. No Cutbank
I, III	Bone Quarry vs. Cathole (Ss)	Ls vs. Ss	No Cutbank vs. Cutbank
III	Bone Quarry vs. Cathole (Ls)	Ls vs. Ls	Cutbank vs. No Cutbank
III	Anvil Rock vs. Acme Quarry	Ls vs. Ls	Ss Boulders vs. No Ss Boulders

[a] Ls denotes limestone. Ss denotes sandstone.

[b] Variables are ordered respective to ordering of reaches in second column.

Chapter 5

Erosion by Sculpted Forms[1]

5.1 Chapter Abstract

Recognition of the important roles sculpted forms play in channel erosion has not translated to knowledge of the controls on their growth or appearance. Empirical evidence from sculpted forms eroded into limestones within Buckeye Creek Cave show that the types of flow or vortex structures present within sculptures during floods determine sculpture morphology. Small hemispherical sculptures maintain constant form as they enlarge. These structures occupy fixed locations on channel walls because of their association with joints, styolites, and bedding planes. Taking advantage of the systematic growth and stability of the sculptures, a geometrical model of sculpture growth is presented that relates the effects of sculpture size, form, and wall retreat to the relative erosion efficiencies and excesses required for sculpture growth. Numerical results obtained from the theoretical model reveal that small sculptures must erode more efficiently than large sculptures or they will be removed by wall retreat, and that erosion rates must increase exponentially with increasing concavity. Relative to channel erosion,

[1] The contents of this chapter are also presented in: Springer, G.S. and Wohl, E.E., 2002. Empirical and theoretical investigations of sculpted forms in Buckeye Creek Cave, West Virginia. *Journal of Geology*, 110:469-481.

small sculptures must possess very high interior erosion rates where nearby surfaces are rapidly eroding. Therefore, small sculptures are unlikely to form or persist on rapidly eroding surfaces. The results suggest that sculpture morphology may not be independent of channel erosion rates, and that the location and size of sculpted forms in bedrock channels may reflect a wider array of variables than has previously been supposed. These findings complicate attempts to evaluate knickpoint erosion using sculpted forms because sculpture morphology is not solely dependent upon channel hydraulics.

5.2 Introduction

A fundamental question in the study of bedrock channels is the relationship of sculpted forms to channel erosion. Sculpted forms, which are smooth concavities eroded into channel perimeters, can enhance abrasion and corrosion by directing corrosive and abrasive fluids and particles to channel margins (Table 5.1)(Blumberg and Curl, 1974; Hancock et al., 1998). Hypothetically, morphology of sculpted forms may be related to bulk channel hydraulics, incision rates, or neither (e.g., null and research components of Hypothesis II). If sculpted forms are related solely to channel hydraulics then it may be possible to model erosion of channel segments wherein sculpted forms are the most common erosion features such as portions of Buckeye Creek Cave (Figure 5.1). However, fundamental studies of sculpted forms are lacking and their discrete relationship(s) to channel incision and hydraulics have been the subject of only three previous studies (Alexander, 1932; Blumberg and Curl, 1974; Wohl et al., 1999).

Individual sculptures are the result of localized abrasion and corrosion caused by non-random deflections of near-wall fluids and particles toward a location on the channel

Figure 5.1: Examples of sculpted forms in the narrow canyon passage in Buckeye Creek Cave. A: Field of scallops with a reverse-flow pocket above marker. Note that the pocket lacks the asymmetry of scallops and appears to have enlarged from an especially large scallop. Asymmetrical etchings within the pocket record recirculating flow. Freestream flow is from right to left. B: A bracketed pair of pockets on the inside apex of a channel bend lacking scallops. Freestream flow is from left to right. C: A large lateral pothole with pronounced upward tapering. Scallops record recirculating, descending flow within the lateral pothole. Note Brunton compass for scale. Freestream flow is from right to left.

Table 5.1: Sculpted forms.

Name	Length Range (cm)	Position[b]	Description of Concavity	Selected Reference(s)
Flute	0.5 to 20	Mig.	Tear-drop plan; broad, steep face beneath upstream lip	Allen (1968; 1971)
Lateral Pothole	20 to 200	Fixed	Hemisperical or hemi-elliptical cylinder	Zen and Prestegaard (1994)
Pocket	2 to 20	Fixed	Hemispherical or hemi-elliptical	defined herein
Pothole	5 to 400[a]	Fixed	Cylinder open at top	Alexander (1932); Sato and Hayami (1987)
Scallop	1 to 50	Mig.	Similar to flutes, but more equant; all lips are shared with adjacent scallops	Blumberg and Curl (1974); Lauritzen et al. (1985)
Undulating Wall	100 to 400	Fixed	Channel expansion symmetrical across thalweg; widths taper upward	Wohl et al. (1999)

[a]Diameter
[b]Stability of position atop a surface. Mig. denotes migration across channel walls.

perimeter during floods. Deflection may initially arise from a local protrusion or defect on the channel perimeter, but enhanced erosion at a reattachment point increases the deflection of succeeding flows by excavating a concavity which perturbs flows through streamwise momentum exchange (Blumberg and Curl, 1974).

The ability of sculpted forms to enhance channel erosion is most important where massive or resistant strata suppress quarrying (Hancock et al., 1998). Observational studies have shown that sculpted forms may be the dominant agents of channel incision and widening in such settings (Hancock et al., 1998; Wohl, 1998; Whipple et al., 2000a). Massive and resistant strata are often associated with channel knickpoints that cannot be readily treated by landscape modelers using stream power laws because of uncertain relationships between sculpted forms, channel erosion, channel hydraulics, and basin hydrology (Hancock et al., 1998; Whipple et al., 2000a,b). Future advances in modeling channel incision within knickpoints may thus be dependent upon discerning quantitative

relationships between sculpted forms, channel erosion, hydraulics, and basin hydrology (Hancock et al., 1998; Whipple et al., 2000a).

The assumption that sculpture growth and morphology reflect a response to substrate-induced hydraulics is crucial to the development of empirical or theoretical models of channel incision by sculpted forms in knickpoints. The population statistics of scallops, polygonal sculpted forms that develop within turbulent boundary layers, are known to reflect mean channel hydraulics, and hydraulics may be subsumed into empirical models that accommodate the effects of basin area, channel gradient, and rock resistance (e.g., Blumberg and Curl, 1974; Curl, 1974; Whipple et al., 2000b). However, sculpted forms that directly exchange fluids with flow outside of the turbulent boundary layer have no known statistical correlations with channel hydraulics despite speculation that relationships may exist (e.g., Zen and Prestegaard, 1994; Hancock et al., 1998). Most sculpted forms examined here are large when compared to the turbulent boundary layer, and are developed upon soluble bedrock by corrosion and abrasion. The results are nonetheless applicable to sculpted forms developed upon other substrates because the processes by which sculpted forms are created are independent of substrate (Allen, 1971; Blumberg and Curl, 1974; Curl, 1974). For instance, Wohl et al. (1999) compared the properties of undulating walls to a wide array of substrate variables. No correlation was found between the properties or occurrences of undulating walls relative to substrate variables. This led the authors to conclude that the properties of undulating walls are attributable to channel hydraulics and not substrate characteristics.

Local erosion processes are known to affect whether sculpted forms are present within a channel. Quarrying generally erodes substrate more quickly than abrasion or

corrosion can excavate sculptures, and thus acts to suppress or prevent sculpture formation (Hancock et al., 1998; Whipple et al., 2000a). This does not mean that sculpted forms predominate in all channels that are eroded primarily by abrasion or corrosion. For instance, undulating walls occupy comparatively short reaches of the abrasion-dominated slot canyons examined by Wohl et al. (1999), and other sculpted forms were not observed. Either channel hydraulics preclude sculpture formation elsewhere in the canyons, or other factors need to be considered. Factors not addressed by prior research on sculpted forms include the influence of surface erosion adjacent to sculptures, and the rates of erosion on those surfaces. Isolated sculptures must establish themselves atop an eroding surface by outpacing wall retreat or they will be removed by truncation. If, as hypothesized and explored herein, sculpture growth and morphology are influenced by erosion rates, then morphology may vary atop the same substrate within a channel in a manner that is not purely dependent upon channel hydraulics. This would impose previously unrecognized limits on the usefulness of sculpted forms for paleohydrologic reconstructions and empirical models of channel incision. This study uses the fortuitous association of parasitic sculptures with larger sculpted forms atop eroding walls to simultaneously explore the relationships between sculpture morphology, flow fields, and the effects of erosion rates. The empirical data define relationships between flow fields and sculpture morphology and are used to interpret the results of a theoretical model that relates sculpture growth to erosion of adjacent surfaces. The model output is used to evaluate Hypothesis II, that the geometry of sculpted forms is not related to erosion atop adjacent surfaces.

5.3 Study Reach Characteristics

The sculpted forms examined for this component of the study are found in the slot-like canyon near the upstream entrance to Buckeye Creek Cave (reach F)(Figure 3.2). The canyon passage is 6-m high, 1.5- to 2-m wide, and formed within fossiliferous biomicrites and oosparites. The canyon begins where a 9-m wide, 7-m high passage abruptly ends in a massive sediment plug on river right. Water exits the passage by turning 90° and flowing into the canyon on river left. The bed of the canyon is primarily bedrock and the gradient is equal to the overall stream gradient (0.01 m m^{-1}). Log jams form intermittently at the upstream terminus and mid-point of the canyon. Gravel may accumulate to depths of 30 cm behind the logjams, but is flushed through the canyon following disintegration of the logjams. The canyon follows rectilinear joints that produce five 90° bends. Erosion of bend corners has resulted in smooth, curvilinear plans.

Unlike adjoining passages within the same lithologic units, nearly all surfaces of the canyon are covered by scallops, pockets, and lateral potholes (Figure 5.1). Scallops are common in subterranean stream constrictions as a result of comparatively high velocities and lateral momentum gradients that enhance wall abrasion and corrosion (Curl 1974). The large number of sculpted forms offers a statistically viable population for empirical study of sculpted form morphology.

5.4 Methodology

Sculpted forms cover virtually all surfaces of the narrow canyon passage in Buckeye Creek Cave and three dominant types were recognized: scallops, pockets, and lateral potholes. Using the criteria of Allen (1971) and Blumberg and Curl (1974), scallops are readily identified as polygonal arrangements of concavities with

asymmetrical profiles (Figure 5.1A). Lateral potholes were first described by Zen and Prestegaard (1994) from a paleochannel of the Potomac River, Maryland and are recognized as comparatively large concavities in vertical or near-vertical channel walls. Individual concavities may resemble hollow, bisected cylinders, hemispheres, hemi-ellipses, or upright teardrops (Figure 5.1C). An intermediate class of sculptures was identified during fieldwork and termed pockets. Pockets resemble hollow, bisected hemispheres or hemi-ellipses and are therefore similar in form to lateral potholes. Pocket morphology is more varied than lateral pothole morphology and internal flow fields of pockets are far more diverse (discussed below).

Measurements of scallop, pocket, and lateral pothole dimensions in the canyon were made using rulers and fiberglass tapes. Scallops were measured along their longest axis within two straight segments with parallel walls within the canyon for paleodischarge calculations (e.g., Curl, 1974). Pocket dimensions were measured along three perpendicular axes for all pockets located within 2.5 m of the channel bed (n=50; Figure 5.2A). A similar set of measurements was made for 16 lateral potholes. The orientations of scallops and other asymmetrical etchings within lateral potholes were used to determine internal flow field orientations relative to the freestream. The four possible flow fields are forward, reversed, vertical, and indeterminate (no scallops). Forward flow is defined as flow in the cavity occurring in the same direction as that of flow along the thalweg. Reversed flow is defined as recirculating, vortical flow along a vertical axis in opposition to that in the thalweg. Vertical flow is defined as upward or downward movement of water within a concavity. All four flow fields were represented within the sample of pockets (Table 5.2). Scallops record reverse flow in all lateral potholes.

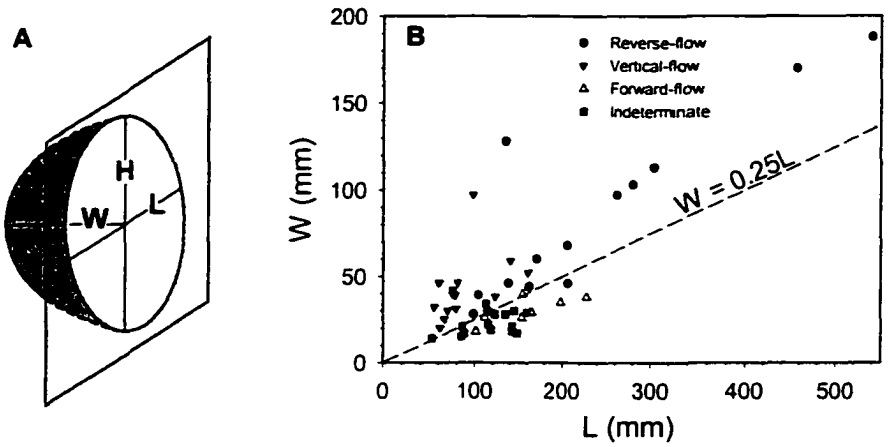

Figure 5.2: A: Schematic diagram of a pocket. The dimensions length (L), width (W), and height (H) were measured for each pocket and lateral pothole. B: A plot of L vs. W by flow classification for all pockets.

Table 5.2: Pocket summary statistics

Flow Direction	n	L (mm)[a,b]	W (mm)[a,b]	H (mm)[a,b]	W/L[a,b]	W/H[a,b]	L/H[a,b]
Forward	7	160 ±45	32 ±10	120 ±26	0.20 ±0.06	0.26 ±0.07	1.29 ±0.28
Indeterminate	15	120 ±30	23 ±6	110 ±35	0.20 ±0.05	0.21 ±0.06	1.09 ±0.22
Reversed	14	230 ±133	83 ±52	270 ±179	0.37 ±0.17	0.32 ±0.10	0.91 ±0.27
Vertical	14	160 ±21	43 ±19	140 ±40	0.51 ±0.19	0.33 ±0.15	0.67 ±0.27
Total	50	150 ±93	46 ±38	170 ±117	0.34 ±0.19	0.28 ±0.11	0.95 ±0.33

[a] L denotes length; W denotes width; H denotes height.

[b] Mean ± one standard deviation.

Empirical and theoretical work by Blumberg and Curl (1974) and Curl (1974) established that the relationships between scallop length (L), channel width (D), and mean flow velocity ($\bar{u}$) in straight reaches of parallel-walled channels can be described by a set of equations that are combined herein to yield:

$$\bar{u} = \frac{\nu}{L_{32}} Re^{*}[2.5(\ln\frac{D}{2L_{32}} - \frac{3}{2}) + B_L] , \qquad (5.1)$$

where ν is kinematic viscosity, L_{32} is the Sauter mean scallop length (L^3/L^2), Re^* is the Reynolds number calculated using the shear velocity, and B_L is a roughness geometry coefficient. Blumberg and Curl (1974) determined that Re^* and B_L are constants with approximate values of 2200 and 9.4, respectively. Thus, by measuring D and L and choosing a temperature-dependent value of ν, estimates can be made of the mean flow velocity ($\bar{u}$), and secondarily, discharge. In straight reaches of the canyon, L_{32} = 4.6 cm. Assuming a water temperature of 10° C, the mean pipe-full velocity in the canyon is estimated as 0.90 m s^{-1} and discharge as 9.5 m^3 s^{-1}. Lauritzen et al. (1985) found empirically that scallops record the upper most flood regime, suggesting that the velocity and discharge estimates are representative of a relatively infrequent, but formative, flow. Validation of this technique has come from comparisons of scallop-based discharge estimates and direct gaging of flood flows (Lauritzen et al., 1985; Lauritzen and Lundberg, 2000).

5.5 Results of Field Study

5.5.1 Origin of Scallops and Pockets

Small pockets are readily distinguishable from scallops by their lack of oversteepened upstream faces (Figure 5.1B). However, the presence of small pockets in

fields of scallops suggests that some pockets may be preferentially enlarged scallops (Figure 5.1A). This may be explained by the fact that 49 of 50 pockets lie on a styolite, joint, or intersection of two or more of these planar features. By inference, pockets represent concavities developed upon small-scale defects in otherwise smooth surfaces and by over-deepening of scallops that develop on defects. Horizontal joints, styolites, and bedding planes are associated with forward-flow pockets whereas vertical-flow pockets invariably follow vertical joints and styolites. The dependence of pockets upon defects suggests that pockets are anchored in place. By comparison, individual scallops migrate laterally as they erode a surface. Reattachment of laminar jets behind small-scale obstacles within the turbulent boundary layer localizes erosion and initiates scallop formation (Blumberg and Curl, 1974). The momentum transfer rate from the freestream determines the reattachment lengths and thereby scallop lengths, but erosion of scallop lips causes lateral migration (Blumberg and Curl, 1974). Large sculpted forms are occupied by flow separations or large, coherent vortices that protrude outside of the turbulent boundary layer and may remain fixed in position only if they enlarge proportionally in all directions.

5.5.2 Pocket Morphology and Internal Flow Fields

Using the asymmetries of small sculptures inside of pockets, three flow fields were identified in pockets: forward, reversed, and vertical. Those pockets without smaller sculpted forms were categorized as indeterminate. Pocket dimensions are summarized by flow category in Table 5.2. The ratio of pocket dimensions can be used to describe pocket morphology (Table 5.2; Figure 5.3A). Larger values of L/W and H/W indicate greater concavity, whereas larger values of L/H indicate greater eccentricity of pocket apertures.

Forward- and indeterminate-flow pockets possess similar form ratios, and statistical tests for differences between W/L are non-significant (p=0.83). Hence, forward- and indeterminate-flow pockets were combined into a single forward-flow category and only three flow categories are used in subsequent analyses. T-test comparisons of form ratios by flow classification yields highly significant differences for all but one comparison (Table 5.3). By inference, the type of flow field present within a pocket determines the morphology of the pocket. Interpreting the ratios in Table 5.2, one sees that forward-flow pockets are elongated in the direction of internal flow (L/H > 1). Vertical pockets are similarly elongated along the direction of internal flow (L/H < 1), and reverse-flow pockets possess essentially equant aperture faces (L/H ≈ 1). The type of flow field present within a pocket may not be fixed. Forward-flow pockets may deepen to become vertical- or reverse-flow pockets, and truncation of these two pockets types can create forward-flow pockets.

Concavity, as measured by values of W/L and W/H, is greatest for reverse- and vertical-flow pockets and least for forward-flow pockets (Table 5.2). The appearance of recirculation in channel enlargements is determined by the degree of concavity. Plotting L vs. W for all pockets shows that non-forward flow occurs in those pockets with W/L > 0.25 (Figure 5.3B). The plot also shows that the three classes have relatively distinct relationships. This result is to be expected given the statistical differences that exist between them (Table 5.2), but the plot indicates that there may be linear relationships between dimension lengths. Linear regression of L, W, and H upon one another by flow classification yields significant correlations for 7 of 9 possible regressions (Table 5.4). From the results in Tables 5.3 and 5.4 the author concludes that, in general, pocket

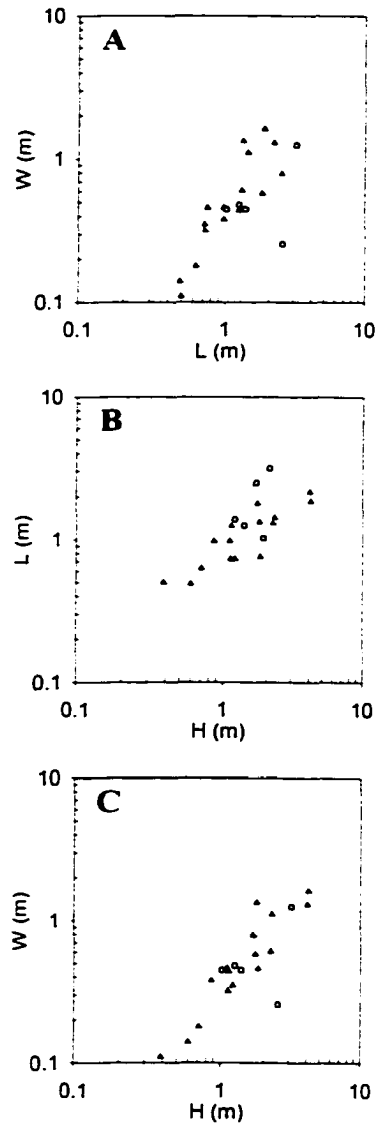

Figure 5.3: Logarithmic plots of axes measurements versus one another for lateral potholes observed in the canyon (triangles) and within quartzites and schists along the Potomac River, Maryland (open circles; Zen and Prestegaard, 1994). Axes lengths scale with one another, which suggests systematic enlargement of lateral potholes. The similarity in forms between the two sets of potholes suggests that their morphology is independent of substrate or erosion processes.

Table 5.3: Comparisons of pocket morphology variables

a. T-test comparisons of W/L values by flow classification.

Flow Direction	Reversed[a]	Vertical[a]	Forward[a]
Reversed	-	-1.97 (0.06)	-3.63 (<0.01)
Vertical	-	-	-5.96 (<0.01)
Forward	-	-	-

b. T-test comparisons of W/H values by flow class.

Flow Direction	Reversed	Vertical	Forward
Reversed	-	-0.015 (0.88)	-3.09 (0.01)
Vertical	-	-	-2.31 (0.04)
Forward	-	-	-

c. T-test comparisons of L/H values by flow class.

Flow Direction	Reversed	Vertical	Forward
Reversed	-	2.35 (0.03)	2.72 (0.01)
Vertical	-	-	5.38 (<0.01)
Forward	-	-	-

[a] Student T-statistic with significance level in parentheses.

Table 5.4: Linear regression of pocket dimensions

Regressing	Flow Direction	Slope	R^2	Significance Level
W on L	Reversed	0.35	0.78	<0.01
	Vertical	0.27	0.21	0.10
	Forward	0.14	0.42	<0.01
W on H	Reversed	0.23	0.64	<0.01
	Vertical	0.16	0.12	0.24
	Forward	0.13	0.25	0.02
L on H	Reversed	0.57	0.59	<0.01
	Vertical	0.46	0.33	0.03
	Forward	0.62	0.55	<0.01

morphology is determined by the type of flow that predominates within the sculpture. This relationship and the gradation of sizes leads to the conclusion that the concavities are self-sustaining and enlarge systematically.

5.5.3 Lateral Potholes

The largest sculpted forms observed in the canyon are lateral potholes (Figure 5.1C). The lateral potholes are of similar shape to those developed in quartzites and schists (Zen and Prestegaard, 1994), but are far more numerous and display a larger size range than described by Zen and Prestegaard (1994). Plots of the dimensions show that lateral potholes enlarge systematically but non-linearly (Figure 5.3).

Scallops within individual lateral potholes of Buckeye Creek Cave record vortex structure and relative flow strengths. Scallops record recirculating flow in all lateral potholes with flows descending at angles of 10-30° from the horizontal. The highest velocities (smallest scallops) occur along the top and downstream surfaces, whereas large scallops suggest flow is slowest along the bottom and upstream surfaces. The distribution of scallop dimensions is consistent with the expected distribution of velocity within a recirculating vortex; comparatively rapid flow enters the downstream end of the vortex, decelerates as it approaches the upstream face, and is least where the vortex radius is greatest. The author was able to briefly observe two small, low-lying lateral potholes during two minor floods and measure internal velocities using a Marsh-McBirney Model 201D water current meter. Vertical, roller-like vortices occupied the sculptures and exchanged fluids with the freestream by turbulent mixing of eddies along the streamwise vortex face. Ephemeral vortices developed at the upstream lip of the lateral potholes and formed an eddy fence along the streamwise face of the larger, coherent vortex. Flow

velocities were greatest at vortex margins and least in vortex cores (0.3 m s^{-1} vs. 0 m s^{-1}); the flow structures approximated forced vortices.

Scallops in lateral potholes and reverse-flow pockets each record recirculating flow, but the two sculpture classes display different shapes; large lateral potholes taper upward (Figure 5.1C), and have log-linear log correlations between axes rather than the linear correlations observed in pockets (Figures 5.2B and 5.3). The differences probably arise from vorticity and pressure gradients, which must influence large vortices more than small ones. Vertical accelerations caused by turbulence in floodwaters may overwhelm hydrostatic pressure gradients over short distances, but hydrostatic forces cannot be ignored over larger scales. For a cylindrical vortex, rotation along any horizontal slice will not be two-dimensional unless vorticity is equal along the vortex axis. However, hydrostatic pressure on the vertical, streamwise vortex face increases with depth, and increasing pressure must be balanced by increasing vortex radius with depth, as seen in the formula for a forced vortex:

$$p_b = \rho C^2 (r_b^2 - r_c^2) + p_c \ , \qquad (5.2)$$

where C denotes vorticity, p denotes pressure, r denotes radius, ρ denotes fluid density, and the subscripts b and c refer to positions at the margin and center of the vortex, respectively (Munson et al., 1993). The variable p_b is equivalent to hydrostatic pressure, which is fixed by flow within the adjacent channel. Radial velocity in a forced vortex is given by:

$$u(r) = C \cdot r \ . \qquad (5.3)$$

In reality, velocity will not vary linearly with radius because of friction at the walls. Vorticity will vary to some degree. However, if a vortex is to possess the gradual

variations in velocity recorded by scallop size gradations, then vorticity cannot be extremely variable within a lateral pothole. Large vertical variations in vorticity would produce horizontal shear planes and prevent formation of a single coherent vortex.

Assuming that vorticity values do not vary dramatically along lateral pothole axes, one may infer that velocity gradients will be greatest where r is least because of the relationship $\bar{u} \propto r^{-1}$. The relationship will not be absolute because of vertical variations in p_c resulting from energy loss. Shearing is proportional to the velocity gradient (du/dr) and will be greatest in the top of lateral potholes where the ratio is greatest. Hence, friction losses per unit area will be greatest near the top of the lateral pothole and a momentum contrast must exist between decelerating fluids in the top of the pothole and forward flow along the overlying, planar wall. Because of the resulting momentum gradient, higher momentum fluids from above the lateral pothole will be exchanged with decelerated fluids of the vortex top resulting in a net vertical inflow of fluids into the vortex. The inflow, in combination with the vertical gradation in radial velocities, establishes a downward component to flow to yield the observed scallop patterns. This process is unlikely to operate until a vortex spans a sufficient depth range such that hydrostatic forces begin to affect the pressure distribution on the streamwise vortex.

5.6 Geometrical Model of Reverse-Flow Pocket Growth

5.6.1 Model Concepts

The relationship of selected sculptures to overall erosion rates can be explored using a geometrical model justified by the correspondence between sculpture flow field and morphology determined from the field study. Reverse-flow pockets display the

strongest dimensional relationships between W, L, and H and are, therefore, interpreted to enlarge systematically (Table 5.4). As a result, it is possible to geometrically model pocket growth given that pocket locations appear fixed by their association with planar defects. Observation indicates that reverse-flow pockets are similar to partial or complete hemispheres (Figures 5.1A and 5.1B). If this is true, these pockets can be modeled using the equations for a circle or sphere. The ratio W/L equals W/H for a hemisphere or partial hemisphere created by removing segments parallel to the aperture face. The mean ratios of W/L and W/H of reverse-flow pockets are not statistically different ($p=0.31$). So, reverse-flow pockets can be modeled as partial or complete hemispheres.

The possible influence of channel erosion rates on sculpture growth can be discerned by geometrically relating sculpture excavation to erosion of adjacent surfaces. Although it is commonly assumed that sculptures form on otherwise slowly or non-eroding surfaces (e.g., Whipple et al., 2000a), channel perimeters are unlikely to be immobile over geologic time, particularly where the substrate is soluble. Radial flow within pockets, lateral potholes, and potholes causes sculptures to enlarge radially while adjacent walls retreat by translation (Figure 5.4). The volume of erosion accomplished by the sculpture must be greater than that accomplished by a patch of wall whose area equals the sculpture aperture area. A translating wall erodes a volume equivalent to $0.25\ \pi\ L_t^2\ ds$ for an increment of wall retreat, ds, within a circular area of diameter L_t. In comparison, a hemispherical pocket must erode a greater volume (ΔV) that is dependent upon L_t^3. The value ΔV is equivalent to the minimum volume of erosion required for non-truncation of a pocket. Conceptually, it is useful to normalize ΔV by dividing it by the volume of bedrock that the wall would have eroded in the absence of the pocket ($0.25\ \pi\ L_t^2\ ds$). This

ratio is the normalized erosion excess that must occur within a pocket to prevent truncation by wall retreat. The ratio is greater than 1.0 for all concave sculptures and will be represented herein as λ.

Recirculation within sculpted forms directs particles and solvents at sculpture interiors because of centripetal forces and rapid deceleration of fluids entering the sculptures. Deflection of erosive substances toward sculpture surfaces increases local erosion rates relative to adjacent surfaces where streamlines parallel channel surfaces (Hancock et al., 1998). Thus, a given volume of erosive fluid removes more substrate than an equal volume flowing across adjacent surfaces; erosive flows within sculptures are more efficient at eroding channel perimeters. This efficiency can be approximated by the ratio $\Delta V/V_I$, which is the volume of bedrock (ΔV) that must be eroded relative to the initial size of a sculpture (V_I) and the volume of fluid it can contain. Holding wall retreat rates constant, larger values of $\Delta V/V_I$ indicate that a pocket must erode proportionally more bedrock per unit volume of erosive fluid; the pocket must be more efficient at erosion to persist. Values of λ and $\Delta V/V_I$ for hemispherical sculptures can be obtained from a geometrical model using the equation for a circle.

5.6.2 Model Construct

Reverse-flow pockets are not perfect hemispheres wherein L = 2W. Pockets are partial hemispheres, which are equivalent to perfect hemispheres that have had disk-like segments removed by slicing parallel to aperture faces. Discrete relationships exist between r, maximum L, maximum W, and W/L for all partial hemispheres. Looking at a cross section on the L-W plane (Figures 5.2A and 5.4), an iterative solution for W_i and L_i can be found for chosen values of radius, r_i, and W/L using the formulas:

$$W_i = r_i - y_i \quad . \tag{5.4}$$

$$L_i = 2 \cdot x_i \quad , \tag{5.5}$$

$$r_i^2 = x_i^2 + y_i^2 \quad , \tag{5.6}$$

where equation (5.6) defines a circle and x_i and y_i are the arc end points shown in Figure 5.4. Radial growth with constant W/L represents the minimum condition whereby pockets persist, because a decrease in W/L is equivalent to truncation. Given an increment of wall retreat, ds, the minimum values of L and W needed to ensure a constant value of W/L can be determined by iteratively solving equations (5.4) thru (5.6) twice for two successive positions of a pocket subject to the condition that,

$$y_{i-1} = y_i + ds \quad . \tag{5.7}$$

Iterative solution of the equations yields all the values necessary to evaluate pocket areas for positions 1 and 2 in Figure 5.4. Volumes are obtained by integrating areas about the y-axis (Figure 5.4).

Calculation of λ and $\Delta V/V_1$ requires calculation of ΔV. Examination of Figure 5.4 reveals that ΔV is not equal to $V_2 - V_1$, because V_2 encompasses a region, area OAC in Figure 5.4, which is eroded by flow across the adjacent wall. Thus, the volume of bedrock eroded by the pocket is actually $V_2 - V_{OAC} - V_1$ (Figure 5.4). Numerically, it is convenient to solve this problem by evaluating V_{OAC} as $V_{PCAQ} - V_{POAQ}$ and employing the formula:

$$\Delta V = V_2 - V_1 - (V_{PCAQ} - V_{POAQ}) = \pi\left[\int_{y_2}^{r_2}(r_2^2 - y^2)dy - \int_{y_1}^{r_1}(r_1^2 - y^2)dy\right] -$$

$$-2\pi\left\{\int_{y_1}^{y_2} y\sqrt{r_2^2 - y^2}\,dy - \int_{y_1}^{y_2} y\left[\frac{x_2 - x_1}{y_2 - y_1}\cdot y + \left(x_1 - \frac{x_2 - x_1}{y_2 - y_1}\cdot y\right)\right]dy\right\} \quad . \quad (5.8)$$

Having previously solved for the unknown variables on the right side of equation (5.8), ΔV can be directly obtained by evaluating the integrals. Note that V_{PCAQ} is calculated by integrating the area beneath an arc of radius r_2 around the y-axis. The arc spans the distance y_2-y_1 or ds on the y-axis (equation 5.7). The volume V_{POAQ} is obtained by integrating the area beneath a line occupying the x-y plane around the y-axis. The slope of the line (m) is defined by the angle at which the pocket rim retreats into the wall (Figure 5.4):

$$m = \frac{x_2 - x_1}{y_2 - y_1} \quad . \quad (5.9)$$

The choice of coordinate systems is responsible for the apparent inversion of the well-known equation for the slope of a line (equation 5.9).

5.7 Model Results

Having constructed a model that allows determination of the erosion efficiencies ($\Delta V/V_1$) and excesses (λ) necessary for the persistence of reverse-flow pockets, it is possible to numerically evaluate the effects of size (r), form (W/L), and wall retreat (ds) on pocket growth. Using a ds-value of 0.001 m, the variables r_1 and W/L were independently varied to generate the data summarized in Figure 5.5. The ratio $\Delta V/V_1$ varies substantially with changes in pocket size (r) and form (W/L). The highest erosion

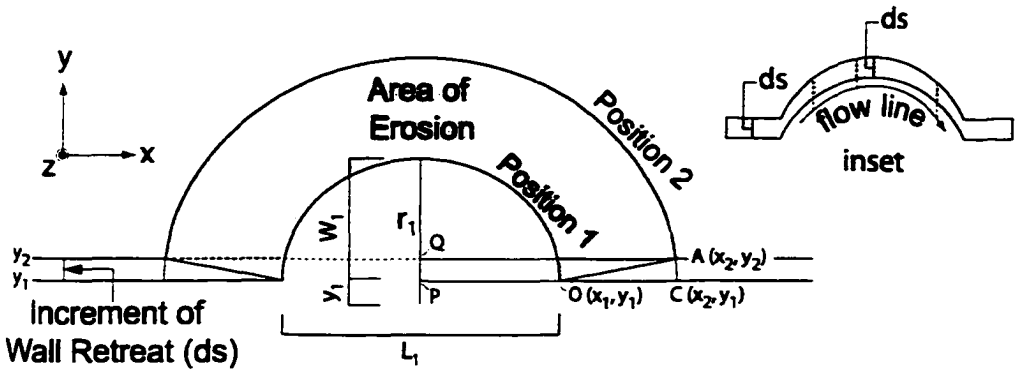

Figure 5.4: Cross section on the L-W plane through an ideal hemispherical pocket at two stages of radial growth (see Figure 5.2). Volumes are calculated by integrating areas around the y-axis after iteratively solving for unique values of x_1, x_2, r_2, W_1, W_2, L_1, and L_2 given prescribed values of y_1, r_1, ds, and W/L. However, the change in volume between the two pocket positions must be corrected for the area/volume OAC which is eroded by flow along the adjacent wall. The geometrical model assumes constant W/L, which is the minimum condition for non-truncation of pockets. In the case of radial enlargement, constant W/L also means a relative increase in pocket size between any two positions, and that W_2-W_1 is always greater than ds. The inset shows the hypothetical situation wherein constant form is maintained by pure translation of pocket walls. Erosion within the pocket would necessarily occur at widely different angles to flow lines of recirculating fluids (dashed lines). Thus, the possibility of pure translation is rejected given that there is no known mechanism to cause systematic, varying inclinations of solvent and abrasive particle attack relative to a flow line.

efficiencies are required of small pockets and those that are especially shallow or concave (Figure 5.5A). The minimum value of $\Delta V/V_1$ is achieved at W/L=0.27, a value that is coincidently close to that required for recirculation (W/L=0.25, Figure 5.3B). As a result, a pocket is optimally poised for growth once recirculation is achieved because efficiency requirements are at their lowest and any erosion beyond the low $\Delta V/V_1$-value equals growth relative to the pace of wall retreat. In contrast to erosion efficiencies, erosion excesses (λ) are only slightly affected by size (Figure 5.5B). Instead, λ-values increase exponentially as pocket concavity increases; a deepening pocket must erode ever-greater volumes relative to wall erosion or it will be truncated. This primarily reflects a geometrical property of partial hemispheres; the ratio of aperture area to volume declines as W/L increases, and area is proportional to L^2 and volume to L^3. Varying the increment of wall retreat, ds, causes a change in $\Delta V/V_1$ that is directly proportional to the change in ds. For instance, a ten-fold decrease in ds produces a ten-fold decline in $\Delta V/V_1$. Values of λ increase non-linearly as a function of W/L because of the geometrical peculiarities previously described for pocket volumes and aperture areas. Small pockets have the largest increases in λ-values for increased values of ds and are therefore more sensitive to changes in the increment of wall retreat than large pockets.

5.8 Discussion

The model results seen in Figure 5.5A show that small pockets must be relatively more efficient at erosion than large sculptures or they will be removed by wall retreat. As pockets grow, they must erode proportionally greater volumes of bedrock in the face of constant wall retreat. This is offset by commensurate increases in fluid volumes, which

cause a decline in minimum efficiencies with increasing sculpture size (Figure 5.5A). In contrast, erosion excesses increase dramatically with increasing concavity (Figure 5.5B). Thus, the principle constraint on sculpture growth is the efficiency with which particles and solvents can erode sculpture interiors. Hypothetically, a sculpture will achieve a concavity that reflects the maximum erosion potential of fluids in the pocket, and that is associated with a stable vortex. Wall retreat would truncate over-deepened sculptures because the necessary erosion volumes would exceed the capability of the pocket. Simultaneously, anomalously shallow pockets would deepen because the required erosion efficiencies ($\Delta V/V_I$) and excess (λ) are least and excess erosion is therefore more probable. From examination of Figure 5.2, the reverse-flow pockets form a relatively straight line with a slope of 0.345 (Table 5.4). This ratio is inferred to be optimum for vortex stability and pocket growth amid wall retreat in the canyon.

Rates of wall retreat and relative volume increases can be constructed by dividing the associated variables by a time interval, dt. The large erosion efficiencies and relative volumes required of pockets on rapidly retreating channel perimeters make pocket growth most probable where wall retreat is slowest or erosion efficiencies are increased by secondary factors. For instance, the soluble canyon walls in Buckeye Creek Cave are presumably retreating at a non-trivial rate. In such situations, model results indicate that small pockets must enlarge quickly or be removed by wall retreat. This explains why 98% of all pockets in the canyon lie on defects. Such discontinuities localize and accelerate erosion and could give rise to flow perturbations that over-deepen scallops or create pocket-excavating vortices (e.g., Hancock et al., 1998). Without bedrock defects, pocket erosion would be suppressed by rapid wall retreat and truncation of incipient

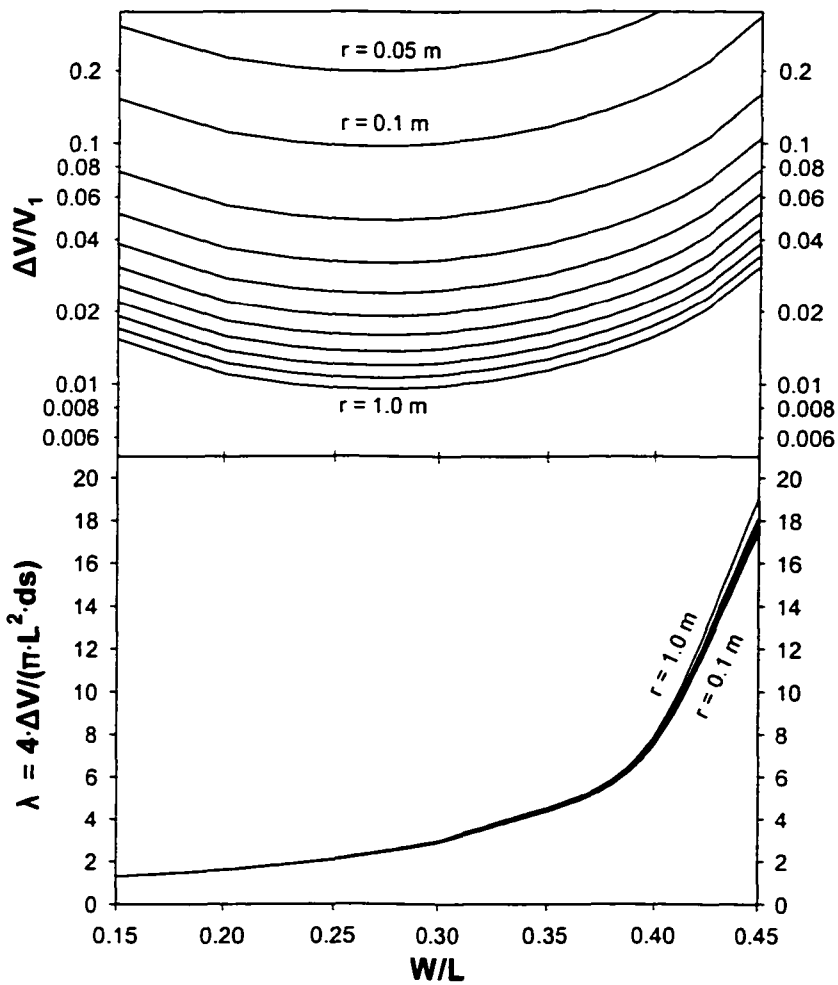

Figure 5.5: Model results for ds=0.001 m. A: Curves representing the minimum normalized volume increase ($\Delta V/V_1$) that must occur to prevent pocket truncation by wall retreat. A $\Delta V/V_1$ ratio of 0.30 indicates that a pocket must erode a volume equal to 30% of its initial volume (V_1) to prevent truncation. B: Curves representing the excess erosion a pocket must accomplish relative to wall erosion to prevent pocket truncation. A λ-value of 2.09 indicates that flow in a pocket must erode a volume equal to 209% of that eroded by the adjacent wall or the pocket will be truncated.

forms. Large, lateral potholes in the canyon do not possess intimate associations with planar weaknesses and this is expected given that $\Delta V/V_t$-values decline with increasing sculpture size (Figure 5.5A).

High erosion rates may suppress the formation of small sculpted forms because extremely high efficiencies must be maintained for small sculptures to grow. By inference, high erosion rates must prevent the formation of large sculpted forms in some channels by suppressing small sculpted forms because the empirical data suggest that small, reverse-flow pockets enlarge to become lateral potholes. However, variations in erosion rates and hydraulics within a channel may create localized zones wherein conditions are favorable for initiation of sculpted forms. Hancock et al. (1998) reported rapid bedrock erosion along the Indus River with rates as high as 4 mm a^{-1} and noted that sculpted forms only appear in zones of large-scale flow separation. The current results suggest that extremely high erosion rates preclude development of stable sculpted forms except in sheltered zones. However, large-scale flow separation is not required to generate sculptures. For instance, pockets and lateral potholes are found upstream, downstream, and at the apices of interior and exterior bends in the canyon. The lack of association with larger separation zones suggests that large sculpted forms do not require deflection of flow lines by large upstream obstacles. Additionally, Hartshorn et al. (2000) report that bedrock bedform amplitudes vary systematically across large, high gradient streams in Taiwan despite unchanging substrate types in individual cross sections. Bedform amplitudes are least in thalwegs and greatest on channel banks where stream velocities and erosion rates are slowest. In light of the results of the theoretical model, it

is posited here that their unexplained observations reflect the inability of sculptures to persist and develop into large sculptures where erosion rates are highest.

If the analyses are correct, the morphology of a sculpted form developed within a separation zone may not be representative of overall channel hydraulics and is not suitable for empirical models of channel hydraulics or erosion without additional study. Because relative erosion efficiencies and excesses increase rapidly with increasing concavity, there must also be a relationship between erosion rates and sculpture concavities. High erosion rates may limit sculpture concavities because they require the greatest efficiencies and excesses. The relationships identified on the basis of the theoretical model lead to rejection of null Hypothesis II, that the geometry of sculpted forms is not related to erosion atop adjacent surfaces. Sculpture geometries are at least co-dependent upon local incision rates.

The possible dependence of sculpture concavities on erosion rates complicates attempts to correlate sculpture properties with channel incision rates and hydraulics. Although very little is known about the relationship of sculpted forms to channel erosion, it is evident that additional work is required and that future studies may need to simultaneously address sculpture morphology, erosion rates, and channel hydraulics.

5.9 Conclusions

Hemispherical and hemi-elliptical sculpted forms enlarge systematically and exploit planes of weakness in Buckeye Creek Cave, West Virginia. The type of flow found within the sculpture determines the precise morphology of individual sculptures. Sculptures preferentially enlarge in the direction of flow along prominent, planar

weakness unless a recirculating vortex forms. Recirculating vortices tend to produce concavities whose apertures are circular when small and tapering upward when large. Tapering occurs because of the effects of hydrostatic pressure on the large vortices with vertical axes. The largest sculpted forms in Buckeye Creek Cave are lateral potholes that apparently grow from small sculptures. A model of sculpture growth reveals that wall retreat imposes limitations on small sculptures. Small sculptures are more sensitive to the rate of wall retreat because they must erode proportionally greater volumes of bedrock for lesser volumes of fluid. Because small sculptures give rise to larger sculptures, channel incision by large sculptures is unlikely amid rapid wall retreat.

The results lead to rejection of null Hypothesis II, that the geometry of sculpted forms is not related to erosion atop adjacent surfaces. Sculpture morphology is not independent of erosion of adjacent surfaces. Therefore, there are practical limits to the use of sculpted forms for making inferences about overall channel hydraulics or erosion processes.

Chapter 6

Profile Maintenance in a Fluviokarst Basin

6.1 Chapter Abstract

Unit stream power and shear stress decline 3-to-30 fold as Buckeye Creek flows from atop insoluble strata, into a fluviokarst depression, and through Buckeye Creek Cave. These changes occur in concert with lengthwise changes in particle sizes, which decline rapidly across an alluvial reach atop the fluviokarst depression floor. Shear stress, unit stream power, and particle sizes are lowest in Buckeye Creek Cave where the majority of erosion features in the stream channel are associated with corrosion. Values are highest where evidence of quarrying and abrasion are common, which is atop a shale and quartz sandstone boulders in an alluvial reach, respectively. The association of higher values of unit stream power and shear stress with the distribution of mechanical incision is posited to represent lengthwise adjustments of channel hydraulics to account for differences in incision driving forces atop insoluble and soluble substrates. Namely, incision of soluble strata requires less input of mechanical energy because chemical energy provides the primary impetus for incision.

The change in particle sizes atop the alluvial reach may be the result of longitudinal sorting and storage of coarse sediment atop the karst depression. It is posited that coarse sediment transport is incompatible with corrosion-dominated incision because coarse sediment transport is improbable where shear stress is low.

6.2 Introduction

Reach-scale hydraulics and energy expenditure have been hypothesized to reflect local adjustments to rock resistance in stable, incising bedrock streams (e.g., Wohl and Merritt, 2001). Correlations between channel hydraulics and substrate resistance have been studied primarily in non-karst streams or streams with drainage areas in excess of 100 km^2 (e.g., Baker and Pickup, 1987; Wohl, 1993; Wohl et al., 1994; Wohl and Merritt, 2001). Although strong associations between hydraulics and substrate resistance have been made, no study has been able to show a correlation between reach hydraulics and incision processes. For instance, bed shear stress may correlate positively with quarrying because shear stress is one of the phenomena that mobilizes and detaches blocks of bedrock from channel beds (Hancock et al., 1998).

This chapter examines correlations between channel hydraulics and evidence of incision processes in Buckeye Creek, the principal channel in a 14 km^2, fluviokarst basin (Figures 3.4 and 3.7). Evidence of quarrying, abrasion, and corrosion are found in separate portions of Buckeye Creek. Presumably, Buckeye Creek has adjusted channel and valley geometries to reflect the varied importance of corrosion for incision of different substrates. The research hypothesis is evaluated that mean bed shear stress (τ)

and unit stream power (ω) are useful indices for estimating the ability of the stream to erode by means other than corrosion (e.g., Corollary Hypothesis I). Presumably, the hydraulic variables will assume relatively low values where chemical energy supplants mechanical energy as the primary impetus for channel incision.

Corollary Hypothesis I and the associated research hypothesis are evaluated by examining relationships between ω, τ, $\bar{u}$, inferred incision processes, lithology, and geomorphic history in a headwater stream incising sandstone, shale, and limestone. The eight reaches examined are incising limestone and shale, although two of the study reaches are alluvial, with the stream flowing over insoluble grains supplied from upstream (Tables 3.1 and 6.1)(Figure 6.1). The assumption is made that incision indices and stream processes in adjacent reaches can be compared when modeling floods of similar instantaneous runoff values.

Model values of ω, τ, $\bar{u}$ are generated in an open channel model, HEC-RAS. All reaches in the cave are modeled as open channel flow because passage sizes are large and closed conduit modeling of the study reaches is not possible because there is no information available concerning head loss or friction factors in the study reaches. No assumptions are made about the possibility that large, cave-filling floods can generate larger values of τ and ω than those obtained from the open channel models. Rather, the assumption is made that the modeled open channel flood provides a useful datum with which to begin a quantitative exploration of hydraulic and incision processes in streams flowing across multiple substrates.

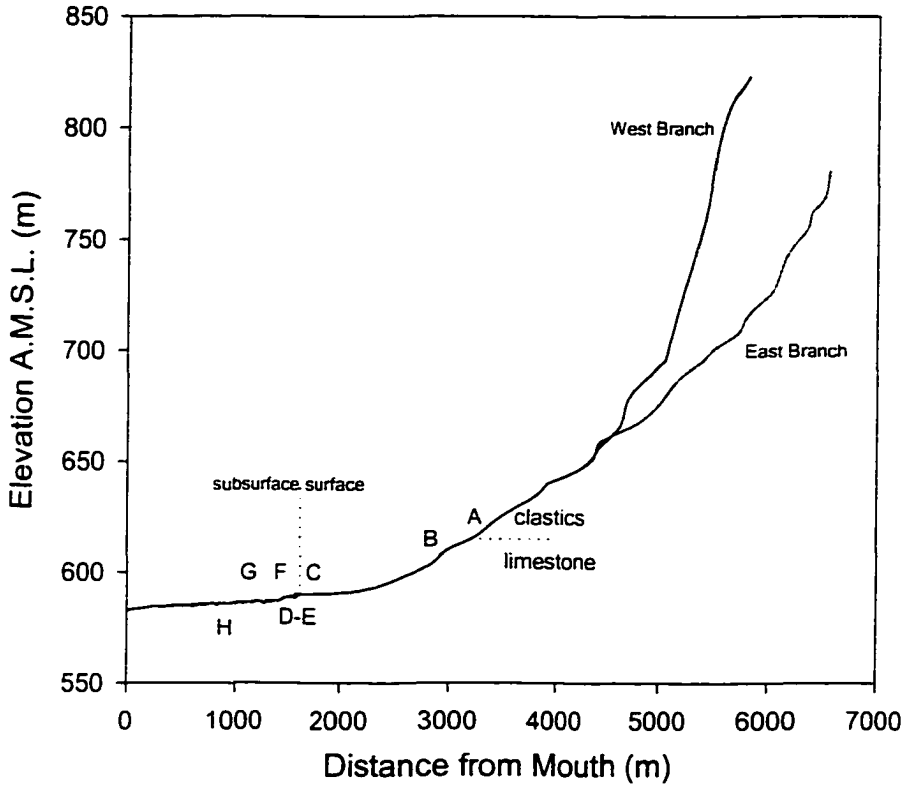

Figure 6.1: Longitudinal profile of Buckeye Creek with reach locations denoted by letters (see Table 3.1 for reach properties).

Table 6.1: Incision Processes and Model Results for Buckeye Creek

Reach	Model Discharge	Bed Lithology	Alluvial or Bedrock	Incision Processes[a]	Average Cross Section Values ω $(W m^{-2})^b$	τ $(N m^{-2})^b$	ū $(m s^{-1})^b$
A	2.4 $m^3 s^{-1}$	Shale	bedrock	Q	190 ± 180	95 ± 73	1.6 ± 0.6
B	2.7 $m^3 s^{-1}$	Limestone	alluvial	Ab[c]	150 ± 40	90 ± 18	1.6 ± 0.1
C	7.3 $m^3 s^{-1}$	Limestone	alluvial	n/a	35 ± 21	30 ± 11	1.1 ± 0.2
D	9.4 $m^3 s^{-1}$	Limestone	mixed	Q, C	81 ± 150	40 ± 51	1.2 ± 0.7
E	9.4 $m^3 s^{-1}$	Limestone	bedrock	C	60 ± 83	28 ± 26	1.6 ± 0.7
F	9.4 $m^3 s^{-1}$	Limestone	bedrock	C	6 ± 3	8 ± 3	0.6 ± 0.1
G	9.4 $m^3 s^{-1}$	Limestone	bedrock	C	34 ± 23	22 ± 10	1.4 ± 0.3
H	9.4 $m^3 s^{-1}$	Limestone	alluvial	n/a[d]	43 ± 31	26 ± 12	1.5 ± 0.4

[a] Ab denotes abrasion; P denotes plucking; Q denotes quarrying; C denotes corrosion. Order reflects inferred relative roles.

[b] Mean ± one standard deviation.

[c] Abrasion is diminishing sandstone boulders atop an alluvial bed.

[d] Evidence of corrosion is found on bedrock banks, but there are no bedrock bed exposures.

6.3 Controls on Profile Development in Buckeye Creek

6.3.1 General Profile

Buckeye Creek is a tributary to Spring Creek, which acts as base level for the catchment (Figures 3.4 and 6.1)(Dasher and Balfour, 1994). The two major branches of Buckeye Creek rise atop Butler Mountain and a flanking ridge. A flat, upland surface underlain by resistant sandstone lies atop Butler Mountain and streams draining eastward to Buckeye Creek are consuming this surface during headward retreat. The top of the nearly horizontal sandstone fixes the upper elevation of streams, which drain off the mountain. As a result, profile relief and concavity are increasing as Buckeye Creek and Spring Creek incise. Similar situations exist throughout the Appalachians. Locally, there are no streams draining similar escarpments that do not flow across carbonates at their

downstream termini. Therefore, it is difficult to evaluate the influence of carbonate versus clastic outcrops on regression equations describing each profile class (e.g., White and White, 1983). However, the Buckeye Creek profile is similar to Spring Creek where Spring Creek is incising clastics and eroding headward into an upland surface of the Appalachian Plateau (Figure 6.2). Although not conclusive, the similar profile shapes argue that the general shape of the Buckeye Creek profile is similar to Spring Creek despite the chemically weak strata found in the lower portion of the Buckeye basin.

As the principle stream in a fluviokarst basin, Buckeye Creek flows into a karst depression and then through a cave for the last 1.6 km of its course. The channel rapidly changes from a bedrock stream to alluvial as it enters the fluviokarst depression, and an upward convexity is present in the stream profile just upstream of the depression (Figure 6.1). Tributaries flowing off Butler Mountain also sink, although the associated caves systems are considerably smaller and shorter than Buckeye Creek Cave. The distance these streams flow across the limestone before sinking or entering caves appears to be related to the logarithm of basin area, although limited available data preclude a definitive statement for the Buckeye Creek catchment streams (Figure 6.3). Similar relationships have been observed for many other karst streams, although no quantitative explanation of the relationship has been given (Miller, 1996).

6.3.2 Profile in Buckeye Creek Cave

There are major differences in channel and valley architecture between Buckeye Creek and typical headwater surface streams. The subterranean profile of the creek is not the product of uninterrupted downcutting, but instead reflects modification of a

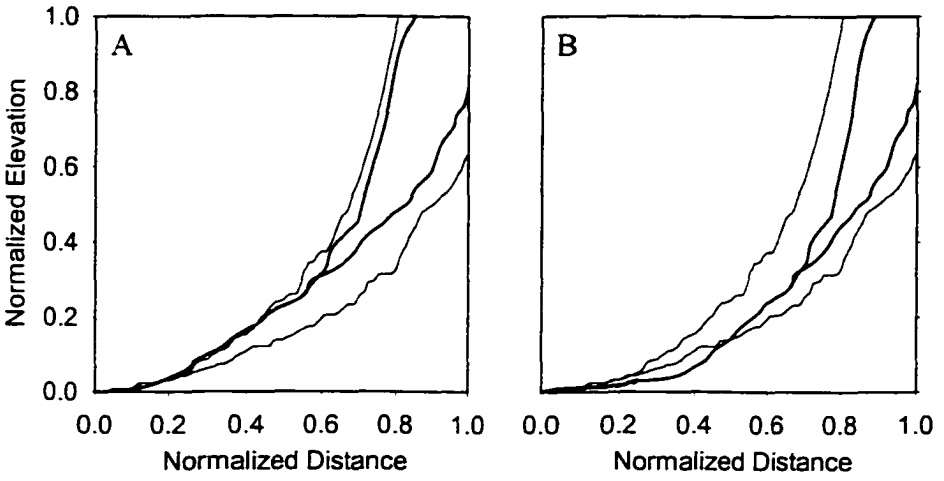

Figure 6.2: A: Normalized profiles of Buckeye Creek (bold) and Spring Creek where each creek drains 13.2 km^2 and is ~4.4 km long. Each reach has two major branches (shown). The Buckeye Creek profile ends at the upstream mouth of Buckeye Creek Cave. Note similarities of profiles despite Spring Creek flowing entirely atop clastics. B: The streambed in Buckeye Creek Cave extends another 1.6 km downstream of the cave entrance to Spring Creek without a significant increase in drainage area. Hence, Buckeye Creek must incise a greater length of channel for the same collection area. Inclusion of the additional channel causes the Buckeye Creek profile to appear slightly more concave, but the overall profile shape is similar to Spring Creek.

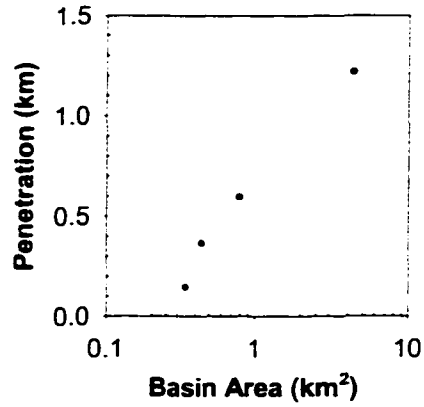

Figure 6.3: Distance streams rising on Butler Mountain flow across limestone before sinking underground (penetration). Basin area includes only the area of each stream that lies atop Butler Mountain or subsidiary ridges underlain by clastic strata.

groundwater route that diverted flow from higher passages separated from the active stream passage by intervening bedrock (Figure 3.10).

The hydrologic controls on the Darcian groundwater route that was enlarged to form the active stream passage in Buckeye Creek Cave were, in effect, the boundary conditions for the modern, subterranean stream profile. The progenitor conduits are preserved in the cave as half-tubes atop bedding planes. Half-tubes appear as bottomless pipes with circular or elliptical cross sections in passage ceilings. Half-tubes enlarge from smaller pathways atop bedding planes and insoluble strata, where preferential flow of groundwater flow initiates conduit formation. Initially, corrosion causes upward growth but incision of underlying units eventually cause half-tubes to become relict features in passage ceilings (White, 1988; Ford and Williams, 1989). Half-tubes were the initial pathways in two distinct segments of Buckeye Creek Cave, which are separated by a narrow canyon that circumvents a collapse. The upstream segment is 200 m long and

extends from the cave entrance to the narrow canyon (reach F in Figure 6.1). Half-tubes in this segment are found atop a bedding plane separating two similar limestones, although collapse has destroyed all but a few segments of the initial tube. Downstream of the canyon, the passage is in the hanging wall of a high-angle reverse fault and half-tubes are developed atop a calcareous siltstone. The passage alternately follows short segments of older passages and smaller passages that began as tubes atop the siltstone for the remaining 1 km of the cave stream.

The initial gradient of the groundwater path was not smooth, but meandered in the vertical direction in response to planar meanders across the dip slope, small-scale folds, and exploitation of pre-existing pathways. The vertical meanders produced phreatic loops, which are passages that descend below a permanent water surface and then rise to become air-filled again (Ford and Williams, 1989). The loops are preserved as vertical constrictions in the modern channel, where passage ceilings approach sediment covered channel beds. A comparison of siltstone and thalweg elevations in the hanging wall reveals little similarity between the modern stream gradient and a siltstone, which guided initial profile development (Figure 6.4); the modern profile is apparently evolved from, but no longer solely dependent upon, the profile of groundwater pathways that set the boundary conditions for subsequent profile development.

6.4 Methods of Incision and Passage Enlargement

6.4.1 Incision Processes

6.4.1.1 Overview. The transition from Darcian groundwater flow to discrete conduit flow is marked by substantial changes in flow, sediment transport, and erosion

regimes (White, 1988; Ford and Williams, 1989; Palmer, 1991). The siltstone was probably not incised and breached by corrosion alone. Presumably, quarrying and abrasion were important processes during passage enlargement because the stream is quarrying the siltstone by physically detaching small blocks while simultaneously toppling larger blocks by dissolving an underlying limestone at the only location where the streambed is currently siltstone (Figure 6.4).

6.4.1.2 Incision in Study Reaches. As discussed in Chapter 4, evidence of incision mechanisms was sought during data collection in each of the nine reaches examined in Buckeye Creek. Quarrying was identified on the basis of step-like ledges with missing and detached blocks. Abrasion was identified by the presence of potholes with grinders and other sculpted forms (Hancock et al., 1998). Corrosion was identified by the presence of scallops and solution tubes in soluble strata (Blumberg and Curl, 1974; Springer et al., 1997). Many sculpted forms are created by abrasion and solution, so anastomose tubes and corrosion pitting were especially valuable evidence of corrosion (Figure 6.5).

Using the criteria above, quarrying was recognized in the headwater reach (reach A in Figure 6.1), cave entrance (reach D), and trunk reach (reach E)(Table 6.1). Abrasion is presumably important in the narrow canyon, reach F, in Buckeye Creek Cave because the walls of the canyon are entirely covered by sculpted forms. However, sculpted forms in limestone can be the product of abrasion and corrosion (Blumberg and Curl, 1974; Curl, 1974). There is, at present, no way to discern the relative roles of abrasion and corrosion in the types of sculpted forms observed in the narrow canyon. Therefore, both processes are assumed to be important. Abrasion was of unambiguous importance at one

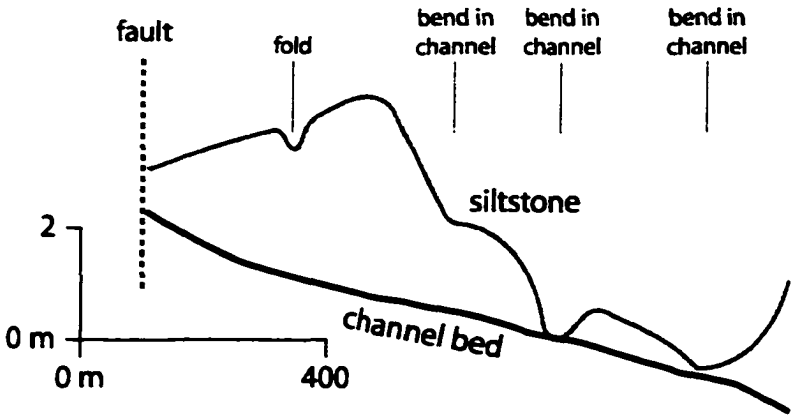

Figure 6.4: Longitudinal profile of Buckeye Creek streambed and siltstone in cave beginning at downstream terminus of narrow canyon and ending at Spencer Cave. The gradient of the streambed does not closely follow the siltstone, although the associated passages initially formed atop the siltstone.

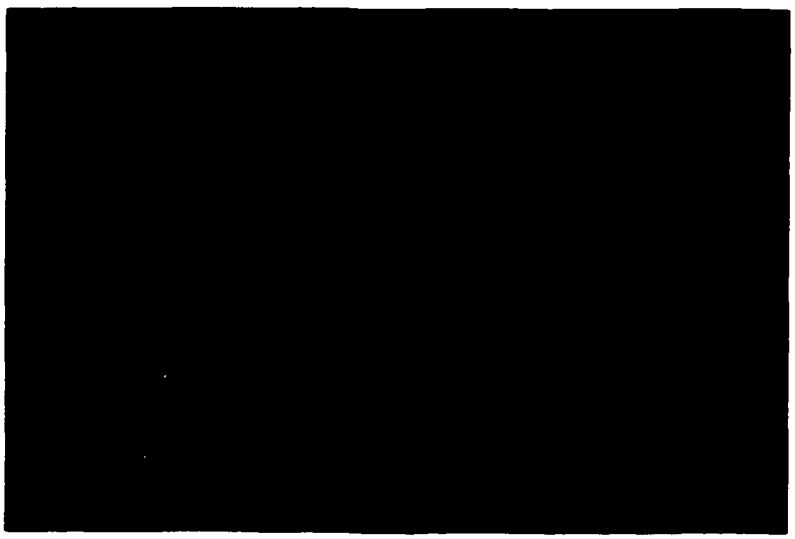

Figure 6.5: Intact bedrock undercut by corrosion in reach E. Corrosion along joints and bedding planes that bound large blocks aid their quarrying. Eventually, blocks are detached from the bed or topple from banks.

location in Buckeye Creek Cave where small potholes with grinders were observed on the channel bed (Figure 6.6). The potholes are found where the stream breaks through a sparsely jointed, silty limestone. Blocks of this rock unit topple into a deep pool at the downstream lip of the potholed channel step. A nearby collapse and vertical constriction precluded open channel modeling at this locale.

Quarrying of limestone was most pronounced between reaches A and B, which is also a pronounced upward convexity in the longitudinal profile (Figure 6.1). The channel in this segment is extremely complex, with many small steps and waterfalls atop bedrock that precluded one-dimensional modeling of channel hydraulics (Figure 3.6A). Quarrying is readily recognized from the association of detached blocks with outcrops and large fraction of limestone cobbles and boulders atop the bed (up to 50%). Corrosion phenomena are absent except at the downstream terminus of the segment where anastomose tubes are found in small boulders and cobbles.

Abrasion may be an important agent for diminishing sandstone boulders at the upstream terminus of the depression floor where the accumulation of insoluble clasts has created an alluvial reach (reach B and vicinity in Figure 6.1). Sandstone boulders are found in the channel and atop the adjacent floodplain. Many of these boulders may have been deposited as debris flows debouched onto the depression floor or during especially high magnitude floods. Regardless of their origin, boulders in the modern channel have been stable long enough for floods to excavate sculpted forms in them (Figure 6.7). The coarseness of the boulders and their lack of downstream transport effectively armors underlying bedrock, which is not exposed in the vicinity of the reach. Presumably, the

limestone is being incised by collapse of small karst conduits (impenetrable flow paths are known to exist near reach B), during knickpoint passage, or during infrequent exposure by catastrophic floods. In either case, similar processes were not observed anywhere else in Buckeye Creek, so the local change in incision processes presumably reflects the creek entering the depression with commensurate changes in flood and debris flow processes.

Observation in Buckeye Creek Cave revealed many features that have been previously associated with corrosion (White, 1988; Ford and Williams, 1989; Palmer, 1991). Observed corrosion features include: (i) sculpted forms, (ii) corrosion bells (Figure 6.8), (iii) large smooth surfaces free of block detachments, and (iv) elliptical tubes; corrosion is inferred to be important in all of the reaches developed atop limestone (Table 6.1). However, the beds of these reaches are often mantled with thick or impenetrable deposits of stream sediments (Figures 3.6B and 3.11A,B). In such cases, the role of corrosion was inferred from the degree of corrosion smoothing and sculpting of passage walls at floor level. The role of corrosion in channel incision is best observed in the trunk (reach E) and narrow canyon (reach F)(Figures 6.5 and 6.9). Corrosion tubes lie beneath channel banks and undercut large blocks, which subsequently topple into the cave stream where perennial flow can diminish them (Figure 6.5). Scallops and other corrosion-related sculpted forms cover the bed and walls of the narrow canyon (Figure 6.9). Corrosion may occur beneath the alluvial sediments mantling many reaches between sediment-mobilizing floods, but previous studies conclude that insoluble stream sediments effectively shield cave floors from corrosion (White, 1988).

Figure 6.6: Floor pothole with grinders between reaches F and G. Pothole is being carved by abrasion in an argillaceous limestone that forms a step in the channel, which is retreating headward. Flow is to left. Note pencil for scale.

Figure 6.7: Pothole-like sculpted forms eroded into the downstream face of a boulder in reach B. The sculptures are created by abrasion and imply stability of the boulder in the channel. Note pen for scale.

Figure 6.8: Ceiling bells etched by corrosion in reach G. Arrow identifies the siltstone that guided passage development. Undercutting of passage walls and quarrying of the siltstone is causing the passage to widen. Photograph courtesy of Ed McCarthy.

Figure 6.9: Scallops and a pocket (above pen) created by corrosion and abrasion in the narrow canyon (reach F). Scallops are found on all rock types, but are especially well-developed in limestone caves (Blumberg and Curl, 1974). Flow is from right to left.

6.4.2 Lateral and Upward Passage Enlargement

The vast majority of cave passages begin as sub-centimeter pathways along zones of favorable hydraulic conductivity. Erosion, principally in the form of corrosion, enlarges the cross-sectional area of the flowpath until a discrete conduit is formed (Palmer, 1991). Initially, these conduits must reflect the role of Darcian groundwater processes and corrosion in their cross sections and evolution. If a conduit experiences frequent or perennial pipe-full flow, then cross sections will often be elliptical or round in shape because corrosion attacks all conduit surfaces (White, 1988; Ford and Williams, 1989). Accumulation of insoluble or immovable detritus on the bed or development atop

relatively insoluble strata will cause preferential growth in the vertical dimension (White, 1988; Ford and Williams, 1989). Stoping is a common means of upward growth; blocks are detached from ceilings by collapse and removed from the underlying cave stream by corrosion (White, 1988).

Whether a passage is enlarging primarily by corrosion or stoping can be inferred from passage morphology. Irregular, angular walls and ceilings are readily identified as products of stoping, and angular blocks of ceiling rock may be found underneath them. Passage perimeters are typically smooth where corrosion predominates (White, 1988; Ford and Williams, 1989). Stoping is occurring in the 9-m-wide trunk reach (reach E in Figure 6.1). Passage walls are irregular except where collapse has failed to remove 2-m-wide elliptical tubes. Measurements of fracture directions on the walls of this reach are telling (Figure 3.13); where the passage is actively stoping, fracture orientations lack the strong bimodal distribution expected of regional joint sets (e.g., White, 1988). These fractures are forming as stoping undercuts walls and ceilings. Fracture orientations and densities are different in blocks containing the elliptical tube that acted as the initial pathway. The walls are sparsely jointed and fractures are consistently strike-oriented. Presumably, lateral erosion along bedding planes led to partial collapse of the original tube, which destabilized adjacent walls and led to fracturing of the host limestones as greater passage widths increased tension in the surrounding bedrock (e.g., White, 1988).

Corrosion is the primary means of upward passage enlargement in reaches F, G, and H, although lateral and vertical stoping is also present in reach H. Passage ceilings display smooth surfaces, as opposed to irregular surfaces from block detachment, and

corrosion bells wherein floodwaters preferentially enlarge ceiling joints (Figure 6.8). The associated passages are elliptical, with preferential horizontal growth on river left caused by collapse induced by lateral erosion of a calcareous siltstone in passage walls (Figure 6.8). Smaller elliptical tubes are found atop the siltstone in some passage ceilings and record passage initiation atop the siltstone. Breaching of the siltstone eventually led to lateral erosion because the friable siltstone is structurally weak and weathers to centimeter- and decimeter-scale blocks.

A combination of corrosion and stoping is especially important in the constriction near the downstream terminus of the Watergate reach (Figures 3.11D and 4.2). Upward corrosion is exposing the base of the siltstone, which subsequently collapses. The siltstone is exposed in passage walls and ceilings of the Watergate termini. As a result, collapse is decreasing the length of the constriction as undercutting of the siltstone proceeds toward the center of the reach. Eventually, this longitudinal-oriented stoping will remove the portion of the siltstone bed in the passage ceiling and thereby remove the constriction.

6.5 Values of Hydraulic Variables Along the Longitudinal Profile

6.5.1 Model Output

All reaches were modeled in HEC-RAS using discharge values obtained by multiplying drainage area above each reach by an instantaneous runoff value (Table 3.1). Estimates of ω, τ, and $\bar{u}$ were obtained directly from HEC-RAS. Model results are provided in Table 6.1 and Figure 6.10C,D.

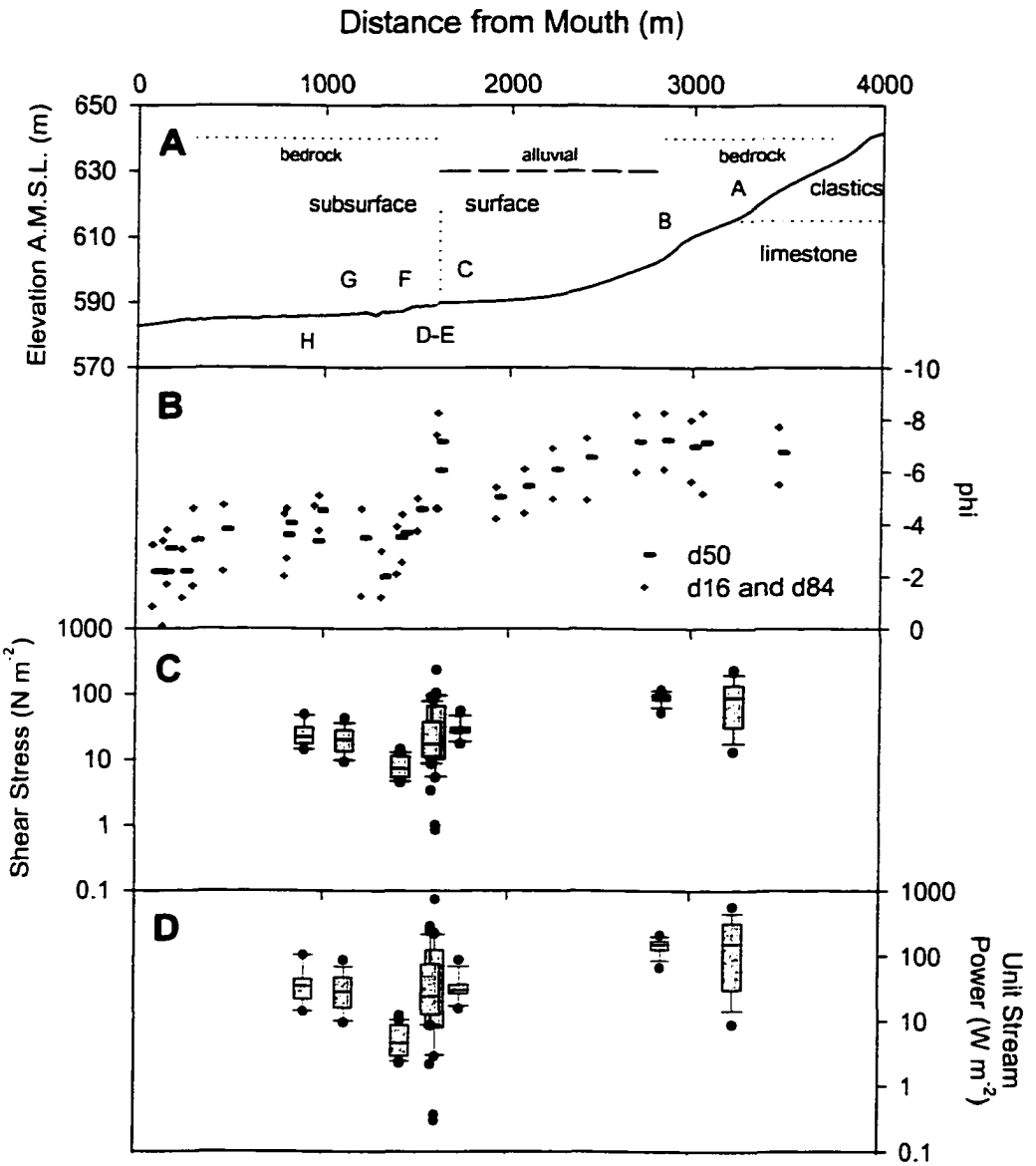

Figure 6.10: Longitudinal distribution of reach variables. A: Longitudinal profile with reach locations identified by letters and reach classifications noted. B: Mean clast sizes along stream as determined using Wolman counts and sieving. C: Box plot of shear stress values. D: Box plot of unit stream power. Note log scale of y-axes in plots C and D. Details discussed in text.

Changes in the distribution of ω and τ are in general agreement with observed changes in grain sizes (panel B versus panels C and D in Figure 6.10). Grain size, ω, and τ peak at the downstream terminus of an upward concavity in the channel profile (Figure 6.10). Values decline as the stream flows across the depression floor, but abruptly increase at the cave entrance where the entrance constriction, a locally steep bed gradient, and coarse talus from the overlying cliff increase flow depth, energy loss, and mean velocity. Values of ω and τ are low throughout the rest of the cave because of low velocities associated with channel geometry (described below).

6.5.2 Sensitivity Analyses

6.5.2.1 Evaluation Techniques. Student t-tests and the Student-Newman-Keuls (SNK) multiple comparison test for significant differences among means were used to assess sensitivity to backwater effects and roughness values. The SNK procedure is also used for reach comparisons (see Chapter 4).

6.5.2.2 Subcritical vs. Critical Flow. Subcritical flow is known to prevail in the cave entrance for large floods (reach D)(Figure 4.1). Calculations that begin with the normal depth boundary condition yield critical flow at several locations in the entrance. Therefore, the downstream WSE was raised from the normal depth until subcritical flow prevailed throughout the reach. This has the effect of overestimating reach values of ω and τ, because actual flow depths may be deeper for the model discharge. Comparison of output values for subcritical versus critical flow yielded significances of 0.14 and 0.18 for ω and τ, respectively. The lack of a significant difference and observations of subcritical flow led to use of the subcritical values in subsequent analyses.

6.5.2.3 Roughness Estimates. Channelized flow has received virtually no quantitative treatment in caves; therefore the effect of Manning's n values chosen for model reaches must be addressed. Sensitivity analyses were performed on the visually estimated roughness value (n_o) by performing model runs with roughness values that were 50% and 200% of n_o. The sensitivity of model output to different roughness values can be assessed by comparing statistical groupings of the reaches as functions of roughness values (Figure 6.11). All three model runs produce high shear stress values for surface and entrance reaches, but all three SNK analyses distinguish between surface, cave entrance, and distal cave segments. Fewer significant differences are recognized among the cave and surface reaches for the $n=2*n_o$ data, but groupings preserve the trend seen in the other two; large, low gradient passages downstream of the canyon yield low shear stress values and group separately from surface segments and those near the cave entrance (Figure 6.11).

6.5.3 Reach Comparisons

When $n=n_o$ SNK groupings of ω and τ distinguish between reaches A, B, and D and reaches atop the karst depression floor and in Buckeye Creek Cave (C, E-H). Reaches A, B, and D are steep with coarse cobble beds and in-channel boulders. Reaches A and B are not significantly different from one another, but their means differ from all other means except for τ in reach D, where the entrance constriction and talus produce deep flow depths and a relatively steep energy gradient.

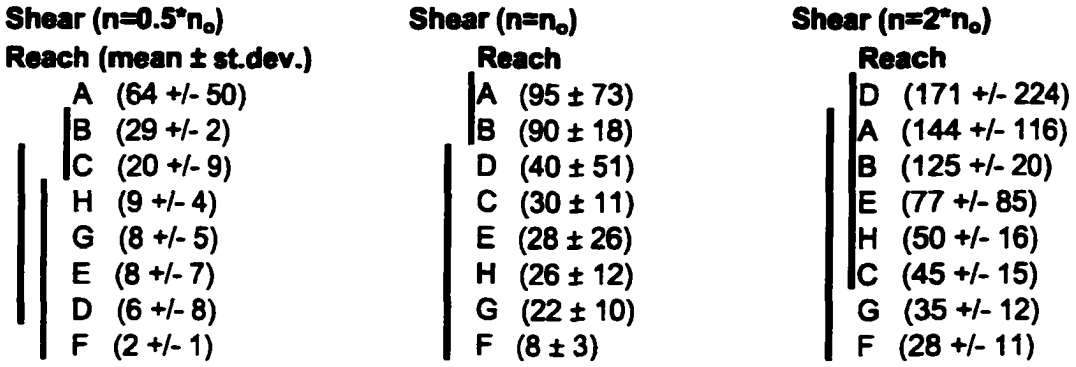

Figure 6.11: Comparisons of mean shear stress (τ) between reaches as classified using the Student-Newman-Keuls (SNK) multiple-comparison method in SAS for different values of Manning's n (SAS Institute Inc., 2000). See text for discussion.

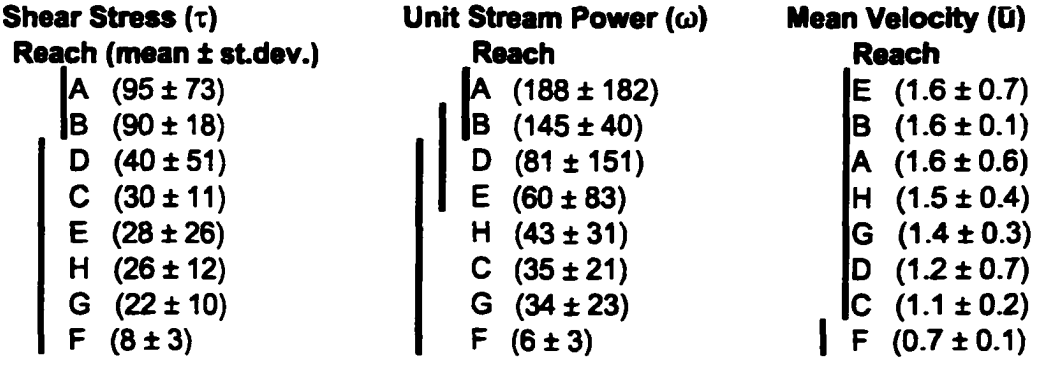

Figure 6.12: Comparisons of selected variables between reaches as classified using the Student-Newman-Keuls (SNK) multiple-comparison method in SAS for visually estimated values of Manning's n (SAS Institute Inc., 2000). See text for discussion.

6.5.4 Model Results Applied To Quarrying

The ability to mobilize individual, unprotected blocks on the streambed is proportional to $\bar{u}$ (Carling et al., 2002). Quarrying presumably requires velocities higher than those required to mobilize individual blocks because attachment forces and opposing normal forces must be overcome if a block is to be removed from intact bedrock surfaces (Hancock et al., 1998). Reach E possesses the highest mean velocity of all low ω and τ reaches identified by the SNK procedure; therefore this reach can serve as a useful test of the ability of the stream to quarry in the cave and downstream terminus of the fluviokarst depression. Using equations that describe the critical velocity required to mobilize detached blocks atop a smooth surface, the minimum velocities (U_c) necessary to mobilize limestone blocks in the bed of reach E can be determined (see Chapter 2). For two intact blocks readily accessible on the bed in reach E, $U_c = 3.7$ m s^{-1}.

6.6 Discussion

6.6.1 Incision Processes in Buckeye Creek

Absolute values of ω and τ modeled along Buckeye Creek are low for an actively incising, bedrock stream. Models of channel hydraulics in bedrock rivers typically yield values of $\omega > 200$ W m^{-2} and $\tau > 50$ N m^{-2}. Values of ω and τ are especially low in the karst depression and cave, where ω and τ are more typical of an alluvial river than a comparatively steep, mountain stream (Table 6.1)(Figure 6.12)(Baker and Pickup, 1987; Nanson and Croke, 1992; Wohl and Ikeda, 1998; Wohl et al., 2001).

The estimate of U_c for blocks in the channel bed in reach E is less than that estimated by the hydraulic model. This can be interpreted to suggest that the cave stream is unable to mobilize unprotected blocks of equal size to those in the bed for the modeled flood. Estimates of $\bar{u}$ are still lower in all other in-cave and karst depression reaches. This result is in general agreement with the absence of limestone clasts atop riffles in reach E and elsewhere in the cave.

On the basis of observations, quarrying is occurring in reaches A and D. Detached blocks and stepped bedrock surfaces are present in these reaches, which also display two of the highest values of ω and τ calculated for the study reaches. Reach B also has comparatively high values of ω and τ, but abrasion is recorded by sculpted forms on insoluble boulders on the alluvial bed. In contrast to reaches A, B, and D, low values of ω and τ are estimated for reaches wherein evidence of corrosion is most common (Table 6.1)(Figure 6.12). The association of high values of ω and τ with evidence of mechanical erosion and low values where evidence of corrosion predominates causes a failure to accept the null hypothesis that τ and ω values are similar in Buckeye Creek where evidence of corrosion is most numerous and are highest where evidence of mechanical incision is most numerous (Corollary Hypothesis I).

The minimal evidence of quarrying and abrasion suggests that low values of ω and τ observed in the limestone reaches are not compatible with quarrying or abrasion. Block mobilization is directly aided by high shear stress values (Hancock et al., 1998), but the relationship between ω and quarrying is indirect. Steep energy slopes increase ω and some energy sinks, such as macroturbulence, can aid block detachment by generating large

pressure fluctuations (Mathes, 1947). However, other energy sinks may produce little or no quarrying (e.g., energy lost in flow separations behind tree boles). Therefore, only a broad link between ω and quarrying is posited for further study.

6.6.2 Profile Maintenance and Stability

6.6.2.1 Profile Form. The relatively smooth longitudinal profile, probable grading to Spring Creek, and similarity to a comparable profile developed entirely atop clastics, imply profile stability in Buckeye Creek, despite the longitudinal transition from quarrying and abrasion to corrosion. The inferred state of equilibrium in turn implies that reaches developed atop limestone and clastics are coupled such that constant incision is maintained in each reach despite distinctly different erosion phenomena.

6.6.2.2 Inferences about Profile Integration. The hydraulics associated with the chemical and mechanical incision regimes may be incompatible with maintenance of a supply-limited bedrock stream system atop both soluble and insoluble strata for available discharge. Theoretically, large values of ω and τ atop the downstream limestones would lead to excess erosion through quarrying, thus creating profile disequilibria. Similarly, constant incision and maintenance of the stable longitudinal profile would be improbable atop clastics with low values of ω and τ. Localized mechanical energy expenditure as a function of substrate resistance has been reported from many large streams, but such partitioning has primarily been studied in streams that are supply-limited with respect to bedload (e.g., Baker and Pickup, 1987; Wohl, 1993; Wohl et al., 1994). Headwater streams, such as Buckeye Creek, are charged with sediment by hillslopes of narrow, deeply incised valleys. Simultaneously, maintenance of a stable profile is dependent upon

having a net long-term balance between sediment produced and transported out of a basin. However, low values of ω and τ atop downstream limestones are incompatible with transport of coarse bedload (Figure 6.10). Therefore, significant longitudinal changes in channel hydraulics as a stream flows from atop clastics to carbonates must also be accompanied by commensurate adjustments in sediment transport processes or else the influx of insoluble grains from clastic rocks would cause aggradation where low values of ω and τ are maintained, and downstream incision would cease.

On the basis of the association of particular erosion phenomena with certain hydraulic regimes, it is posited that equilibrium in profile shape and sediment mass balance is maintained in Buckeye Creek by longitudinal changes in sediment transport regimes. Sediment caliber declines rapidly as the stream enters and crosses the karst depression. Simultaneously, stream classification changes from bedrock to alluvial and back to bedrock in the cave. Coarse sediment storage at the upstream terminus of the karst depression and longitudinal sorting would explain why gravel is the dominant bedload in the downstream portion of the depression and cave (Figure 6.10). Presumably, mass balance flux is maintained by gravel transport during small to moderate floods, which are more likely to transport gravel than cobbles or boulders. Gravel bars were observed to have been mobilized between visits on a few occasions from 1999 to 2001 despite a drought-induced paucity of floods.

Ultimately, the alluvial reach may be a morphology adjustment wherein stream processes alter the sediment transport regime such that the different τ regimes can operate in a relatively smooth, concave channel of short length. The corrosion-dominated reaches

are characterized by relatively low values of τ, which is an important determinant of sediment transport (Bagnold, 1966). Therefore, the alluvial reach may adjust the size of bedload sediment such that long-term sediment transport is continuous throughout the channel despite large absolute differences in τ. Such a reality, if true, would help explain the observations of Miller (1996), that the distance streams flow across limestone is proportional to drainage area. Such a relationship exists for the small number of streams rising on Butler Mountain (Figure 6.3). Longer distances of flow across floodplains in the narrow valleys of the depression presumably afford greater storage capacity. Ultimately, debris-laden streams may sink only after mean bedload particle size has diminished such that a balance exists between the hydraulic regimes necessary for incision and sediment transport. This conjecture requires further study because it implies that the floor of the karst depression in the Buckeye catchment is as much the result of fluvial as karst processes.

6.6.2.3 Incision by Debris Flows. The role of mass wasting events in channel incision in the surface reaches is unknown. Debris flows can be extremely erosive in small headwater channels (Cenderelli and Kite, 1998; Springer et al., 2001). Moreover, the momentum of debris flows ensures that they will flow some minimum distance before depositing entrained boulders (Springer et al., 2001). There is considerable evidence of debris flow activity in low-order channels atop Butler Mountain, and coarse boulder accumulations in reach B may have been deposited by debris flows (Figure 3.9).

Debris flows are effective at quarrying and stream channels downstream of eroded channel segments may experience extensive aggradation (Benda, 1990). The maximum

distance of the limestone/clastic transition from potential sources of debris flows is 3 km, but low-order tributaries enter the channel immediately above and below the contact. Reported runout lengths of debris flows elsewhere in the Appalachians are as long as 3 km (Cenderelli and Kite, 1998; Springer et al., 2001), so it is possible that debris flows occasionally sweep across the convexity and reach the upstream terminus of the karst depression. If so, it is probable that quarrying and coarse sediment deposition in and upstream of reach B are not entirely functions of the channel processes examined for this study.

6.6.2.4 Profile Stability. The 1.2-km-long alluvial reach that dominates the fluviokarst depression floor is not compatible with long-term profile stability unless the underlying bedrock is removed such that the valley profile remains stable. No sinkholes are present along the surface course of Buckeye Creek and no known caves underlie the stream course. Therefore, it is possible that long-term excavation of the valley floor is not accomplished entirely by corrosion beneath the insoluble sediments shielding the bedrock. If so, there must be periodic incision and bedrock exposure in the alluvial reach or the Buckeye Creek profile would be destabilized by aggradation associated with influx of headwater-derived sediment and lack of valley floor incision.

Incision is known to be episodic in Buckeye Creek Cave (Figure 3.10), as it is in most fluviokarst caves. Long periods of relative stability alternate with vertical avulsions that lead to abandonment of stream channels (Palmer, 1987; Palmer, 1991). The effect of these avulsions must propagate headward through the drainage basin. Presumably, the alluvial reach would experience incision and extensive scour of floodplain sediments.

White and White (1983) report the presence of abandoned straths in a fluviokarst basin in Tennessee, where a fluviokarst stream is also graded to a large-order stream. The straths were interpreted to be abandoned fluviokarst depression floors. They tentatively interpreted the straths to represent periods of baselevel stability. In light of inferences made for Buckeye Creek, these straths may represent former depression floors abandoned during headward recession of a knickpoint created when an associated cave stream avulsed to a new, lower stream passage. Cave levels are known to reflect the elevation of base level streams (Granger et al., 2001), therefore the supposition does not conflict with the idea suggested by White and White (1983).

Episodic incision inside of Buckeye Creek Cave is not compatible with maintenance of a stable profile because Spring Creek is presumably incising continuously (ignoring bed elevation fluctuations brought about by climate shifts). However, avulsions in stream caves need not cause abandonment of passages throughout the length of the cave. For instance, Buckeye Creek is currently avulsing to a lower stream passage near the Spencer Cave entrance and the narrow canyon (reach F) is an avulsion brought about by collapse of a slightly higher passage. The effect of incremental avulsion would be to maintain grading and drive lower relief, more frequent knickpoints throughout the stream network. This hypothetical model would better explain the relative thinness of clastic sediments on the Buckeye Creek floodplain because lengthy periods of no incision would yield thick alluvial deposits.

6.7 Conclusion

Magnitudes of ω, τ, and sediment size decline markedly in the downstream direction in Buckeye Creek. The lowest estimated values of ω and τ are found where evidence of corrosion is most abundant. Values are highest where evidence of quarrying and abrasion are present. On the basis of these results, there is a failure to accept the null hypothesis that, τ and ω are similar in Buckeye Creek where evidence of corrosion is most numerous and highest where evidence of mechanical incision is most numerous (Corollary Hypothesis I).

The decline in sediment sizes is coincident with declines in estimated values of ω and τ. The coincident changes in relative substrate solubility, hydraulics, sediment size, and inferred incision processes are therefore posited to represent adjustment of channel processes such that chemical and mechanical erosion act separately, but congruently, to maintain a graded profile in Buckeye Creek. Coarse sediment, which is not readily transportable under low τ predicted in a cave channel, is stored in a 1.2-km-long alluvial reach that couples bedrock reaches in the headwaters and cave. Coarse clasts are preferentially deposited in the alluvial reach and mean clast size declines from -7ϕ at the upstream end of the alluvial reach to -4ϕ in the cave.

Chapter 7

Profile Maintenance in a Large Mountain River

7.1 Chapter Abstract

Unit stream power and shear stress are highest atop insoluble strata versus soluble strata in paired reaches of the Greenbrier River, West Virginia. Mean reach values of shear stress and unit stream power are highest atop resistant sandstone, 880 W m^{-2}, and least atop shales and limestones. The lowest mean value of unit stream power, 40 W m^{-2}, is achieved where the river is flowing atop limestones away from valley walls. However, for constant relative solubility of the channel bed, unit stream power and shear stress are consistently higher in reaches that interact strongly with hillslopes. Unit stream power and shear stress vary by an order of magnitude between reaches containing and lacking: (i) vertical bedrock cutbanks, and (ii) large boulders.

Evidence of quarrying and abrasion is most numerous where unit stream power and shear stress are largest. The association of large unit stream power and shear stress values with evidence of mechanical incision is posited to represent lengthwise adjustments of channel hydraulics to account for differences in forces driving incision atop insoluble and soluble substrates. Namely, incision of soluble strata requires less

input of mechanical energy because chemical energy provides the primary impetus for incision.

7.2 Introduction

Reach-scale hydraulics and energy expenditure are believed to reflect local adjustments to substrate resistance in stable, incising bedrock streams (e.g., Wohl and Merritt, 2001). For instance, it has been hypothesized that flow velocities may be adjusted over geological time to be swiftest atop extremely resistant and massive strata, which cannot be readily quarried by floodwaters. High water velocities increase the ability of suspended tools to abrade channel margins and this would theoretically allow the associated reaches to maintain congruent incision with other channel segments (Hancock et al., 1998; Whipple et al. 2000a,b). Therefore, mean water velocity ($\bar{u}$) may be useful as a crude index of the capability of a graded stream to incise bedrock (Hancock et al., 1998). Hypothetically, bed shear stress (τ) and unit stream power (ω) may be useful indices of quarrying capabilities (Hypothesis I). However, values of ω, τ, and $\bar{u}$ may not be simple functions of substrate resistance because hillslope interactions and other confounding influences may be reflected in reach-scale channel hydraulics (Hypothesis III). This chapter examines correlations between ω, τ, $\bar{u}$, inferred incision processes, bed resistance, and hillslope interactions in a stable bedrock river incising sandstone, shale, and limestone.

7.3 Methods of Incision

Evidence of incision mechanisms was sought during data collection in each of the five reaches examined in the Greenbrier River. Using the criteria outlined in Chapter 4, the principle incision mechanisms in each reach were identified (Table 7.1). Corrosion was evident in all limestone reaches (e.g., Figure 7.1). Quarrying is enhanced at Acme Quarry by corrosion widening of block-bounding joints (Figure 7.2). Evidence of abrasion was only observed at Anvil Rock where sandstone boulders display potholes up to a meter in diameter, flutes on upstream faces, and complex sculpted forms on downstream faces (Figure 7.3). Abrasion is especially prevalent where large boulders constrict the channel, where abrasion is diminishing boulders (Figures 7.3 and 7.4). These boulders are not part of the channel substrate because they are derived from the canyon rim, but concavity of the longitudinal profile in the canyon and pervasive excavation of sculpted forms atop sandstone boulders strongly suggest that the boulders impede incision of the limestone substrate (Figures 3.3C, 7.3, 7.4). The abrasion may be aided by the rapidity of local mean channel velocities (Table 7.1).

The role of quarrying atop limestone can be evaluated by the fraction of locally derived clasts on the riverbed. Bedload of the Greenbrier River is primarily sandstone and conglomerate clasts derived from local and headwater sources. The Greenbrier River first crosses limestones of the Greenbrier Group at Renick. Hence, limestones observed on the bed are presumably derived from adjacent hillslopes or the riverbed. The fraction of limestone clasts is highest atop a limestone bed where evidence of quarrying was

Figure 7.1: Irregular, corroded limestone clasts from atop a riffle in the Cathole reach. Corrosion presumably occurs prior to and during transport. Penny for scale.

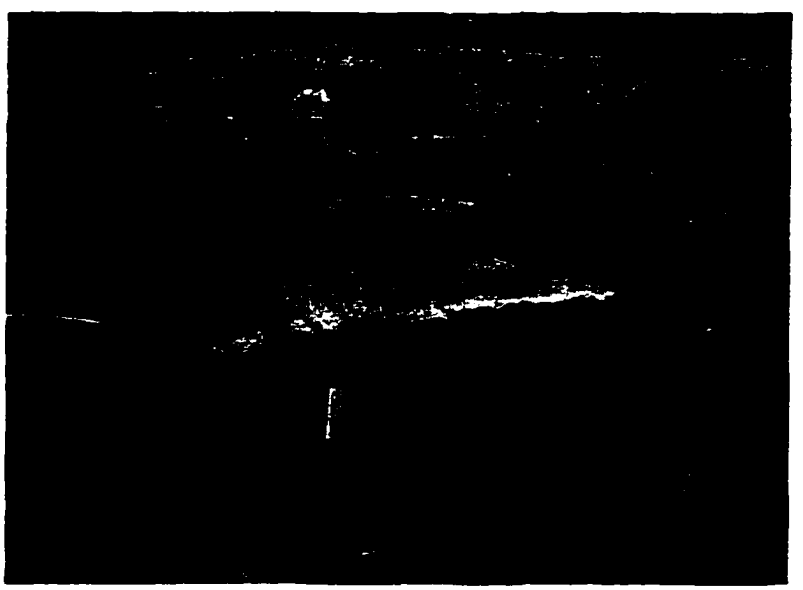

Figure 7.2: Quarried block of limestone detached from bed of the Acme Quarry reach by corrosion along bounding joints. Vertical tubes mark upward or downward flow of water during floods. Tubes in attached blocks intersect sub-horizontal anastomose tubes atop underlying bedding planes. Note 17.8 cm high field notebook for scale.

Table 7.1: Incision Processes and Model Results for Greenbrier River

Reach	Model Discharge	Bed Lith.	Bedrock Cutbank?	Incision Processes[a]	% Ls Clasts[b]	Mean Depth	Mean Top Width (m)	Hydraulic Radius (m)	ω (W m^{-2})[c]	τ (N m^{-2})[c]	$\overline{u}$ (m s^{-1})[c]
Anvil Rock	2300 $m^3 s^{-1}$	Ls	Yes	Ab+Q+C	8.0	8.5	80	8.5	720 ± 170	170 ± 30	4.3 ± 0.4
Acme Quarry	2300 $m^3 s^{-1}$	Ls	Yes	C+Q	10.7	7.4	111	7.4	400 ± 190	120 ± 40	3.3 ± 0.7
Mile-27	1800 $m^3 s^{-1}$	Ss	Yes	Q	0.0	5.0	148	5.0	250 ± 80	90 ± 20	2.8 ± 0.3
Bone Quarry	1800 $m^3 s^{-1}$	Ls	No	C	0.7	9.5	131	9.5	40 ± 20	30 ± 7	1.6 ± 0.3
Cathole	1800 $m^3 s^{-1}$	Ls	Yes	C+Q	4.3	5.4	110	5.4	410 ± 130	110 ± 20	3.5 ± 0.4
		Sh	Partial	Q		6.0	116	6.0	180 ± 70	60 ± 20	2.8 ± 0.4
		Ss	Yes	Q		4.7	103	4.7	880 ± 70	200 ± 10	4.4 ± 0.1

[a] Ab denotes abrasion; Q denotes quarrying; C denotes corrosion. Order reflects inferred relative roles.

[b] Percent of bedload clasts that are limestone. Minimum n of 300.

[c] Mean ± one standard deviation from atop riffles except for shale values at Cathole. Shale only outcrops in pool.

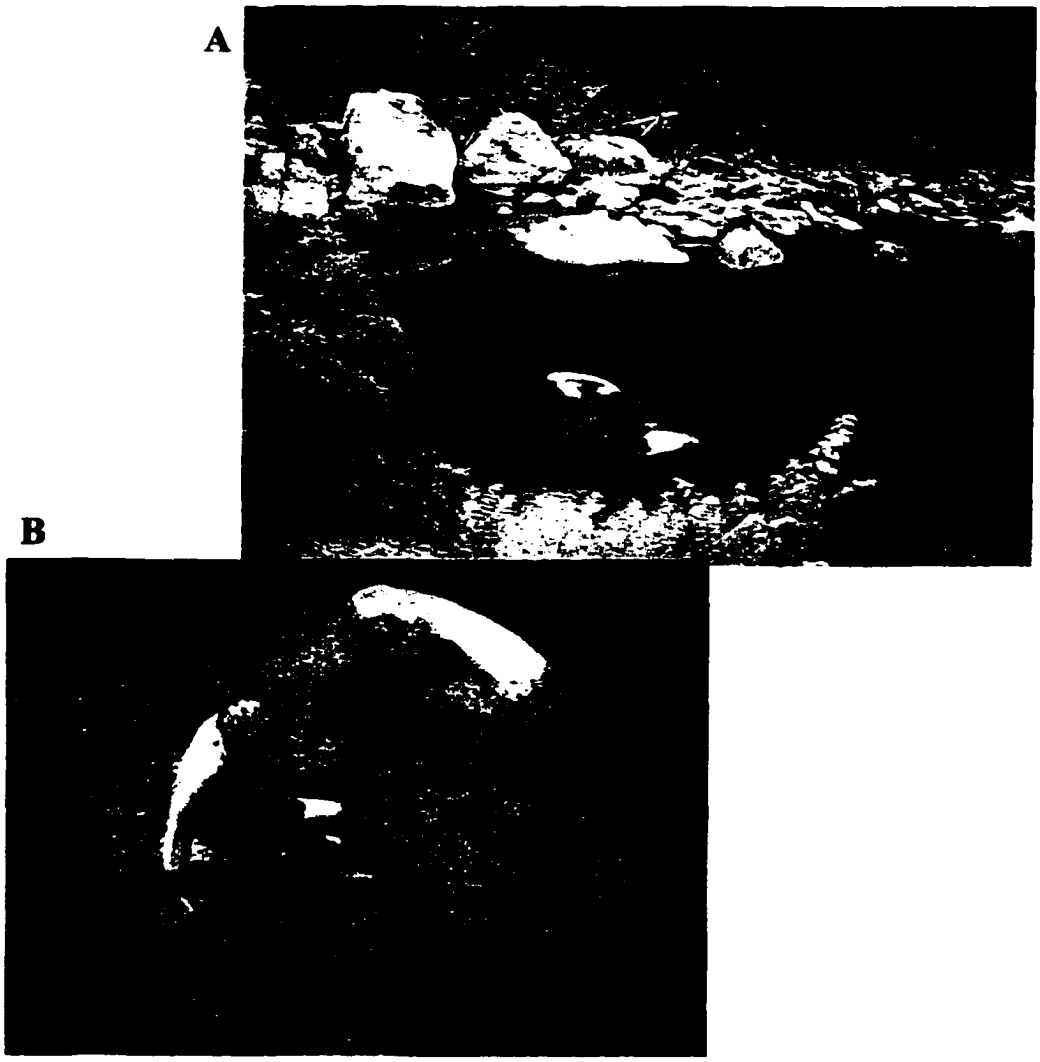

Figure 7.3. A: Colluvial apron composed of sandstone boulders on river right in Anvil Rock reach. B: Large boulder in center of channel at apron seen in A (location identified by B in frame A). Abrasion has formed large potholes atop the boulder. Note gravel-size grinders in largest pothole and smaller pothole beside model. Flow is from right to left.

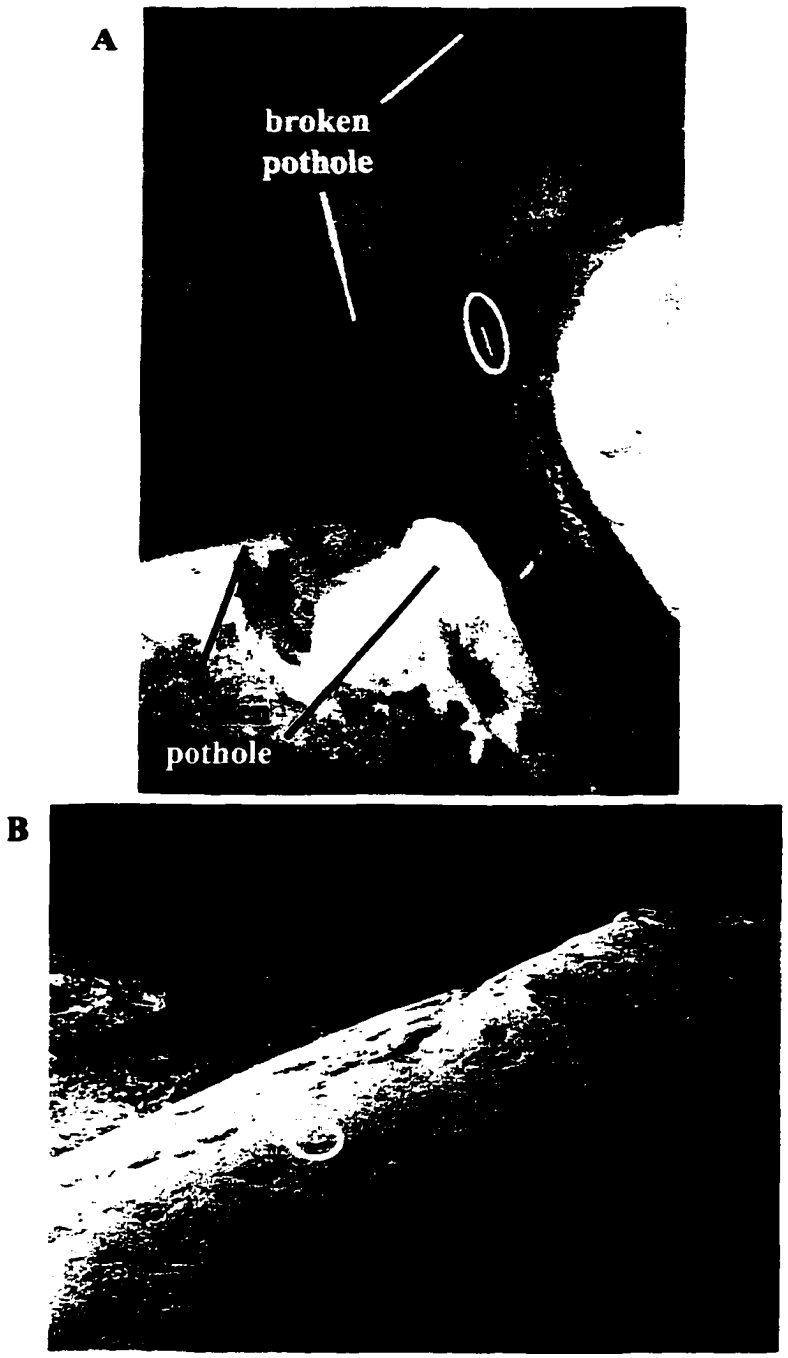

Figure 7.4. A: Broken pothole formed at intersection of two joints in a large sandstone boulder in the Anvil Rock reach. The pothole enhanced tensional forces across the joint and caused the boulder to split. Note marking pen for scale. B: Abraded and crudely fluted surface of a large sandstone boulder in the Anvil Rock reach. Flow is from left to right. Note penny for scale.

observed and least where corrosion is inferred to be the only means of river incision by a lack of quarried surfaces (Table 7.1).

7.4 Results

7.4.1 Modeling Output

All five reaches were modeled in HEC-RAS using estimates of the 100-yr discharge (Table 7.1)(Chapter 4). Estimates of ω, τ, and $\bar{u}$ were obtained directly from HEC-RAS. Model results are provided in Table 7.1. Values of ω range from 40 W m^{-2} atop limestone at Bone Quarry to 880 W m^{-2} atop sandstone in the Cathole reach. Values of τ range from 30 W m^{-2} atop limestone at Bone Quarry to 200 W m^{-2} atop sandstone in the Cathole reach. ω and τ are codependent because each shares three calculation terms (equations 1.1, 1.3, 1.4). Because of the codependence, only the results of comparisons of ω are presented below.

7.4.2 Preplanned Comparisons of Reach Results

7.4.2.1 Bone Quarry versus Mile-27. The channel bed is composed of limestone in two of the three reaches at Renick (Figure 3.3). The Mile-27 and Bone Quarry reaches are underlain by sandstone and limestone, respectively (Table 3.2). These two straight reaches do not receive coarse sediment from adjacent hillslopes, and Selby rock hardness scores are similar (Table 3.2). Despite their similarities, ω and τ are statistically distinct between the two reaches (Table 7.2). The lowest values are achieved atop limestones in the Bone Quarry reach (Table 7.1). ω averages 40 W m^{-2} in the Bone Quarry reach despite expansive bedrock exposures. For comparison, 200 W m^{-2} has been suggested as the

Table 7.2: Results of Hypothesis Tests for Unit Stream Power

Hypotheses	Reaches Compared	Substrate Comparison[a,b]	Geomorphic setting Comparison[a,b]	T-statistic (Significance)	Test Outcomes[c] I	III
I	Bone Quarry vs. Mile-27	Ls vs. Ss	No Cutbank vs. No Cutbank	4.3 (0.05)	CA	n/a
I	Cathole (Ls) vs. Cathole (Ss)	Ls vs. Ss	Cutbank vs. Cutbank	4.8 (0.02)	CA	n/a
I, III	Cathole (Ls) vs. Mile-27	Ls vs. Ss	Cutbank vs. No Cutbank	1.8 (0.15)	FR	FR
I, III	Bone Quarry vs. Cathole (Ss)	Ls vs. Ss	No Cutbank vs. Cutbank	18. (0.03)	CA	CA
III	Bone Quarry vs. Cathole (Ls)	Ls vs. Ls	Cutbank vs. No Cutbank	5.0 (0.04)	n/a	CA
III	Anvil Rock vs. Acme Quarry	Ls vs. Ls	Ss Boulders vs. No Ss Boulders	2.7 (0.04)	n/a	CA

[a] Ls denotes limestone. Ss denotes sandstone.

[b] Variables are ordered respective to ordering of reaches in second column.

[c] FR denotes failure to reject the null hypothesis. CA denotes that the null hypothesis cannot be accepted and that the model values are more supportive of the research hypothesis.

typical lower limit for ω in bedrock streams and a value of 180 W m^{-2} is achieved atop nearby shales (Table 7.1)(Nanson and Croke, 1992).

Gradient is steeper in the Bone Quarry reach, but the mean hydraulic radius (R) of 8.6 m at Bone Quarry is significantly greater than the mean of 4.8 m at Mile-27 (d.f.=12; statistical significance <0.001)(Table 7.2). Top widths at Bone Quarry and Mile-27 are 131 m and 148 m, respectively. The larger hydraulic radii at Bone Quarry reflect greater cross-sectional flow areas and depths. The larger depth causes τ to decline proportionally less relative to ω at Bone Quarry than in any other reach (ω/τ)(equation 1.4).

7.4.2.2 Values Atop Limestone and Sandstone at Cathole. The 1.4-km-long Cathole reach spans outcrops of limestone, shale, and sandstone (Figure 3.3B). The river is incising bedrock cutbanks into the limestone and sandstone. The sandstone is being quarried as large, thin blocks of sandstone that mantle portions of the reach. Blocks may only be 10 cm thick even when a- and b-axis lengths are 1.5 m. Evidence of corrosion is pronounced atop limestones of the Cathole reach (Figure 7.1). Angular quarried blocks are virtually absent, although limestone clasts are common atop riffles where corrosion-liberated blocks comprise a large fraction of the limestone bedload (Table 7.1)(Figure 7.1). Bedrock is exposed extensively in pools atop the limestone and sandstone, but ω and τ are statistically distinct as functions of lithology (Table 7.2). Hydraulic radius and depth are significantly larger atop the limestone (statistical significance of 0.05 and 0.002 for each comparison, respectively).

7.4.2.3 Cathole (Ls) versus Mile-27. The Mile-27 reach is incising sandstones, but lacks a bedrock cutbank. The thinly cross-bedded sandstone is yielding decimeter-sized,

plate-like blocks and cubic blocks with axis lengths of a few decimeters. Cathole (Ls) is incising limestone beneath a bedrock cutbank, but there is little visual evidence of quarrying. Values of ω are not significantly different between the two reaches (statistical significance of 0.15). The two reaches were chosen for comparison because of the interaction of substrate and geomorphic setting variables (Tables 4.1 and 7.2). The interaction term effectively tests Hypotheses I and III simultaneously.

7.4.2.4 Bone Quarry versus Cathole (Ss). These two reaches were also chosen because of substrate and geomorphic setting interactions, although the interaction is the opposite of the Cathole (Ls) versus Mile-27 comparison (Table 7.2). The Bone Quarry versus Cathole (Ss) comparison is the most significant of all comparisons made for the Greenbrier River; the statistical significance of the comparison is 0.03.

7.4.2.5 Bone Quarry versus Cathole (Ls). These two reaches are flowing atop limestone near the base of the Greenbrier Group. But, Bone Quarry is isolated from the valley wall by low terraces and a floodplain while a limestone cutbank lines river right in the Cathole reach. Therefore, relative substrate solubility is constant but geomorphic setting is not. The statistical significance of the comparison is 0.04 despite the similarity in bed composition.

7.4.2.6 Anvil Rock versus Acme Quarry. These two reaches are flowing atop limestone, but the Anvil Rock reach receives insoluble boulders from the overlying valley while the Acme Quarry reach does not. The statistical significance of the comparison is 0.04. As discussed in Chapter 1, no statistical comparisons are made between these two

reaches and those near Renick because of the possibility of asynchronous response to base level fall or knickpoint propagation between the two segments.

7.5 Evaluation of Reach Comparisons and Hypothesis Tests

7.5.1 Concepts

The reaches examined in Greenbrier River were chosen to evaluate the general hypothesis that the river has minimized ω and τ where the presence of a soluble substrate affords the river an additional source of energy for river incision, chemical energy. Although causality cannot be definitively established by this study, the results should either support or contradict the conjecture. Hypothesis I should aid this qualitative assessment. Similarly, the confounding effect of hillslope interactions is evaluated using Hypothesis III. Presumably, the supply of coarse sediment to the channel will be associated with higher values of ω, τ, and $\bar{u}$ because these variables may be associated with the ability of the stream to quarry and abrade (Corollary Hypothesis I).

7.5.2 Effects of Relative Substrate Solubility and Geomorphic Setting

7.5.2.1 Relative Substrate Solubility. Hypothesis I is evaluated in four of the six comparisons (Table 7.2). The null hypothesis of no effect upon ω for soluble and insoluble strata cannot be accepted for three of the four comparisons; ω is greater atop insoluble bedrock than atop soluble bedrock.

The null hypothesis cannot be rejected for the Cathole (Ls) versus Mile-27 comparison; ω is not statistically different between the limestone- and sandstone-floored reaches. This comparison was made between a limestone-bound reach with a bedrock

cutbank and a sandstone-floored reach lacking a cutbank. The bedrock cutbank supplied coarse sediment from rockfalls and may be the result of lateral incision. Presumably, the limestone has higher ω and τ because it must incise and transport or diminish coarse sediment supplied by the hillslope. The coarse sediment presumably shields the bed from directed corrosive attack and the soluble sediment supplied by the bedrock cutbank presumably causes hyporheic fluids to have higher pH, which would diminish their ability to corrode the bed. If the reach is incising laterally, as is suspected, additional energy must be expended over geologic time.

7.5.2.2 Geomorphic Setting. Among the three Renick reaches, values of ω, τ, and $\bar{u}$ are highest where the river is incising bedrock cutbanks (Table 7.1). Hypothesis III is evaluated in four of the six comparisons (Table 7.2). The null hypothesis of no effect for geomorphic setting cannot be accepted for three of the four comparisons; ω is greater where a reach is interacting directly with the adjacent hillside relative to a reach lacking the same interaction.

The null hypothesis cannot be rejected for the Cathole (Ls) versus Mile-27 comparison; ω is not statistically different between the cutbank and no cutbank reaches. However, as discussed previously this comparison is complicated by term interactions wherein the limestone reach is associated with a bedrock cutbank and the sandstone reach is not. This outcome supports the research hypothesis that, stream reaches abutting valley walls or receiving coarse, insoluble sediment from hillsides will display higher values of ω and τ than reaches lacking such confounding influences. Having previously found that reaches underlain by soluble strata are associated with lower values of ω and τ, the higher

value for Cathole (Ls) can be interpreted to represent the effect of the bedrock cutbank and coarse sediment supplied by oversteepened valley walls. Lateral incision would further support this argument, but further work must be done to establish whether this process is active in the reaches examined.

The relative roles of quarrying versus corrosion in the Acme Quarry and Anvil Rock reaches are unknown, but several observations suggest that the two processes are related to one another. Joint spacing is wide in both reaches, with minimum block widths on the order of 1-to-3 m. Detached and intact blocks are diminished by corrosion and abrasion (Figure 7.5), but corrosion is effective in simultaneously diminishing and liberating blocks (Figure 7.2). Quarrying of blocks may partly reflect the massive strata in both reaches, but must also reflect high values of ω and τ that have arisen in response to the insoluble sandstone boulders. Response to these boulders presumably extends outside of the Anvil Rock reach, because the longitudinal profile is convex upward over a longer distance (Figure 3.3C).

7.5.3 Association of Incision Mechanisms with Hydraulic Variables

Corollary Hypothesis I, that quarrying and abrasion are associated with higher values of ω, τ, and $\tilde{u}$, can be qualitatively evaluated using the model output. Modeled values of ω and τ are least at Bone Quarry where visual evidence of corrosion greatly outnumbers evidence of quarrying or abrasion (Table 7.1). The highest model values are found atop sandstone in the Cathole reach, which is notable for the presence of large, distinctively thin blocks of quarried sandstone on the bed. Between these two extremes, ω is statistically lower atop limestone at Cathole than atop sandstone (Table 7.2). Evidence

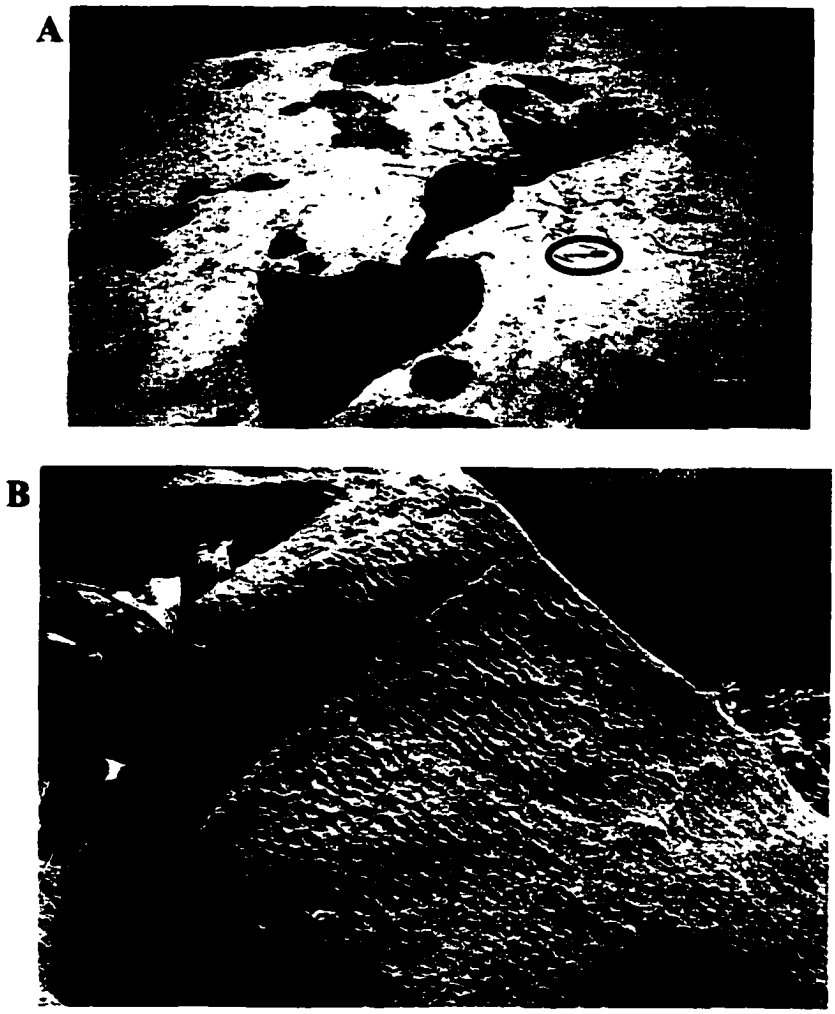

Figure 7.5. A: Potholes formed by abrasion and corrosion in the vicinity of the Anvil Rock reach. These potholes are found where the channel is free from sandstone boulders. By inference, the energy required to erode the sandstone boulders also causes abrasion to be an important component of limestone erosion in adjacent reaches. Note marking pen for scale (inside oval). Flow is toward viewer. B: Scallops eroded into an intact limestone block in the Acme Quarry reach. The scallops are excavated by a combination of corrosion and abrasion. Note corrosion widening of joint near top of boulder, and penny for scale.

of corrosion predominates atop the limestone, whereas evidence of quarrying pervades the sandstone-floored reach.

A comparison of incision phenomena versus ω in the remaining reaches is complicated by the apparent influence of hillslope interactions on ω (section 7.5.2). The Bone Quarry versus Cathole (Ss) comparison is between reaches where evidence of corrosion and quarrying each predominate and the comparison supports the conjecture. However, the presence of a bedrock cutbank in the sandstone-bound reach may exaggerate the difference between the two reaches. Similarly, the Cathole (Ls) versus Mile-27 comparison is complicated by hillslope interactions.

There is qualified support for the research component of Corollary Hypothesis I, that ω and τ are least in Greenbrier River where evidence of corrosion is most numerous and highest where evidence of mechanical incision is most numerous. However, the confounding effect of hillslope interactions cannot be ignored.

7.6 Discussion

Differences between individual variables as functions of relative rock solubility (limestone versus sandstone) are statistically significant, for a criterion of 0.05, among reaches with similar hillslope interactions. By inference, lower values of ω and τ atop soluble rock in the Greenbrier River may reflect a hydraulic adjustment to the chemical weakness of soluble strata. Namely, mechanical energy expenditure is maximized atop insoluble strata because mechanical incision processes erode those strata. The nature of the adjustments may be geometrical; hydraulic radius is larger atop limestones. This has

the effect of lessening boundary-generated energy expenditure relative to reaches with smaller radii and increases the area available for corrosion (e.g., Leopold et al., 1964).

The ability of the Greenbrier River to incise by corrosion does not translate to universally low values of ω and τ atop limestones or an absence of quarrying atop limestones; incision mechanisms and values of ω, τ, and $\bar{u}$ vary significantly among the limestone reaches examined. Values of ω, τ, and $\bar{u}$ are largest where the river is excavating bedrock cutbanks and receiving coarse sediment from valley walls (Table 7.1); comparison of individual reaches of the Greenbrier River suggests that relationships between channel hydraulics and erosion processes may be obscured by hillslope interactions (Table 7.2). For instance, corrosion is independent of hydraulic processes but this does not mean that the erosion process will be uniformly expressed as low ω and τ values because incision indices in the Greenbrier River are not merely functions of the chemical resistance of the bed substrate. Values of ω, τ, and $\bar{u}$ atop limestone may be higher than those atop sandstone if the limestone reach interacts more strongly with the valley wall, as is the case for the comparison of Cathole (Ls) vs. Mile-27 (Tables 7.1 and 7.2). Similarly, incision indices atop limestone may be equivalent to those atop resistant sandstone if the limestone reach receives coarse sandstone boulders from adjacent hillslopes, as is the case for Cathole (Ls) versus Anvil Rock.

Profile equilibrium is not assumed for the entire Greenbrier River, although incision rates in the study segments are similar. However, the apparent adjustment of ω and τ atop soluble and insoluble strata suggests that congruent incision prevails at least at the scale of the study segments. This raises the question of how the different reaches are

coupled, such that different hydraulic regimes prevail atop the different substrates. This study only examined one reach spanning multiple substrates, Cathole. Incision mechanisms apparently change across the 1.4-km-long Cathole reach in conjunction with changes in channel geometry. Hydraulic radius is largest atop limestone, and differences in channel width, depth, and area atop sandstone and limestone produce different values of incision-related hydraulic variables (Table 7.1). These changes in channel geometry occur in association with a 1-km-long pool, which is the largest pool observed in this river segment. The effect of the pool is to maximize depth and thereby τ atop limestone and shales of the Cathole reach, because greater depth is required to drive flow across the 500-m-long section of reversed gradient at the downstream end of the pool. Mechanical energy expenditure is enhanced atop sandstone at the downstream end of the pool by decreases in depth and width, which presumably enhances boundary roughness and probably turbulence generation Whether other stream reaches spanning other lithologic contacts have similar relationships between hydraulics and substrate resistance will require investigation of additional reaches and rivers.

7.7 Conclusions

The Greenbrier River incises by corrosion, quarrying, and abrasion. The chemical and physical resistance of the channel bed, as well as hillslope interactions, determines the relative importance of individual incision mechanisms. Corrosion predominates atop soluble strata where the river interacts minimally with the valley wall and receives no coarse sediment from adjacent hillslopes. The ability to incise by corrosion alone

translates to minimal modeled values of ω, τ, and $\bar{u}$, which are posited to be crude indices of incision capability for channels atop insoluble strata. Values of ω, τ, and $\bar{u}$ increase where the river flows beneath bedrock cutbanks regardless of bed solubility. However, the largest modeled values of ω, τ, and $\bar{u}$ are where the river is simultaneously excavating a bedrock cutbank and incising sandstone. Moreover, values of ω, τ, and $\bar{u}$ are high where the river receives coarse sandstone boulders from the valley wall, but is incising limestone. Many of the massive boulders may be too large to move and are being diminished by abrasion.

Chapter 8

Profile Maintenance in Bedrock Streams Incising Soluble Strata

8.1 Overview of Findings

Bedrock streams use a variety of phenomena to incise including quarrying, abrasion, and corrosion. The longitudinal distribution of incision mechanisms varies as a function of substrate in Buckeye Creek and the Greenbrier River. Evidence of corrosion is more common than evidence of quarrying atop soluble strata and evidence of quarrying is most common atop insoluble strata. Unit stream power (ω) and bed shear stress (τ) are highest atop insoluble substrates in both streams. However, insoluble strata are not uniquely associated with elevated values of ω and τ. Hillslope interactions such as cutbank excavation and large influxes of insoluble, coarse sediment produce measurable responses in values of ω and τ atop limestones in Greenbrier River (Table 7.2). Coarse sediment is not being transported throughout Buckeye Creek and boulders are being diminished by abrasion or effectively diminished through sorting in the floodplain atop the karst depression. Sculpted forms locally enhance abrasion and corrosion. The morphology of the sculpted forms is not entirely a function of hydraulics.

8.2 Discussion: Findings in Context

8.2.1 Covariance of Incision Processes and Hydraulics

Previous studies have established that model estimates of unit stream power and shear stress are highest where resistant strata outcrop in streambeds (Baker and Pickup, 1987; Wohl, 1993; Wohl et al., 1994; Wohl and Ikeda, 1998; Wohl and Merritt, 2001). Qualitative observations have been used to hypothesize that bed gradient and energy expenditure adjust in bedrock rivers according to the resistance of the underlying bedrock and its longitudinal distribution (Hancock et al., 1998; Whipple et al., 2000a,b). These changes may be complex because some strata cannot be eroded by more than one of the three common erosion mechanisms. For instance, effectively insoluble strata that are particularly massive may simultaneously resist quarrying and corrosion. Therefore, it is possible that bedrock streams will adjust their gradient and velocities to incise these strata by abrasion (Hancock et al., 1998; Whipple et al., 2000a,b). However, no studies have shown quantitatively that hydraulics and incision processes co-vary in a bedrock river because most studies have examined solitary reaches.

The variations in substrate, inferred incision processes, and modeled values of hydraulic variables are generally consistent with the hypothesis that streams simultaneously adjust channel processes and incision processes such that congruent incision is maintained throughout. The results are not conclusive because only two streams and thirteen reaches were examined. But, the results lend the first quantitative support to the conjecture and suggest the need for future studies.

The present results also allow the first statements to be made about the relative influences of geomorphic setting and basin scale on channel processes. Coarse sediment loading is apparently expressed as high values of ω and τ in Greenbrier River, regardless of relative bedrock solubility. This implies that geomorphic setting is more important for determining reach hydraulics than substrate in many reaches. The apparent relationship of the alluvial reach atop the karst depression in the Buckeye Creek catchment may also be related to geomorphic setting. But, as a headwater stream the Buckeye Creek may be incapable of simultaneously incising by corrosion and transporting coarse boulders.

8.2.2 Basin-Scale Models of Bedrock Channels

Establishing the relationships between substrate, incision processes, and hydraulics is necessary for development of second-generation models of longitudinal profile development in bedrock rivers. Existing models of bedrock stream profiles typically attempt to describe stream variables as functions of local basin area (A), slope (S), and rock resistance (k)(Howard, 1994). Values of k are often back calculated where incision rates are known, but k-values may vary by five orders of magnitude even where lithology is similar (Snyder et al., 2000). The variability of k is, presumably, a consequence of the variability in channel hydraulics as functions of hillslope interactions and incision mechanisms, which may occur independently of channel substrate. For instance, comparison of two limestone-floored reaches, Bone Quarry and Cathole, show a 10-fold difference in ω because the river is excavating a bedrock cutbank in the Cathole reach. Corrosion is the primary incision mechanism in both reaches, but the Cathole reach receives coarse sediment from the cutbank and is incising laterally, so values of ω

and τ are necessarily higher than atop the Bone Quarry reach, which is isolated from the valley wall by low floodplains and terraces.

Longitudinal variations in stream behavior are even more pronounced in the headwater catchment, Buckeye Creek. Maintenance of a stably incising, graded profile atop insoluble and soluble strata is accomplished by varying ω and τ by three orders of magnitude. The stream has adjusted to these differences by forming a 1.2-km-long alluvial reach that acts as a sorting mechanism. The importance of coarse, colluvial sediment is further seen in the limestone-bound, Anvil Rock reach wherein hydraulic variables are elevated, facilitating abrasion of sandstone boulders. Current bedrock channel models do not allow for such a complex response because these first-generation models generally fail to couple hillslope processes with channel processes and do not allow for non-systematic changes in channel width, depth, and slope (e.g., Howard, 1994; Snyder et al., 2000). Second-generation models will need to include empirical variables that relate channel interaction with valley walls and influxes of coarse sediment. The present study suggests that the empirical data may be obtained by performing space substitutions, whereby variable response to similar substrates is examined by modeling multiple reaches with different geomorphic boundary conditions.

8.2.3 Relationship of Incision Processes to Channel Hydraulics

8.2.3.1 Corrosion. Corrosion is not uniquely associated with a particular hydraulic regime in the slowly incising bedrock streams examined. Channel hydraulics vary in statistically recognizable ways where corrosion is the primary incision mechanism, but many confounding variables are recognized for Buckeye Creek and Greenbrier River. The most important confounding variable is valley wall interactions, which includes both

bedrock cutbanks and influx of colluvial sediment. The total variability in values of ω and τ atop soluble strata being incised by corrosion is 30-fold. However, corrosion is associated with extremely low values of ω and τ where the streams are interacting minimally with the valley wall. In such cases, values are more typical of lowland, alluvial rivers than mountain streams as defined by Nanson and Croke, 1992. The geomorphic factors that influence hydraulic variables for a single incision mechanism were discernable because multiple reaches were compared.

8.2.3.2 Quarrying and Abrasion. The small number of study reaches that were dominated by quarrying and abrasion preclude any strong conclusions to be made about the relationship that exists between the processes and channel hydraulics or substrate. Although it is evident that model values are generally higher atop insoluble substrates, the significance of the absolute differences is unknown pending modeling of other sandstone, siltstone, and shale reaches.

8.2.3.3 Sculpted Forms and Incision. Sculpted forms are known to be important agents of channel incision in caves and are believed to play important roles in channel incision atop resistant strata (Curl, 1974; Wohl, 1993; Hancock et al., 1998; Wohl et al., 1999; Whipple et al., 2000a,b). Erosion in sculpted forms may be the primary means of channel incision or sculpted forms may weaken attachment forces such that quarrying is possible after a period of preparation (Wohl, 1993). Sculpted forms occur in large numbers in some reaches of Buckeye Creek and Greenbrier River. Presumably, erosion inside sculpted forms dominates incision and passage enlargement in reach F of Buckeye Creek Cave because they cover all channel surfaces.

Abrasion of sandstone boulders in the Greenbrier River is associated with a narrowing of the channel and a local increase in the bed gradient. These adjustments have been observed atop many different substrates being eroded by sculpted forms (Wohl, 1993; Whipple et al., 2000a,b). The diminishing of sandstone boulders by sculpted forms in Greenbrier River and in the alluvial reach B in Buckeye Creek, both atop limestone beds, raises a philosophic issue as to whether the river is incising by corrosion, or corrosion and abrasion, in the associated reaches. As used *stricto senso*, bed incision in these reaches does not include pothole and sculpture excavation atop sandstone boulders. But, channel geometry and hydraulics are adjusted to maximize velocity and energy expenditure such that the boulders are diminished. As such, channel properties and values of $\bar{u}$, τ, and ω are more typical of a sandstone-bound channel than limestone (e.g., Wohl, 1993). By virtue of these observations it seems reasonable to argue that abrasion of the sandstone boulders is significant enough to conclude that abrasion is a primary means of channel incision, *senso facto*.

8.3 Conclusion

In general, unit stream power and shear stress are least where Buckeye Creek and Greenbrier River are incising soluble strata and highest where the streams are incising insoluble strata. Unit stream power, shear stress, and velocity vary as a function of incision processes and to a lesser degree channel substrate. Confounding variables, such as delivery of coarse sediment to both channels, causes large responses as evaluated using hydraulic variables. By implication, no single relationship exists between substrate resistance and channel hydraulics in the streams examined. Nonetheless, channel

segments developed atop soluble and insoluble strata are integrated with one another by discrete phenomena. As a result, stream profiles are relatively smooth despite significant longitudinal changes of substrate and incision processes.

References Cited

Alexander, H.S. 1932. Pothole erosion. *Journal of Geology*, 40:305-337.

Allen, J.R.L. 1968. On criteria for the continuance of flute marks, and their implications. *Geologie en Mijnbouw* 47:3-16.

Allen, J.R.L. 1971. Transverse erosional marks of mud and rock; their physical basis and geological significance. *Sedimentary Geology*, 5:165-385.

Atkinson, T.C., 1977. Diffuse flow and conduit flow in limestone terrain in the Mendip Hills, Somerset (Great Britain). *Journal of Hydrology*, 35:93-110.

Bagnold, R.A., 1966. An approach to the sediment transport problem from general physics. U.S. Geological Survey Professional Paper 422-I.

Baker, V.R. 1988. Flood erosion. *In:* Baker, V.R., Kochel, R.C., Patton, P.C. (Editors), Flood Geomorphology. Wiley-Interscience, Chicago, p. 81-95.

Baker, V.R. and Pickup, G., 1987. Flood geomorphology of the Katherine Gorge, Northern Territory, Australia. *Geological Society of America Bulletin*, 98:635-646.

Benda, L., 1990. The influence of debris flows on channels and valley floors in the Oregon Coast Range, U.S.A.. *Earth Surf. Processes and Landforms*, 15: 457-466.

Berggren, W.A., Kent, D.V., Swisher, C.C., and Aubry, M., 1995. A revised Cenozoic geochronology and chronostratigraphy. *In:* Berggren, W.A., Kent, D.V., Aubry, M., Hardenbol, J. (Editors), Geochronology, time scales and global stratigraphic correlation. Special Publication of the Society for Sedimentary Geology, 54:129-212.

Blumberg, P. G. and Curl, R. L. 1974. Experimental and theoretical studies of dissolution roughness. *Journal of Fluid Mechanics*, 65:735-751.

Burbank, D.W., Leland, J., Fielding, E., Anderson, R.S., Brozovic, N., Reid, M.R., and Duncan, C., 1996. Bedrock incision, rock uplift and threshold hillslopes in the northwestern Himalayas. *Nature*, 379:505-510.

Cardwell, D.H., Erwin, R.B., and Woodward, H.P. 1968. Geologic map of West Virginia: West Virginia Geologic and Economic Survey, scale 1:250 000, 2 sheets.

Carling, P.A., Hoffmann, M., and Blatter, A.S., 2002. Initial motion of boulders in bedrock channels. *In:* House, K., Webb, R., Baker, V.R., and Levish, D.R. (Editors), Ancient Floods, Modern Hazards: Principles and Applications of Paleoflood Hydrology, Water Science and Application Volume 5. American Geophysical Union Monograph, Washington, D.C., 147-160.

Cenderelli, D.A. and Kite, J.S., 1998. Geomorphic effects of large debris flows on channel morphology at North Fork Mountain, eastern West Virginia, USA. *Earth Surf. Processes and Landforms*, 23: 1-19.

Coward, J.M.H., 1975. Paleohydrology and streamflow simulation of three karst basins in southeastern West Virginia. Unpublished PhD thesis, McMaster University, Canada, 394 p.

Curl, R. L. 1974. Deducing flow velocity in cave conduits from scallops. National Speleological Society Bulletin, 36(2):1-5.

Dasher, G.R., and Balfour, W.M., 1994. The caves and karst of the Buckeye Creek Basin, West Virginia Speleological Society Bulletin 12, West Virginia Speleological Society, Barracksville, West Virginia, 238 p..

Deike, G.H. and White, W.B., 1969. Sinuosity in limestone solution conduits. *American Journal of Science*, 267:230-241.

England, J., 1999. Expected Moments Algorithm: At-site flood frequency estimation with historical/paleohydrologic data [DOS program]. Denver, Colorado, U.S. Dept. of the Interior, Bureau of Reclamation.

Farrant, A.R., Smart, P.L., Whitaker, F.F., and Tarling, D.H., 1995. Long-term quaternary uplift rates inferred from limestone caves, Sarawak, Malaysia. *Geology*, 23:357-360.

Ford, D.C. and Williams, P.W., 1989. Karst geomorphology and hydrology, Unwin Hyman, London, 601 p.

Gale, S.J., 1984. The hydraulics of conduit flow in carbonate aquifers. *Journal of Hydrology*, 70:309- 327.

Gilbert, G.K., 1877. Report on the geology of the Henry Mountains: Geographical and geological survey of the Rocky Mountain region: Washington, D.C., Government Printing Office, 106 p.

Gillieson, D., 1996. Caves: Processes, Development, and Management. Blackwell Publishing, 353 p.

Granger, D.E., Fabel, D., and Palmer, A.N., 2001. Pliocene-Pleistocene incision of the Green River, Kentucky, from radioactive decay of cosmogenic ^{26}Al and ^{10}Be in Mammoth Cave sediments. *Geological Society of America Bulletin*, 113(7):825-836.

Hack, J.T., 1957. Studies of longitudinal stream profiles in Virginia and Maryland. U.S. Geological Professional Paper 294-B, 45-97.

Hancock, G.S., Anderson, R.S., and Whipple, K.X, 1998. Beyond power, bedrock incision process and form. *In:* Tinkler, K.J. and Wohl, E.E., (Editors), Rivers over rock: Fluvial processes in bedrock channels, AGU Monograph 107:35-60.

Hartshorn, K.; Hovius, N.; and Sligerland, R. 2000. Bedform amplitude in bedrock river channels [poster]. American Geophysical Union Fall Meeting, Abstracts with Programs, American Geophysical Union, Washington, D.C., p. F489.

Hydrologic Engineering Center 1998a. HEC-RAS, River analysis system, version 2.2 [program]. Davis, California, U.S. Army Corps of Engineers.

Hydrologic Engineering Center, 1998b. HEC-RAS River Analysis System: Hydraulic Reference Manual. U.S. Army Corps of Engineers, Davis, California, 189 p.

Howard, A.D., 1980. Thresholds in river regimes. *In:* Coates, D.R and Vitek, J.D (Editors), Thresholds in geomorphology. George Allen and Unwin, London, p. 227-258.

Howard, A.D., 1994. A detachment-limited model of drainage basin evolution. *Water Resources Research*, 30: 2261-2285.

Howard, A.D., 1998. Long profile development of bedrock channels: Interaction of weathering, mass wasting, bed erosion, and sediment transport. *In:* Tinkler, K.J. and Wohl, E.E. (Editors), Rivers Over Rock: Fluvial Processes in Bedrock Channels. American Geophysical Union Monograph 107, Washington, D.C., p. 297-319.

Howard, A.D., Dietrich, W.E., and Seidl, M.A., 1994. Modelling fluvial erosion on regional to continental scales. *Journal of Geophysical Research*, 99(B7):13971-13986.

Johnson, W., 1972. Impact strength of materials. Edward Arnold Publishing, New York, 361 p.

Johnson, P.A. and Gomez, B., 1994. Cave levels and cave development in the Mitchell Plain following base level lowering, *Earth Surface Processes and Landforms*, 19:517-523.

Jones, W., 1997. Karst Hydrology Atlas of West Virginia. Karst Waters Institute Special Publications 4. Charles Town, West Virginia. 111 p.

Knighton, D., 1998. Fluvial forms and processes: A new perspective. John Wiley and Sons, New York. 383 p.

Knighton, A.D., 2000. Profile form and channel gradient variation within an upland drainage basin - River Noe, Derbyshire, *Zeitschrift fur Geomorphologie*, 122:149-164.

Lauritzen, S.-E.; Abbott, J.; Arnesen, R.; Crossley, G.; Grepperud, D.; Ive, A.; and Johnson, S., 1985. Morphology and hydraulics of an active phreatic conduit. *Cave Science* 12(4):139-246.

Lauritzen, S.-E., and Lundberg, J. 2000. Solutional and erosional morphology (of caves). *In:* Klimchouk, A., Ford, D., Palmer, A. and Dreybrodt, W. (Editors). Speleogenesis: Evolution of karst aquifers. National Speleological Society, Huntsville, Alabama, p. 408-426.

Leopold, L.B., Wolman, M.G., and Miller, J.P., 1964. Fluvial processes in geomorphology, Freeman, San Francisco, 522 p.

Mackin, J.H., 1948. Concept of the graded river. *Geological Society of America Bulletin*, 59:632-636.

Matthes, G.H., 1947. Macroturbulence in natural stream flows. *EOS. Transactions of the Am. Geophysical Union*, 28:255-265.

Merritts, D.J., and Vincent, K.R. 1989. Geomorphic response of coastal streams to low, intermediate, and high rates of uplift, Mendocino junction region, northern California. Geol. Soc. of Am. Bull. 109:1373-1388.

McCue, J.B.; Lucke, J.B.; and Woodward, H.P. 1939. Limestones of West Virginia. The West Virginia Geological and Economic Survey, Morgantown, West Virginia, Volume V-12, 560 p.

Microsoft Corporation, 2001. Excel [spreadsheet program]. Seattle, Washington, USA.

Miller, J.R., 1991a. Controls on channel form along bedrock-influenced alluvial streams in south-central Indiana. *Physical Geography*, 12:167-186.

Miller, J.R., 1991b. The influence of bedrock geology on knickpoint development and channel-bed degradation along downcutting streams in south-central Indiana. *Journal of Geology*, 99:591-605.

Miller, T.E., 1996. Geologic and hydrologic controls on karst and cave development in Belize. *Journal of Cave and Karst Studies*, 58:100-120.

Mills, H.H., 1990. Geologic and topographic controls on the rapids of the New River gorge, West Virginia, *Southeastern Geology*, 31:45-62.

Munson, B.R., Young, D.F., and Okiishi, T.H., 1994. Fundamentals of fluid mechanics. John Wiley and Sons, New York, 893 p.

Nanson, G.C., and Croke, J.C., 1992. A genetic classification of floodplains. *Geomorphology*, 4:459-486.

Newson, M.D., 1971. The role of abrasion in cave development. *Transactions of the Cave Research Group of Great Britain*, 13:102-108.

O'Connor, J.E., 1993. Hydrology, Hydraulics, and Geomorphology of the Bonneville Flood, Geological Society of America Special Paper 274, 83 p.

Ott, R.L., 1992. An introduction to statistical techniques. Wadsworth Publishing, Belmont, California, 1051 p.

Palmer, A.N., 1977. Influence of geologic structure on groundwater flow and cave development in Mammoth Cave National Park, Kentucky, USA, International Assoc. of Hydrogeologists, 12th Memoirs, p. 405-414.

Palmer, A.N., 1987. Cave levels and their interpretation. *Bulletin of the National Speleological Society*, 49:50-66.

Palmer, A.N., 1991. Origin and morphology of limestone caves, *Geological Society of America Bulletin*, 103:1-21.

Palmer, M.V., and Palmer, A.N., 1975. Landform development in the Mitchell Plain of southern Indiana: Origin of a partially karsted plain. *Zeitschrift fur Geomorphologie*, 19:1-39.

Pazzaglia, F.J., Gardner, T.W., and Merritts, D.J., 1998. Bedrock fluvial incision and longitudinal profile development over geologic time scales determined by fluvial terraces. *In:* Tinkler, K.J. and Wohl, E.E. (Editors). Rivers Over Rock: Fluvial Processes in Bedrock Channels. American Geophysical Union Monograph 107, Washington, D.C., p. 207-235.

Pease, P.P., Gomez, B., and Schmidt, V.A., 1994. Magnetostratigraphy of cave sediments, Wyandotte Ridge, Crawford County, Indiana: Towards a regional correlation. *Geomorphology*, 11:75-81.

Pisarowicz, J.A. and Maslyn, R.M., 1981. Empirical confirmation of Curl's (1974) flow velocity calculations. *In:* Beck, B.B. (Editor), Proceedings of the Eighth International Congress of Speleology [monograph], Bowling Green, KY, International Union of Speleology, 772-774.

Ritter, D.F., Kochel, R.C., and Miller, J.R ., 1999. The disruption of Grassy Creek: implications concerning catastrophic events and thresholds, *Geomorphology*, 29(3-4):323-338.

SAS Institute Inc., 2000. SAS/STAT statistical analysis program, version 8.0: Cary, NC, SAS Institute.

Sasowsky, I.D., Curry, M.C., Demrovsky, N., Shank, D.A., Springer, G.S., and Benjamin, S.E., 2002. Hydrology and geomorphology of a highly karsted upland: The Greenbrier Valley and Little Levels, West Virginia [abstract], GSA Annual Spring Convention, Lexington, KY.

Sato, S., and Hayami, T. 1987. Potholes in Skikoku, Japan, Part II: Origin of potholes and significance of pothole research, *Memoirs of the Faculty of Education*, Ehime University, Series III Natural Science 7:191-220.

Selby, M.J., 1980. A rock mass strength classification for geomorphic purposes: With tests from Antarctica and New Zealand, *Zeitschrift fur Geomorphologie*, 24:31-51.

Shank, D. and Sasowsky, I.D. 2001. Hydrology and paleohydrology of Windy Mouth Cave, West Virginia: An abandoned spring conduit on the Greenbrier River. In: GSA Abstracts with programs, Annual Meeting, Boston, Massachusetts, 33(6):A 6-7.

Sklar, L.S. and Dietrich, W.E., 1998. River longitudinal profiles and bedrock incision models: Stream power and the influence of sediment supply. *In:* Tinkler, K.J. and Wohl, E.E. (Editors), Rivers Over Rock: Fluvial Processes in Bedrock Channels, American Geophysical Union Monograph 107, Washington, D.C., p. 237-260.

Sklar, L.S., and Dietrich, W.E. 2001. Sediment and rock strength controls on river incision into bedrock. *Geology*, 29:1087-1090.

Smart, C.C., 1988. A deductive model of karst evolution based on hydrological probability, *Earth Surface Processes and Landforms*, 13:271-288.

Smith, J.A., Baeck, M.L., Steiner, M. and Miller, A.J., 1996. Catastrophic rainfall from an upslope thunderstorm in the central Appalachians: The Rapidan storm of June 27, 1995. *Water Resources Research*, 32:3099-3113.

Snow, R.S. and Slingerland, R.L., 1987. Mathematical modeling of graded river profiles. *Journal of Geology*, 95:15-33.

Snyder, N.P.; Whipple, K.X.; Tucker, G.E.; and Merritts, D.J., 2000. Landscape response to tectonic forcing: Digital elevation model analysis of stream profiles in the Mendocino triple junction region, northern California. *Geological Society of America Bulletin*, 112:1250-1263.

Spell, T.L. and McDougall, I., 1992. Revisions to the age of the Bruhnes-Matayama boundary and the Pleistocene geomagnetic polarity timescale. *Geophysical Research Letters*, 19:1181-1184.

Springer, G.S., 2002. Caves and their potential use in paleoflood studies. *In:* House, K., Webb, R., Baker, V.R., and Levish, D.R. (Editors), Ancient Floods, Modern Hazards: Principles and Applications of Paleoflood Hydrology, Water Science and Application Volume 5. American Geophysical Union Monograph. Washington, D.C., 329-344.

Springer, G.S., Kite, J.S., Schmidt, V.A., 1997. Cave sedimentation, genesis, and erosional history in the Cheat River Canyon, West Virginia. *Geological Society of America Bulletin*, 109:524-532.

Springer, G.S., Dowdy, H.S., and Eaton, L.S., 2001. Sediment budgets for two mountainous basins affected by a catastrophic storm: Blue Ridge Mountains, Virginia. *Geomorphology*, 37(1-2):135-148.

Thompson, D.M., E.E. Wohl and Jarrett, R.D., 1999. Velocity reversals and sediment sorting in pools and riffles controlled by channel constrictions. *Geomorphology*, 27:229-241.

Tinkler, K.J., 1997. Critical flow in rockbed streams with estimated values for Manning's n. *Geomorphology*, 20:147-164.

Tinkler, K.J. and Wohl, E.E., 1998. Field studies of bedrock channels. *In:* Tinkler, K.J. and Wohl, E.E. (Editors), Rivers Over Rock: Fluvial Processes in Bedrock Channels. American Geophysical Union Monograph 107, Washington, D.C., p. 261-277.

Whipple, K.S., Hancock, G.S., and Anderson, R.S., 2000a. River incision into bedrock: Mechanics and relative efficacy of plucking, abrasion, and cavitation. *Geological Society of America Bulletin*, 112:490-503.

Whipple, K.S., Snyder, N.P., and Dollenmayer, K., 2000b. Rates and processes of bedrock incision by the Upper Ukak River since the 1912 Novarupta ash flow in the Valley of Ten Thousand Smokes, Alaska. *Geology*, 28:835-838.

White, W. B., 1988. Geomorphology and Hydrology of Karst Terrains, Oxford University Press, New York, 464 p.

White, E.L., and White, W.B., 1968. Dynamics of sediment transport in caves, *Bulletin of the National Speleological Society*, 30:115-129.

White, E.L. and White, W.B., 1983. Karst landforms and drainage basin evolution in the Obey River basin, north-central Tennessee, U.S.A., *Journal of Hydrology*, 61:69-82.

Wohl, E.E., 1992. Bedrock benches and boulder bars: Floods in the Burdekin Gorge of Australia, *Geological Society of America Bulletin*, 104:770-778.

Wohl, E.E., 1993. Bedrock channel incision along Picanniny Creek, Australia, *Journal of Geology*, 101:749-761.

Wohl, E.E. 1998. Bedrock channel morphology in relation to erosional processes. *In:* Tinkler, K.J. and Wohl, E.E. (Editors), Rivers Over Rock: Fluvial Processes in Bedrock Channels. American Geophysical Union Monograph 107, Washington, D.C., p. 133-151.

Wohl, E.E., 2000. Mountain rivers. Am. Geophysical Union Water Resources Monograph 14, Washington, D.C., 320 p.

Wohl, E.E., Greenbaum, N., Schick, A.P., and Baker, V.R., 1994. Controls on bedrock channel incision along Nahal Paran, Isreal, *Earth Surface Processes and Landforms*, 19: 1-13.

Wohl, E.E. and Ikeda, H., 1998. Patterns of bedrock channel erosion on the Boso Peninsula, Japan, *Journal of Geology*, 106:331-345.

Wohl, E.E., Thompson, D.M., and A.J. Miller, 1999. Canyons with undulating walls, *Geological Society of America Bulletin*, 111:949-959.

Wohl, E.E. and Merritt, D.M. 2001. Bedrock channel morphology. *Geological Society of America Bulletin*, 113:1205-1212.

Wohl, E.E., Cenderelli, D., and Mejia-Navarro, M., 2001. Channel changes from extreme floods in canyon rivers. *In:* Anthony, D.J., Harvey, M.D., Laronne, J.B., and Mosley, M.P. (Editors), Applying geomorphology to environmental management. Water Resources Publications, Highlands Ranch, Colorado, 149-174.

Wohl, E.E. and Achyuthan, H., 2002. Substrate Influences on Incised-Channel Morphology, *Journal of Geology*, 110:115-120.

Wolman, M.G., 1954. A method of sampling coarse river-bed material, *Trans. Am. Geophys. Union*, 35:951-956.

Zen E., and K.L Prestegaard, 1994. Possible hydraulic significance of two kinds of potholes: Examples from the paleo-Potomac River, *Geology*, 22:47-50.

Appendix A

Schematics of Study Reaches

This appendix includes schematics of all study reaches as exported from HEC-RAS. Cross section spacing and widths are to scale. Bends are not to scale. Cross section numbers decrease in the downstream direction. Number system is arbitrary, as any combination of descending numbers can be used. The orientations of reaches do not represent the absolute channel azimuths. Detailed reach information can be found in Tables 3.1 and 3.2.

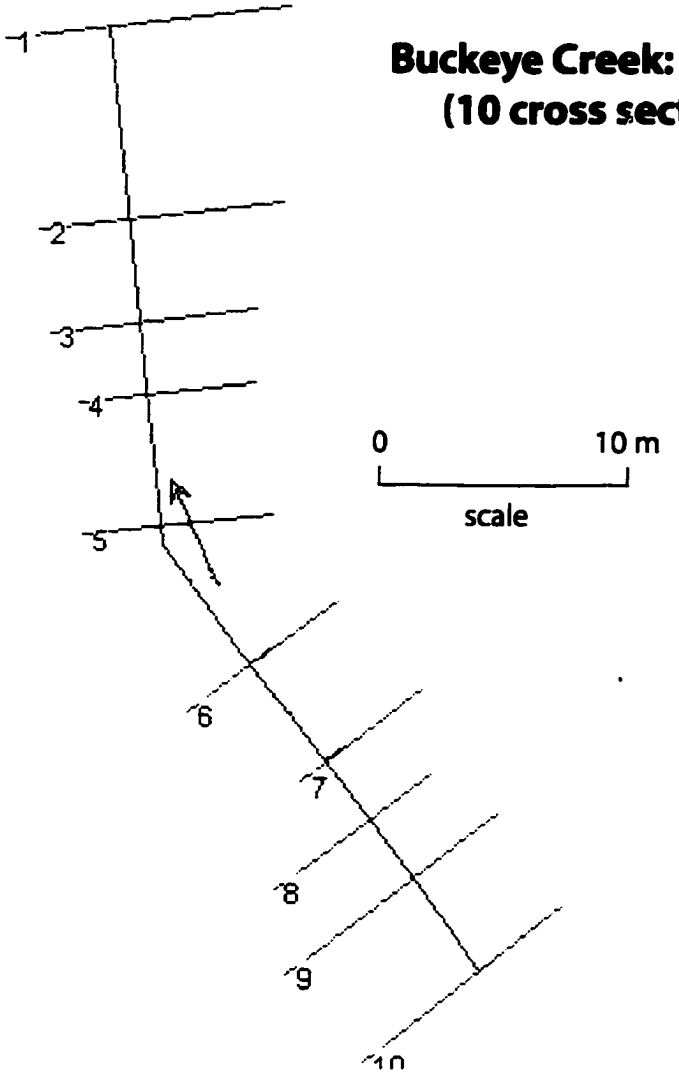

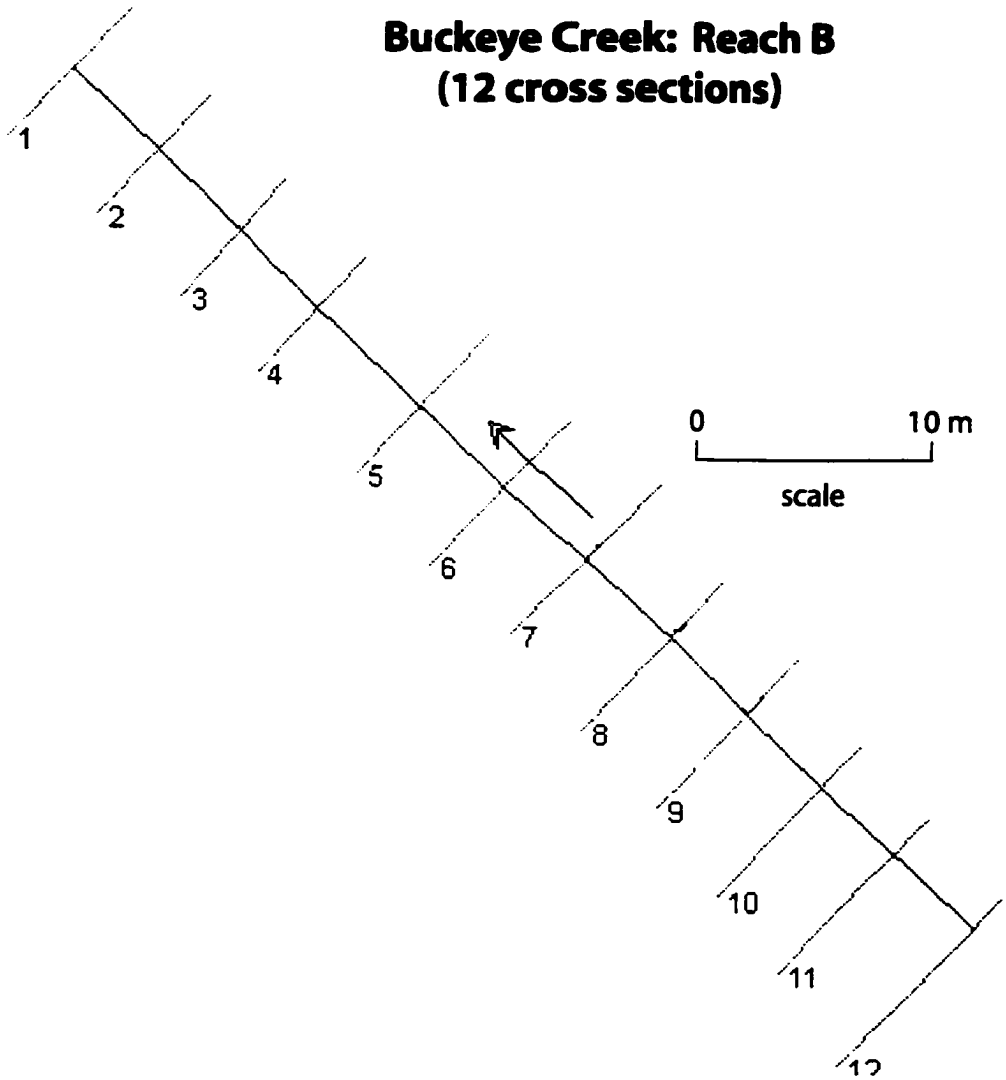

Buckeye Creek: Reach C
(9 cross sections)

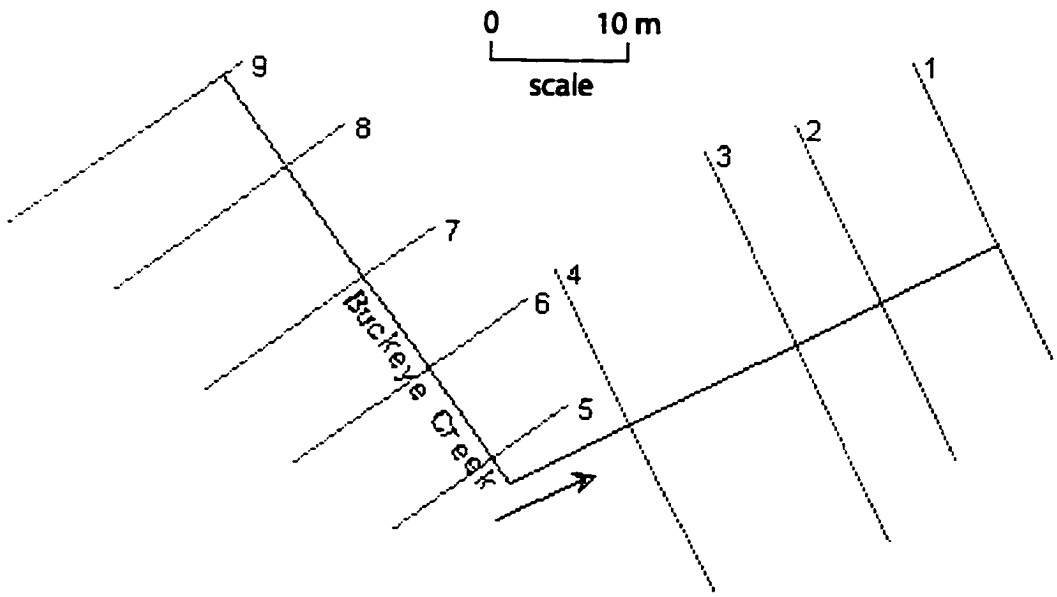

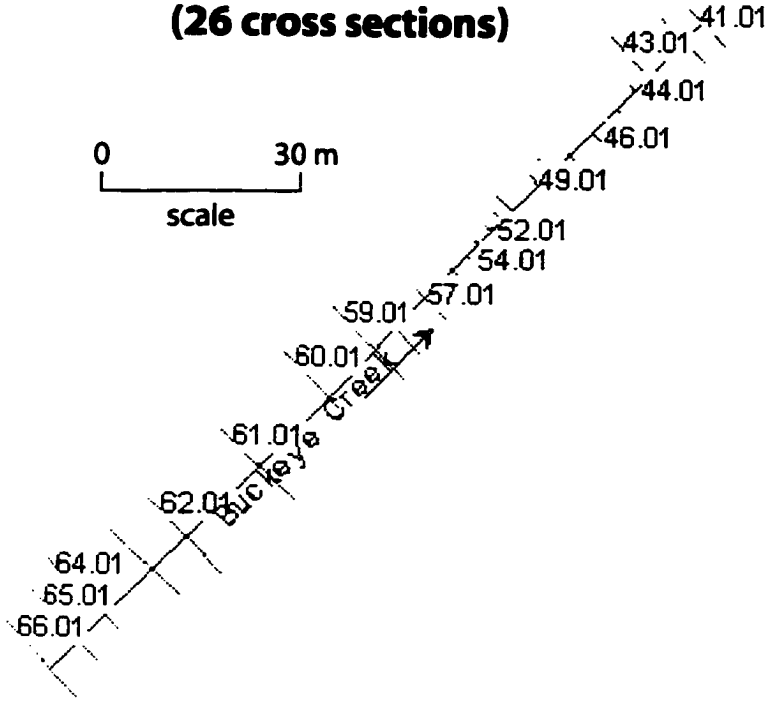

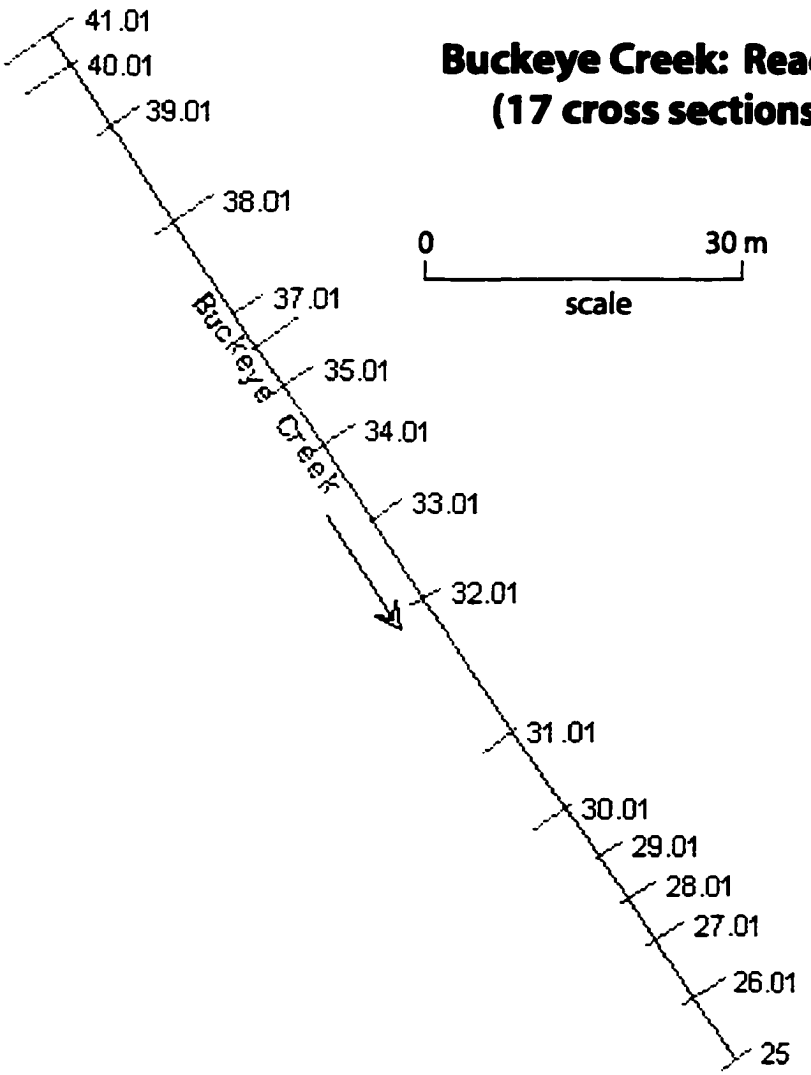

Buckeye Creek: Reach F
(20 cross sections)

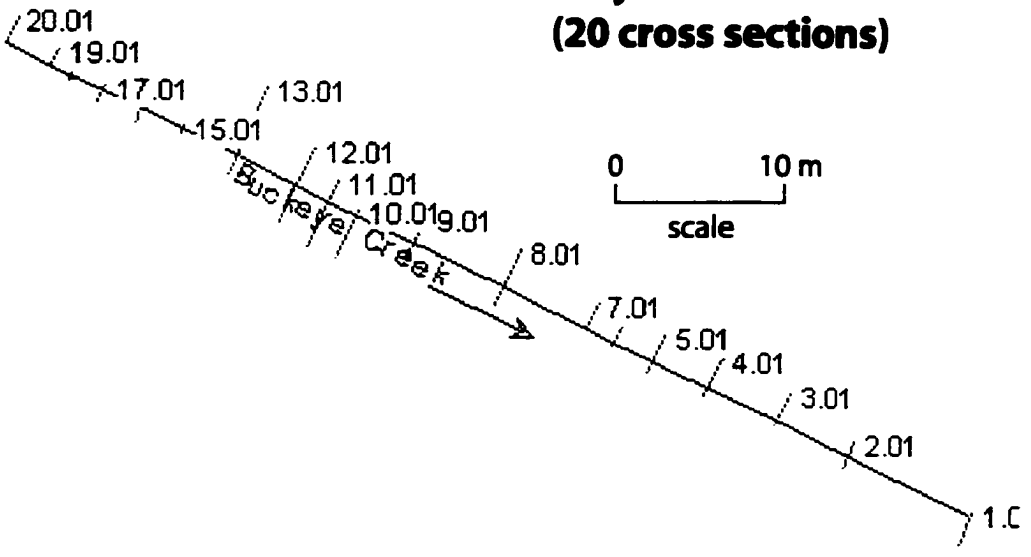

Buckeye Creek: Reach G
(12 cross sections)

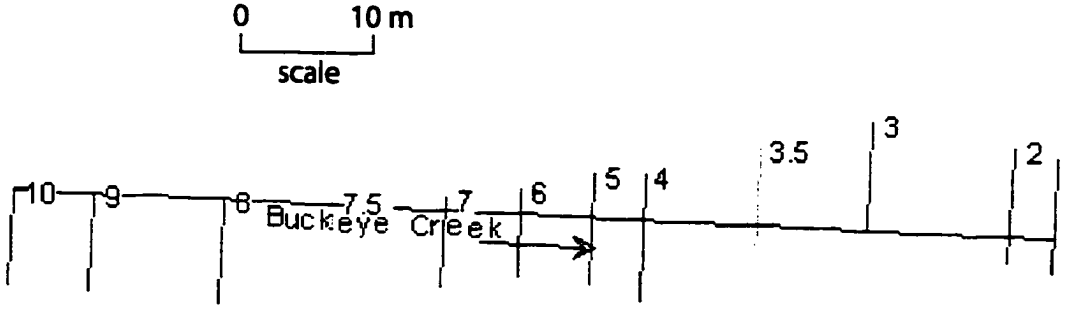

Buckeye Creek: Reach H
(15 cross sections)

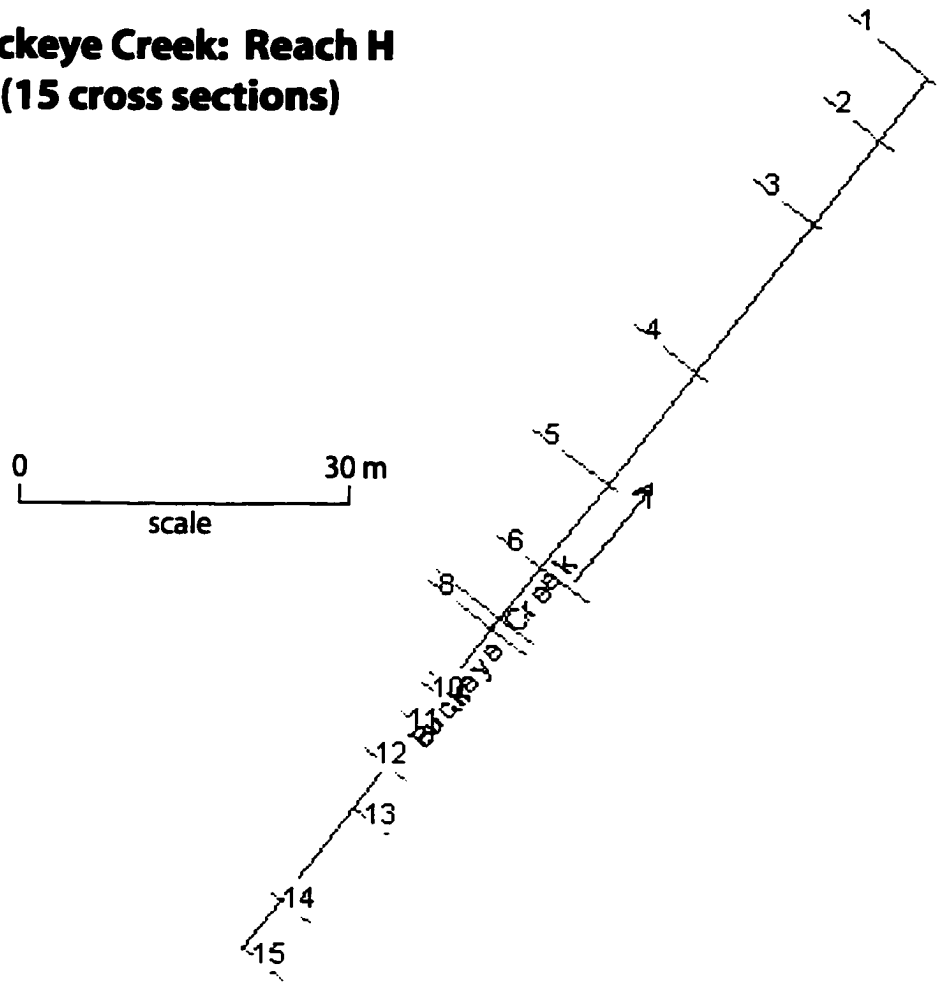

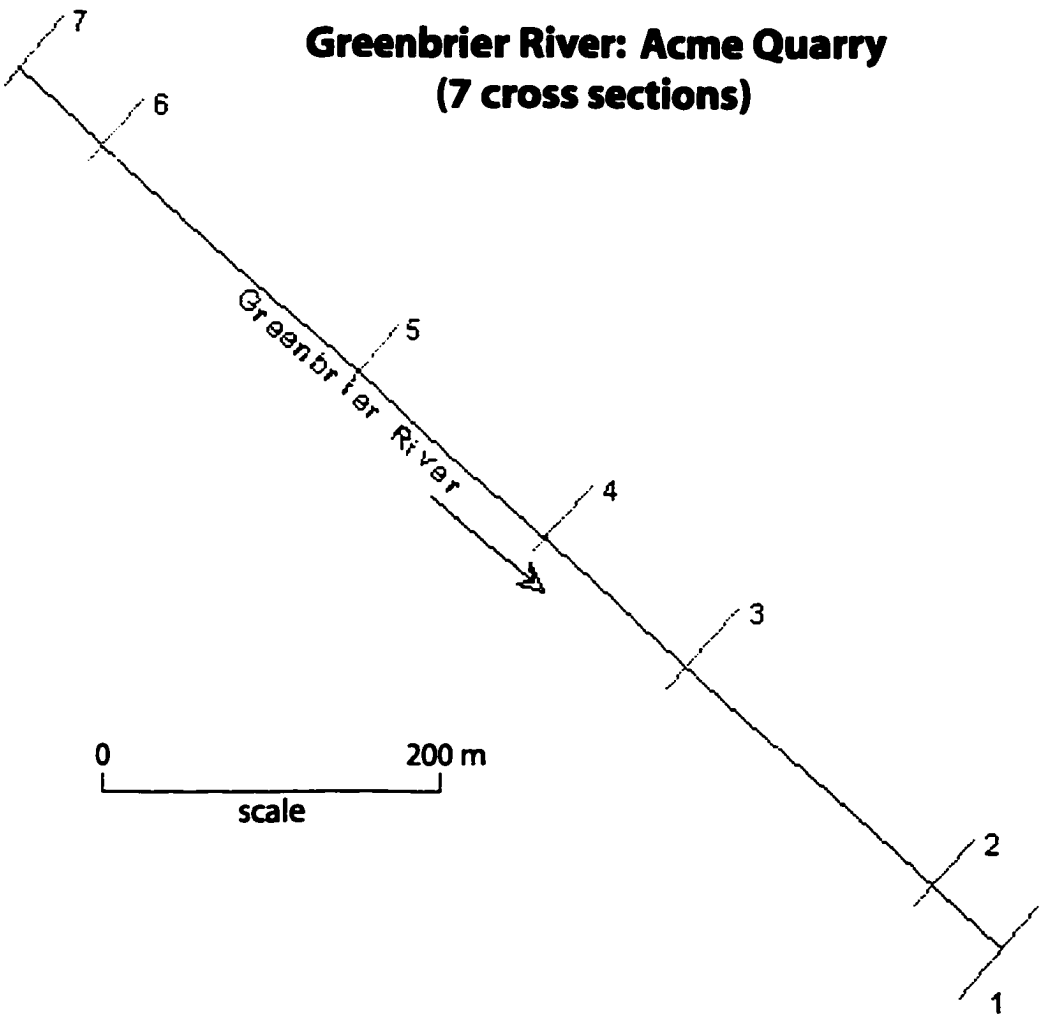

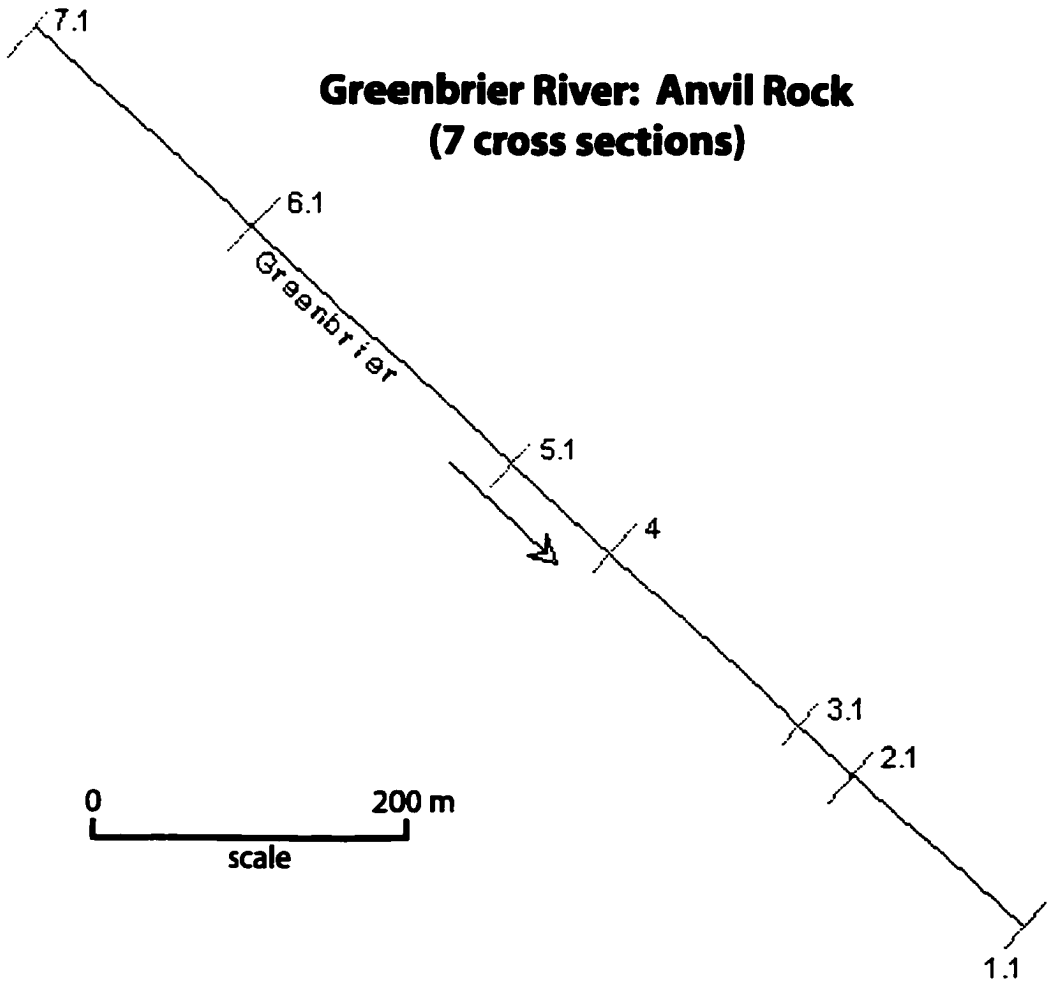

Greenbrier River: Bone Quarry
(8 cross sections)

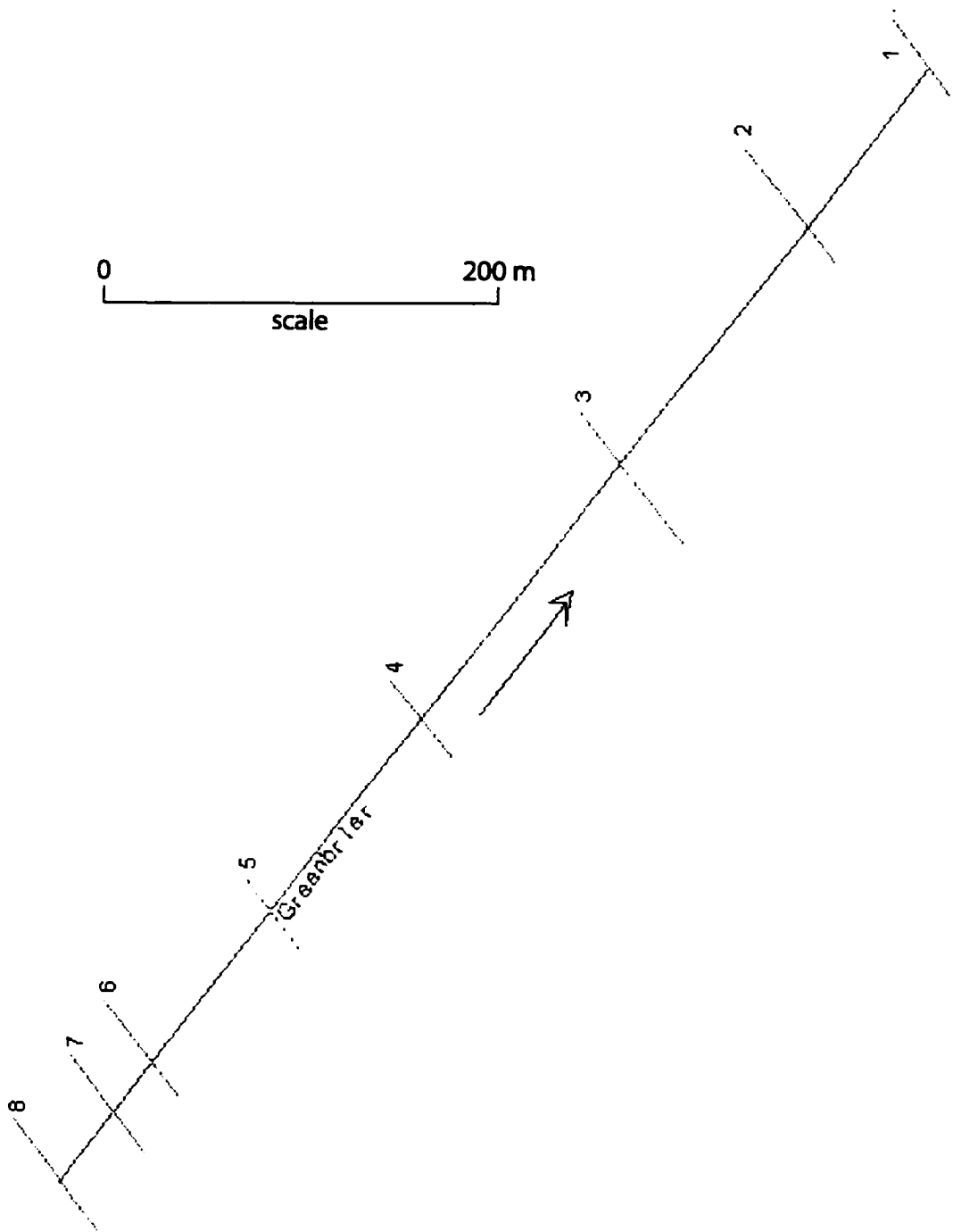

Greenbrier River: Cathole
(12 cross sections)

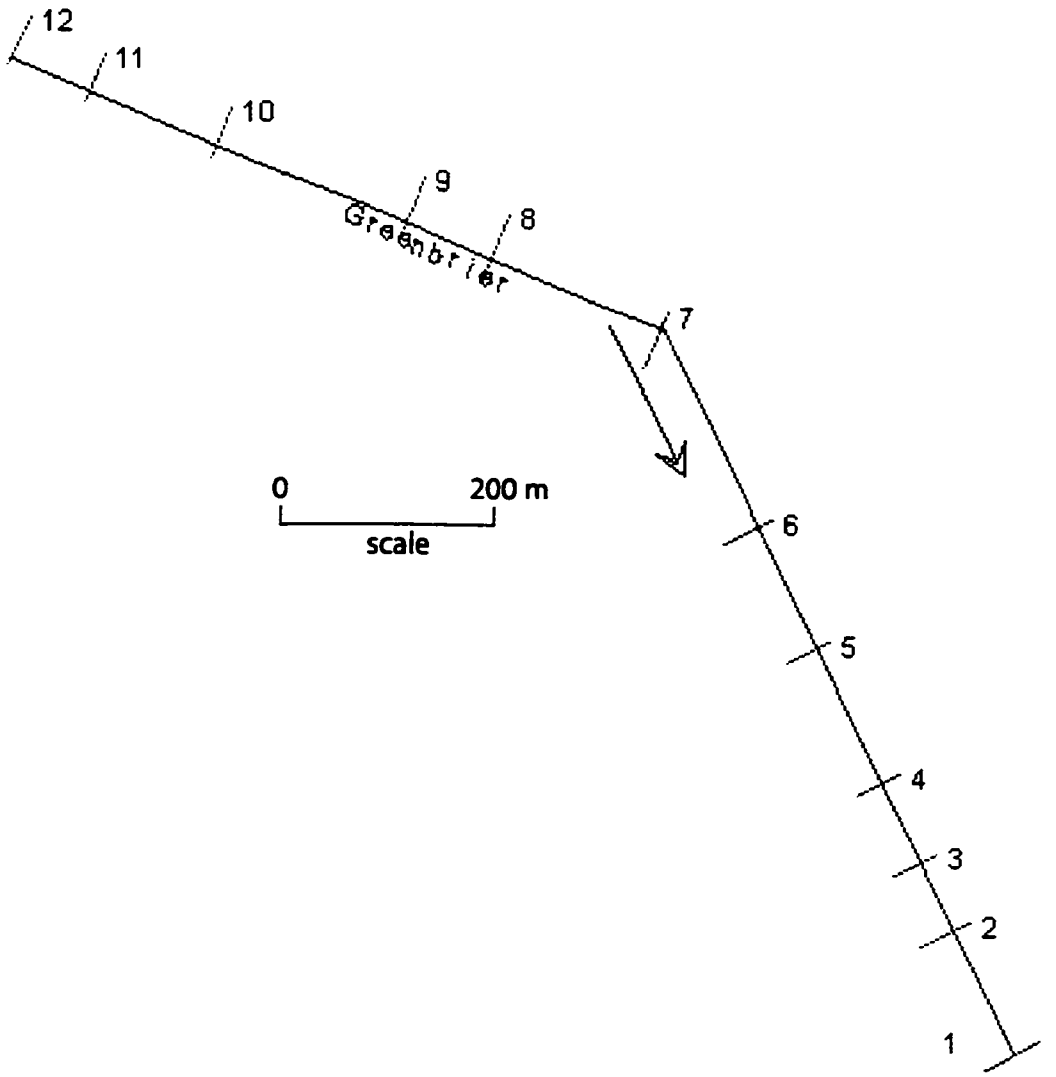

Greenbrier River: Mile-27
(6 cross sections)

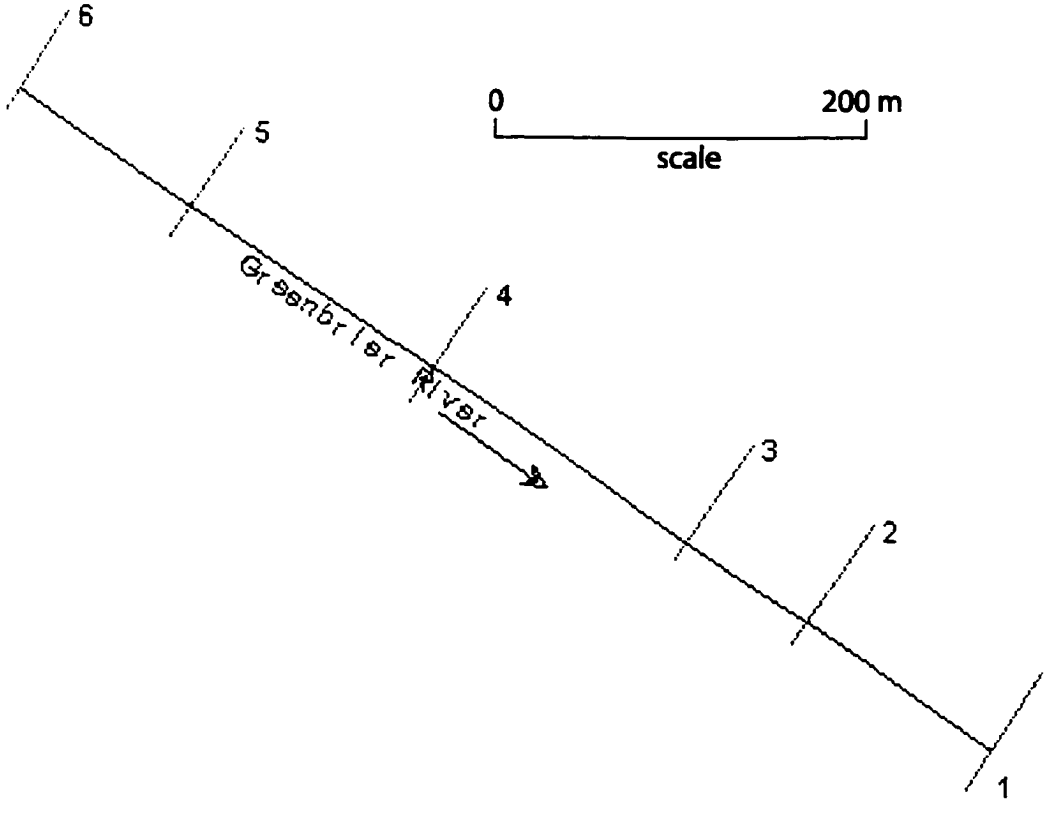

Appendix B

Visual Basic Macro for Reduction of Cross Section Data

This appendix presents the code for a simple macro that can be used in Microsoft Excel for the processing of XYZ cross-section data to a format that is compatible with HEC-RAS (Microsoft Corporation, 2001). Further details are provided in Module 1 (below). Selected screenshots are provided so that interested parties can create a spreadsheet within which to run the code. The author wrote the macro and will provide a copy to any interested parties (laramide@bedrockstreams.org).

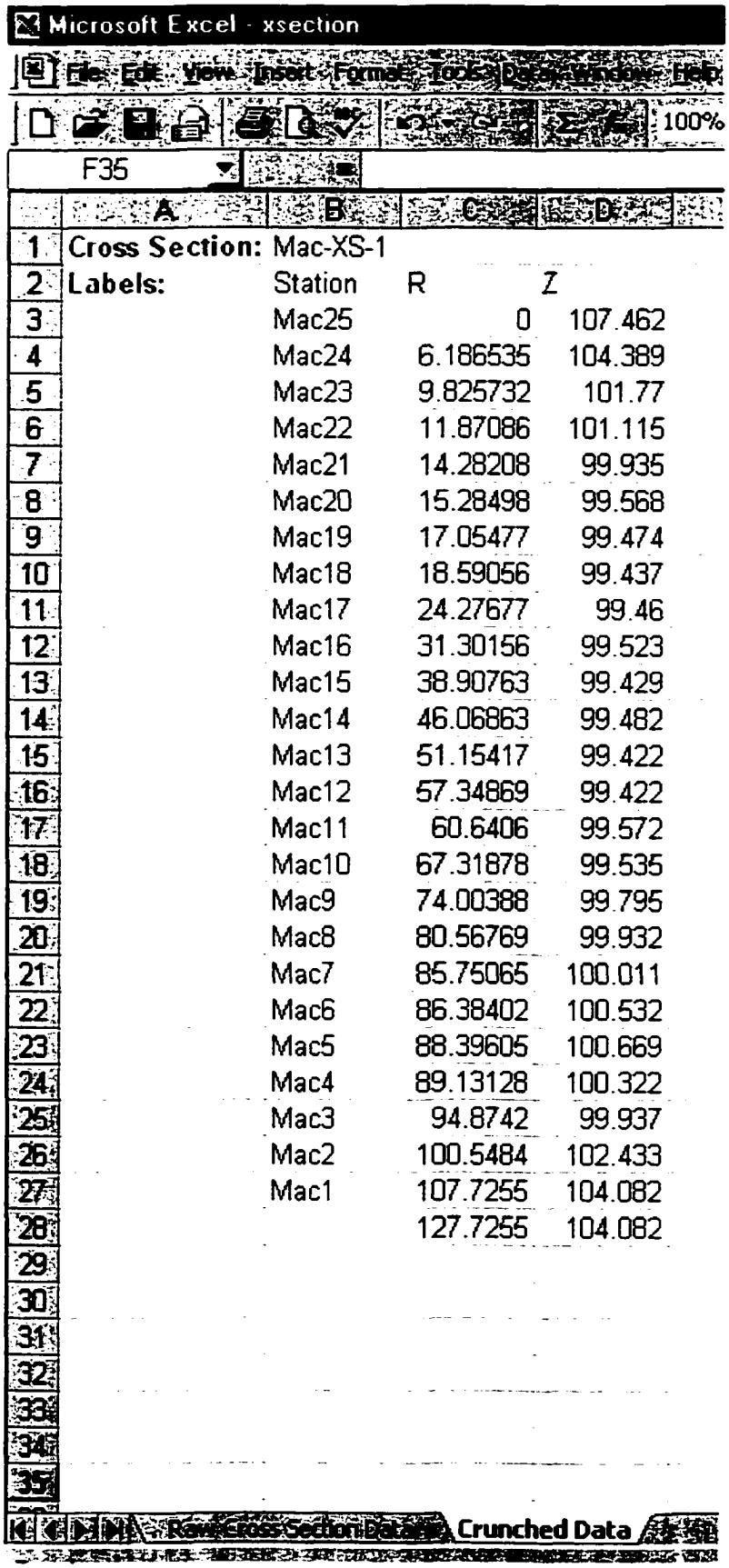

	A	B	C	D
1	**Cross Section:**	Mac-XS-1		
2	**Labels:**	Station	R	Z
3		Mac25	0	107.462
4		Mac24	6.186535	104.389
5		Mac23	9.825732	101.77
6		Mac22	11.87086	101.115
7		Mac21	14.28208	99.935
8		Mac20	15.28498	99.568
9		Mac19	17.05477	99.474
10		Mac18	18.59056	99.437
11		Mac17	24.27677	99.46
12		Mac16	31.30156	99.523
13		Mac15	38.90763	99.429
14		Mac14	46.06863	99.482
15		Mac13	51.15417	99.422
16		Mac12	57.34869	99.422
17		Mac11	60.6406	99.572
18		Mac10	67.31878	99.535
19		Mac9	74.00388	99.795
20		Mac8	80.56769	99.932
21		Mac7	85.75065	100.011
22		Mac6	86.38402	100.532
23		Mac5	88.39605	100.669
24		Mac4	89.13128	100.322
25		Mac3	94.8742	99.937
26		Mac2	100.5484	102.433
27		Mac1	107.7255	104.082
28			127.7255	104.082
29				
30				
31				
32				
33				
34				
35				

Module 1

```
' Cartesian Cross Section Macro
' By Greg Springer
' 17 October 1998

' Notes
' This macro takes cartesian data points along a cross section
' and uses trigonometry to align all the points along a straight
' line connecting the end points of the cross section. The final data
' has two numbers: R and z. R is the distance of the corrected point
' from the RIVER LEFT end point and z is the depth of the station below
' datum. NOTE: Depth is NOT affected by the program nor is it a function
' of the elevation of the end points. It is always relative to your datum!

' The end points are the only points that need to be in a particular
' place or order. The end station for river right must be the first station
' entered (cells E3:G3). The end station for river left is next (cells E4:G4).
' River right is the right bank as you look DOWNSTREAM.

' You should give each cross-section a name, although that is not necessary.
' The name goes in cell B2. The macro will label a cross section 'Zamadius'
' if you do not supply a name.

' All cross section data is stored in the Crunched Data worksheet.
' You can delete the data on the Crunched Data worksheet by selecting it and
' pressing delete. HOWEVER you must leave the headers in cells A1 and A2 or
' the program will crash. The headers say Station and Label.
```

Module 2

```
Sub CrossSectionProcessor()

  ' Count the number of Entries in Station Data
    Dim CNumberofStations As Object
    Set CNumberofStations = Worksheets("Raw Cross Section Data").Cells(5,
5).CurrentRegion

    cNOS = CNumberofStations.Rows.Count

    Dim DStations As Object
    Set DStations = _
        Worksheets("Raw Cross Section Data").Cells(1, 1).Resize(Worksheets("Raw
Cross Section Data"). _
        Cells(1, 1).CurrentRegion.Rows.Count - 1, 1)

    ' Calculate angle between Endpoint stations
    ' The ends points are river right and river left control stations!
    xr = Worksheets("Raw Cross Section Data").Cells(3, 5).Value
    yr = Worksheets("Raw Cross Section Data").Cells(3, 6).Value
    xl = Worksheets("Raw Cross Section Data").Cells(4, 5).Value
    yl = Worksheets("Raw Cross Section Data").Cells(4, 6).Value

    xangleratio = (yr - yl) / (Sqr((xr - xl) ^ 2 + (yr - yl) ^ 2))
    Worksheets("Raw Cross Section Data").Cells(1, 8).Value = xangleratio
    Worksheets("Raw Cross Section Data").Cells(1, 9).Formula = "=ASIN(H1)"
    xangle = Worksheets("Raw Cross Section Data").Cells(1, 9).Value

    ' Clear previous calculations
    For i = 8 To 9
      For j = 5 To cNOS
        Worksheets("Raw Cross Section Data").Cells(j, i).Value = ""
      Next j
    Next i

    'Calculate the individual stations

    ' Start with River Left Control Station
    Worksheets("Raw Cross Section Data").Cells(4, 8).Value = _
      Worksheets("Raw Cross Section Data").Cells(4, 4).Value
    Worksheets("Raw Cross Section Data").Cells(4, 9).Value = 0
    Worksheets("Raw Cross Section Data").Cells(4, 10).Value = _
      Worksheets("Raw Cross Section Data").Cells(4, 7).Value
```

```
' Setting Final Value of River Right Control Station
Worksheets("Raw Cross Section Data").Cells(3, 8).Value = _
   Worksheets("Raw Cross Section Data").Cells(3, 4).Value
Worksheets("Raw Cross Section Data").Cells(3, 9).Value = _
   (Sqr((xr - xl) ^ 2 + (yr - yl) ^ 2))
Worksheets("Raw Cross Section Data").Cells(3, 10).Value = _
   Worksheets("Raw Cross Section Data").Cells(3, 7).Value

' Distance between RR and RL
xlength = (Sqr((xr - xl) ^ 2 + (yr - yl) ^ 2))

'Now the rest!
For i = 5 To cNOS
   xs = Worksheets("Raw Cross Section Data").Cells(i, 5)
   ys = Worksheets("Raw Cross Section Data").Cells(i, 6)
   Worksheets("Raw Cross Section Data").Cells(1, 9).Formula = "=ASIN(H1)"
   stationratio = (ys - yr) / (Sqr((xs - xr) ^ 2 + (ys - yr) ^ 2))
   Worksheets("Raw Cross Section Data").Cells(1, 8).Value = stationratio
   stationangle = Worksheets("Raw Cross Section Data").Cells(1, 9).Value
   stationangle = Abs(stationangle)
   xangle = Abs(xangle)
   gamma = stationangle - xangle
   gamma = Abs(gamma)
   dist = Sqr((xs - xr) ^ 2 + (ys - yr) ^ 2)
   r = dist * Cos(gamma)
   r = xlength - Abs(r)
   Worksheets("Raw Cross Section Data").Cells(i, 8).Value = _
      Worksheets("Raw Cross Section Data").Cells(i, 4).Value
   Worksheets("Raw Cross Section Data").Cells(i, 9) = r
   Worksheets("Raw Cross Section Data").Cells(i, 10) = _
      Worksheets("Raw Cross Section Data").Cells(i, 7)
Next i

' Transfer Data to Crunched Data Sheet
' Sort by Distance from River Left CC

 ' Count the number of Entries in Station Data
Dim CNumberofCrunched As Object
Set CNumberofCrunched = Worksheets("Crunched Data").Cells(1, 1).CurrentRegion

cNOCD = CNumberofCrunched.Columns.Count
```

```
    ' Place Cross Section Name
    xname = Worksheets("Raw Cross Section Data").Cells(2, 2).Value
    If xname = "" Then xname = "Zamadius (No Name Given)"

    Worksheets("Crunched Data").Cells(1, cNOCD + 1).Value = xname

    ' Place Labels
       Worksheets("Crunched Data").Cells(2, cNOCD + 1).Value = _
          "Station"
       Worksheets("Crunched Data").Cells(2, cNOCD + 2).Value = _
          "R"
       Worksheets("Crunched Data").Cells(2, cNOCD + 3).Value = _
          "Z"

    For i = 3 To cNOS

       ' Data
       Worksheets("Crunched Data").Cells(i, cNOCD + 1).Value = _
          Worksheets("Raw Cross Section Data").Cells(i, 8).Value
       Worksheets("Crunched Data").Cells(i, cNOCD + 2).Value = _
          Worksheets("Raw Cross Section Data").Cells(i, 9).Value
       Worksheets("Crunched Data").Cells(i, cNOCD + 3).Value = _
          Worksheets("Raw Cross Section Data").Cells(i, 10).Value
    Next i

    ' Clear out inverse sine cells.
    Worksheets("Raw Cross Section Data").Cells(1, 8).Value = ""
    Worksheets("Raw Cross Section Data").Cells(1, 9).Value = ""

    Range("E3:G4").Select
    Selection.BorderAround Weight:=xlMedium, ColorIndex:=xlAutomatic
    Range("B2").Select
    Selection.BorderAround Weight:=xlMedium, ColorIndex:=xlAutomatic

End Sub


Sub ClearRawDataSheet()

  ' Count the number of Entries in Station Data
    Dim CNumberofStations As Object
    Set CNumberofStations = Worksheets("Raw Cross Section Data").Cells(5,
5).CurrentRegion

    cNOS = CNumberofStations.Rows.Count
```

```
    Dim DStations As Object
    Set DStations = _
        Worksheets("Raw Cross Section Data").Cells(1, 1).Resize(Worksheets("Raw
Cross Section Data"). _
        Cells(1, 1).CurrentRegion.Rows.Count - 1, 1)

    ' Clear previous calculations
    For i = 4 To 10
      For j = 3 To cNOS
        Worksheets("Raw Cross Section Data").Cells(j, i).Value = ""
      Next j
    Next i

    ' Clear Name
      Worksheets("Raw Cross Section Data").Cells(2, 2).Value = ""

    ' Add borders to important cells
    Range("E3:G4").Select
    Selection.BorderAround Weight:=xlMedium, ColorIndex:=xlAutomatic
    Range("B2").Select
    Selection.BorderAround Weight:=xlMedium, ColorIndex:=xlAutomatic

End Sub
```